OLD DOMINION UNIVERSITY RESEARCH FOUNDATION

SCHOOL OF ENGINEERING
OLD DOMINION UNIVERSITY
NORFOLK, VIRGINIA

Technical Report 76-T10

MODELS FOR INFRARED ATMOSPHERIC RADIATION

By

Surendra N. Tiwari

Final Report

Prepared for the
National Aeronautics and Space Administration
Langley Research Center
Hampton, Virginia

Under
Grant NSG 1153

June 1976

SCHOOL OF ENGINEERING
OLD DOMINION UNIVERSITY
NORFOLK, VIRGINIA

Technical Report 76-T10

MODELS FOR INFRARED ATMOSPHERIC RADIATION

By

Surendra N. Tiwari

Final Report

Prepared for the
National Aeronautics and Space Administration
Langley Research Center
Hampton, Virginia 23665

Under
Grant NSG 1153
Henry G. Reichle, Technical Monitor
ESSD - Meteorology Section

Submitted by the
Old Dominion University Research Foundation
Norfolk, Virginia 23508

June 1976

FOREWORD

This is a final report of the work completed during the year 1975-76 on the research project "Radiative Transfer Models for Nonhomogeneous Atmosphere." This work was supported by the NASA-Langley Research Center through Grant NSG 1153. The grant was monitored by Dr. Henry G. Reichle (ESSD-Meteorology Section).

TABLE OF CONTENTS

TABLE OF CONTENTS (continued)

LIST OF FIGURES

LIST OF FIGURES (continued)

LIST OF FIGURES (continued)

LIST OF FIGURES (concluded)

MODELS FOR INFRARED ATMOSPHERIC RADIATION

by

Surendra N. Tiwari[1]

SUMMARY

Different line and band models for infrared spectral absorption are discussed. Radiative transmittance and integrated absorptance of Lorentz, Doppler, and Voigt line profiles are compared for a range of governing parameters. It is found that, for the intermediate path lengths, the use of the combined Lorentz-Doppler (Voigt) profile is essential in calculating the atmospheric transmittance. Narrow band model relations for absorptance are used to develop exact formulations for total absorption by four wide band models. Several continuous correlations for the absorption of a wide band model are presented and each one of these is compared with the exact (numerical) solutions of the wide band models. By employing the line-by-line and quasi-random band model formulations, computational procedures were developed for evaluating the transmittance and upwelling atmospheric radiance. Homogeneous path transmittances were calculated for selected bands of CO, CO_2, and N_2O, and these are compared with available experimental measurements. The importance of line-by-line model for atmospheric work is emphasized. Model calculations were made to determine the upwelling radiance and signal change in the wave number interval of CO fundamental band. These results are useful in determining the effects of different interfering molecules, water vapor profiles, ground temperatures, and ground emittance on the upwelling radiance and signal change. This information is of vital importance in establishing the feasibility of measuring the concentrations of pollutants in the atmosphere from a gas filter correlation instrument flown on an aircraft or mounted on a satellite.

---

[1] Associate Professor, School of Engineering, Old Dominion University, Norfolk, Virginia 23508.

LIST OF SYMBOLS

a	parameter expressing the ratio of Lorentz to Doppler half-width
A	band absorptance, cm^{-1}
$A(u, \beta)$	absorption of a wide band
$\bar{A}$	nondimensional A
A_j	absorptance (total absorption) of a single line (jth line)
$\bar{A}_j$	average value of A_j, dimensionless
$A_{j,\delta}$; $A_{j,D}$; $A_{j,d}$; $A_{j,\infty}$	absorption of jth line over spectral intervals δ, D, d, and ∞ respectively
A_j^*	nondimensional A_j, $A_j^* = A_j/A_n$
A_n	nondimensional constant, $A_n = 2\gamma_D/(\ell n 2)^{1/2}$
$A_N(x, \beta)$	absorption of a narrow band
A_o	band width parameter, cm^{-1}
A_s	absorption of a single line in a linear limit, cm^{-1}
$\bar{A}_s(u, \beta)$	axial or slab band absorptance
$B(\omega, T)$	Planck's function
c	speed of light
$E(\omega)$	upwelling radiative energy
E_D	total upwelling radiative energy in spectral interval $\Delta\omega = D$
$E_G(\omega)$	thermal radiation of ground and atmosphere
$E_R(\omega)$	solar radiation reflected from ground
$E_\phi(\omega)$	solar radiation scattered by the atmosphere without having been reflected by the ground

$E_{R\phi}(\omega)$	solar radiation reflected from ground outside the field of view and scattered by the atmosphere into the field of view
f_j	shape factor of jth line
h	altitude of an aircraft or a satellite
H_s	sun irradiance at the top of the atmosphere
k	Boltzmann constant
K(a, v)	Voigt function
$L(\eta)$	Ladenberg-Reiche function
m	molecular mass of the absorbing medium
p, P	partial pressure of the absorbing medium
S	band intensity or band strength, cm^{-2}
S_j	line intensity or line strength, cm^{-2}
t	line structure parameter, $t = \beta/2$
T	kinetic temperature, °K
T_s	surface or ground temperature
T(z)	temperature of atmosphere at altitude z
u	dimensionless coordinate, $u = Spy/A_o$
$\bar{u}$	pressure path length, cm-atm
W_j	equivalent width of jth spectral line
x	optical path at the line center
X	mass of absorbing gas per unit area
β, β_j	line structure parameter, $\beta = 2t$
γ_j	line half-width of jth spectral line
ε	surface emittance
$\varepsilon(X, p, T)$	total emissivity
ε_j, ε_1	line overlapping parameter
ε_ω	spectral emissivity

θ	sun zenith angle
κ_o	absorption coefficient correlation, cm^{-1}
κ_ω	equilibrium spectral absorption coefficient, cm^{-1}
$\kappa_{\omega j}$	absorption coefficient of jth spectral line, cm^{-1}
τ	radiative transmittance
$\overline{\tau}_{j,D}$; $\overline{\tau}_{j,\delta}$	average transmittance of jth line in the spectral interval D or δ.
τ_ω	spectral transmittance
$\tau_{\omega j}$	spectral transmittance of jth line
ω	wave number, cm^{-1}
ω_j	wave number the center of jth line
ω_o	line center of the main line or band center, cm^{-1}

1. INTRODUCTION

The study of radiative transmission in real (non-homogeneous) atmospheres requires a detailed knowledge of the atmospheric constituents that absorb and emit significantly in the spectral range of interest. One of the important quantities required for calculating the atmospheric transmittance is the absorption coefficient of the atmospheric constituents. An accurate model for the spectral absorption coefficient is of vital importance in the correct formulation of the radiative flux equations that are employed for the reduction of data obtained from either direct or remote measurements.

A systematic representation of the absorption by a gas, in the infrared, requires the identification of the major infrared bands and evaluation of the line parameters of these bands. The line parameters depend upon the temperature, pressure, and concentration of the absorbing molecules and, in general, these quantities vary continuously along a non-homogeneous path through the atmosphere. Even though it is quite difficult to reproduce the real non-homogeneous atmosphere in the laboratory, considerable efforts have been expended in obtaining the absorption coefficients of important atmospheric constituents. With the availability of high resolution spectrometers, it is now possible to determine the line positions, intensities, and half widths of spectral lines quite accurately [1-5].[1] As a result, absorption by the strong infrared bands of gases like CO, CO_2, N_2O, H_2O, CH_4, NH_3, and O_3 are known now quite well.

In theoretical calculations of transmittance (or absorptance) of a band, a convenient line or band model, for the variation of the spectral absorption coefficient, is used. High spectral resolution measurements make it necessary to employ line-by-line models

[1] Numbers in brackets indicate references.

for transmittance calculations. If, however, the integrated signals are measured over a relatively wide spectral interval, then one could employ an appropriate band model. The line models usually employed in the study of atmospheric radiation are Lorentz, Doppler, and combined Lorentz-Doppler (Voigt) line profiles. A complete formulation (and comparison) of the transmittance (and absorptance) by these lines, in an infinite and finite spectral interval, is given in [6-8]. The band models available in the literature are the narrow band models (such as, Elsasser, statistical, random-Elsasser, and quasi-random) and the wide band models (such as, coffin, modified box, exponential, and axial). The expressions for wide band absorptance are obtained from the general formulations of the narrow band models. In radiative transfer analyses, the use of band models results in a considerable reduction in computational time. Essential information on various narrow band models is available in [9-16] and on wide band models in [16-20]. The most appropriate model for atmospheric application is the quasi-random narrow band model which is discussed in detail in [12, 14, 15].

The earth's surface with its temperature in the vicinity of 300°K emits like a black body from the near to the far infrared region of the spectrum. The emission in the infrared range (between 2 and 20 microns) is particularly important because most of the minor atmospheric constituents (i.e., CO_2, N_2O, H_2O, CO, CH_4, NH_3, etc.) absorb and emit this spectral region. The upwelling infrared radiation from the earth's atmosphere, therefore, consists of the modulated surface radiation and the radiation from the atmosphere. This radiation carries the spectral signature of all the minor atmospheric constituents amongst which gases such as CO, CH_4 and NH_3 are called the atmospheric pollutants. Ludwig et al. [4] have explored the possibilities of measuring the amount of atmospheric pollutants through remote sensing. An important method of measuring the pollutant concentration by remote sensing is the passive mode (also called the nadir experiment) in which the earth-oriented detector receives the upwelling atmospheric radiation. The near infrared region is particularly suitable for passive mode measurements simply because the radiation in this region is practically

free from the scattering effects. Radiation in the visible and ultra-violet regions is severely affected by the scattering processes which make meaningful passive mode measurements impossible.

The purpose of this study is to review various line and band models and present analysis procedure for calculating the atmospheric transmittance and upwelling radiance. Various expressions for absorption by different line and band models are presented in sections 2 and 3. Theoretical formulations of atmospheric transmittance are given in section 4, where homogeneous path transmittances are calculated for selected infrared bands. The basic equations for calculating the upwelling atmospheric radiance are presented in section 5, where model calculations are made to study the effects of different interfering molecules, water vapor profiles, ground temperatures, and ground emittances on the upwelling radiance.

2. ABSORPTION BY SPECTRAL LINES

In order to describe the infrared absorption characteristics of a radiating molecule it is necessary to consider the variation of the spectral absorption coefficient for a single line. In general, for a single line centered at the wave number ω_j, this is expressed as

$$\kappa_{\omega j} = S_j \, f_j(\omega, \gamma_j) \, , \tag{2.1}$$

where S_j is the intensity of the jth spectral line and is given by

$$S_j = \int_{-\infty}^{\infty} \kappa_{\omega j} \, d(\omega - \omega_j) \, . \tag{2.2}$$

The line intensity may be described in terms of the molecular number density and Einstein coefficients, i.e., it depends upon the transition probabilities between the initial and final states and upon the populations of these states. For a perfect gas it may

be shown that S_j is a function solely of temperature. The quantity $f_j(\omega, \gamma_j)$ is the line shape factor for the jth spectral line. It is a function of the wave number ω and the line half-width γ_j and is normalized on $(\omega - \omega_j)$ such that

$$\int_{-\infty}^{\infty} f_j(\omega - \omega_j)\, d(\omega - \omega_j) = 1 . \qquad (2.3)$$

Several approximate line profiles have been described in the literature. Most commonly used profiles are rectangular, triangular, Lorentz, Doppler, or Voigt (combined Lorentz and Doppler) profiles. The study of line shapes and line broadening is an active research field. For various reviews on the subject, references should be made to [13, 21-29]. Lorentz, Doppler, and Voigt profiles are of special interest in the atmospheric studies and these are discussed in some detail here.

The line profile usually employed for studies of infrared radiative transfer in the earth's atmosphere is the Lorentz pressure broadened line shape for which the shape factor is such that the expression for absorption coefficient is found to be

$$\kappa_{\omega j} = S_j\, f_j(\omega, \gamma_L) = S_j\, \gamma_L / \left\{ \pi \left[(\omega - \omega_j)^2 + \gamma_L^2 \right] \right\} , \qquad (2.4)$$

where γ_L is the Lorentz line half-width. From simple kinetic theory it may be shown that γ_L varies with pressure and temperature according to the relation

$$\gamma_L = \gamma_{Lo} (P/P_o)^m \, (T_o/T)^n , \qquad (2.5)$$

where γ_{Lo} is the line half-width corresponding to a reference temperature T_o and a pressure P_o. The values of m and n depend, in general, on the collision parameters and on the nature of the molecules. A discussion on the variation of γ_L with P and T is given in [22, 30-32]. The value of $m = 1$ and $n = 0.5$ is employed usually for most atmospheric studies.

The maximum absorption coefficient occurs at $\omega = \omega_j$ and is given by the expression

$$\left(\kappa_{\omega j}\right)_{\omega=\omega j} = S_j/\pi\gamma_L \ . \tag{2.6}$$

The variation of κ_ω over a specific wave number range containing n independent lines is given by

$$\kappa_\omega = \sum_{j=1}^{n} \kappa_{\omega j} \ . \tag{2.7}$$

For Lorentzian line profiles, Eq. (2.7) can be expressed as

$$\kappa_\omega = \sum_j \kappa_{\omega j} = \sum_j S_j \ \gamma_{Lj} / \left\{\pi\left[\left(\omega - \omega_j\right)^2 + \gamma_{Lj}^{\ 2}\right]\right\} \ . \tag{2.8}$$

Note that for the Lorentz line profile, γ_L varies linearly with the pressure. Thus, in a spectral interval containing many lines the discrete line structure will be smeared out at sufficiently high pressure.

For Doppler broadened lines, the absorption coefficient is given by the relation [21, 22]

$$\left.\begin{aligned} \kappa_{\omega j} &= S_j \ f_j\left(\omega, \ \gamma_D\right) \ , \\ \text{where} \\ f_j\left(\omega, \ \gamma_D\right) &= \left(1/\gamma_D\right) \ \left(\ell n \ 2/\pi\right)^{1/2} \ \exp\left[-\left(\omega - \omega_j\right)^2 \ \left(\ell n \ 2/\gamma_D^{\ 2}\right)\right] \ , \\ \gamma_D &= \left(\omega_j/c\right) \ \left(2 \ k \ T \ \ell n \ 2/m\right)^{1/2} \ . \end{aligned}\right\} \tag{2.9}$$

In this equation γ_D represents the Doppler half-width, c is the speed of light, κ is the Boltzman constant, and m is the molecular mass. Doppler broadening is associated with the thermal motion of molecules. From Eq. (2.9) it is clear that the Doppler width depends not only on temperature but also on molecular mass and the location of the line center. For certain atmospheric conditions, therefore, the Doppler and Lorentz widths may become equally important for a particular molecule radiating at a

specific frequency. For comparable intensities and half-widths, however, the Doppler line has more absorption near the center and less in the wings than the Lorentz line (Figure 2.1).

For radiative transfer analyses involving gases at low pressures (upper atmospheric conditions) it becomes imperative to incorporate the combined influence of the Lorentz and the Doppler broadening. The shape factor for the combined profile is given by [21, 22].

$$\left.\begin{aligned} \kappa_{\omega j} &= S_j\, f_j(a, v) = \kappa_o\, K(a, v) \ , \\ \text{where} \\ f_j(a, v) &= \left(1/\gamma_D\right)\, (\ell n\ 2/\pi)^{1/2}\, K(a, v) \ , \\ K(a, v) &= (a/\pi) \int_{-\infty}^{\infty} \{\exp(-t^2)/[a^2 + (v - t)^2]\}dt \ , \\ \kappa_o &= \left(S_j/\gamma_D\right)\, (\ell n\ 2/\pi)^{1/2} = \left(S_j/\sqrt{\pi}\right)\, \left(a/\gamma_L\right) \ , \\ v &= \left[\left(\omega - \omega_j\right)/\gamma_D\right]\, (\ell n\ 2)^{1/2} = \left(\omega - \omega_j\right)\, \left(a/\gamma_L\right) \ , \\ a &= \left[\left(\gamma_c + \gamma_N\right)/\gamma_D\right]\, (\ell n\ 2)^{1/2} \ . \end{aligned}\right\} \quad (2.10)$$

The function $K(a, v)$ defined in Eq. (2.10) is called the Voigt function, γ_c is the collisional broadened half-width and γ_N is the natural line half-width. Usually γ_N can be neglected in comparison to γ_c. At very low pressures (upper atmospheric conditions), however, the contributions from γ_N becomes significant. The combined effect of γ_c and γ_N is frequently represented by γ_L, and the parameter a is interpreted as the ratio of the Lorentz and Doppler half-widths. As the pressure becomes small, γ_L approaches zero and Eq. (2.10) reduces to the absorption coefficient for the Doppler broadened lines which may now be expressed as

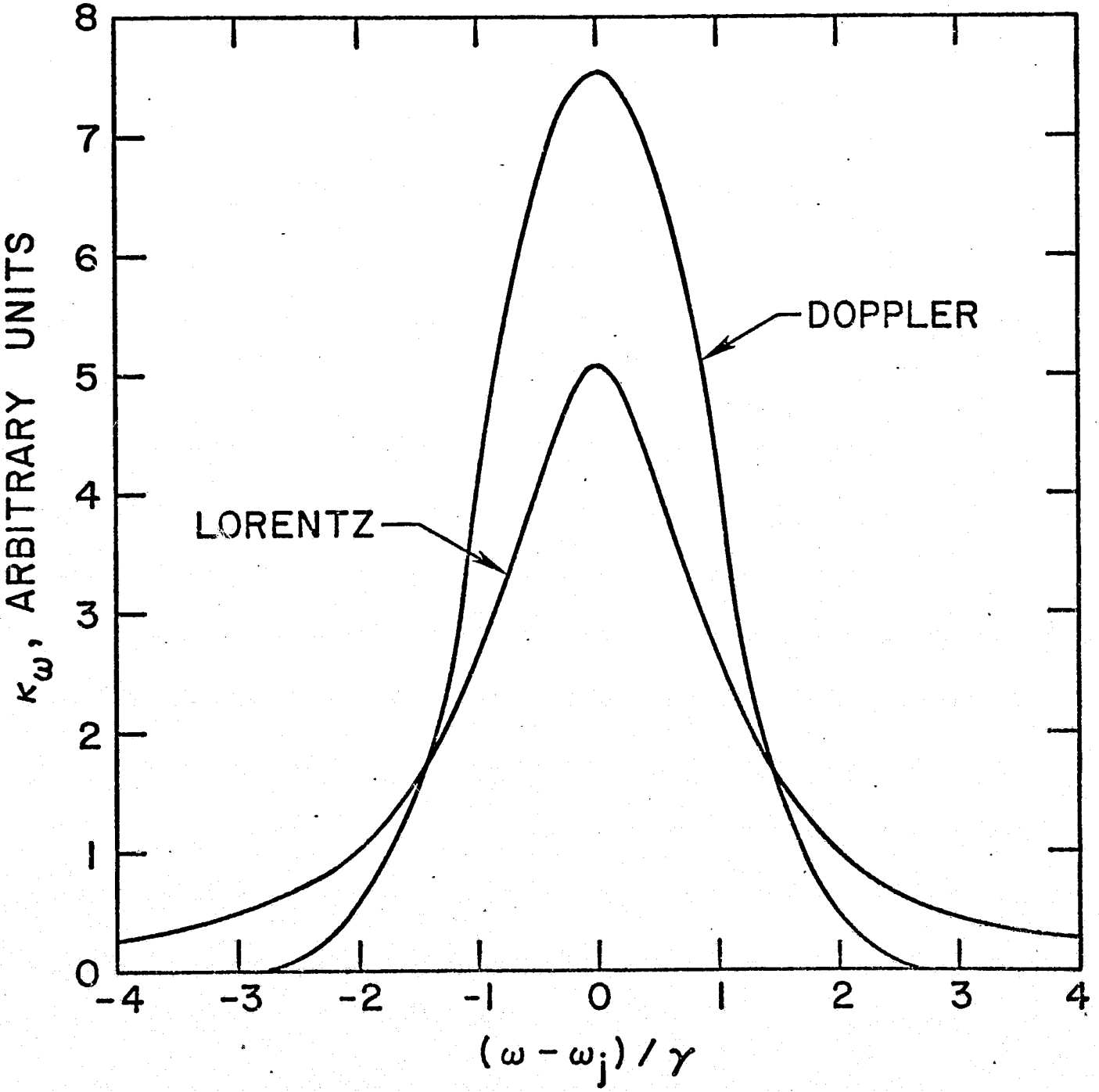

Fig. 2.1 Comparison of Lorentz and Doppler line profiles having equal line intensities.

$$\kappa_{\omega j} = \kappa_o \exp(-v^2) \ . \qquad (2.11)$$

On the other hand, for large pressures, the quantity (γ_L/γ_D) becomes large and Eq. (2.10) reduces to the Lorentzian case, Eq. (2.4). In other words, the Voigt profile assumes the Lorentzian shape in the limit of large v and reduces to the Doppler profile for small a. The Voigt function is referred to as the reduced absorption coefficient with κ_o representing its dimensional constant. The origin and properties of the Voigt function and methods of computing it are reviewed in some detail in [29] where it is shown that $K(a, v)$ is the real part of the complex error function.

Several alternate and approximate forms of the Voigt function, and a number of tabulations of these forms, are available in [21, 22, 29, 33-47]. With the aid of computer programs developed by Hummer [41-43], Young [45, 46], Armstrong [47], Chiarella and Reichel [48], and Gautschi [49, 50], it is now possible to calculate the Voigt function (for an extended range of parameters) to an accuracy of better than six significant figures.

A simple closed form approximation to the Voigt profile that is valid over a useful range of parameters is given, in terms of the present nomenclature, by [35, 39, 51]

$$\kappa_{\omega j}/\kappa_{\omega o} = \left[1 - (\gamma_L/\gamma_V)\right] \exp\left\{-11.088\left[(\omega - \omega_j)/\gamma_V\right]^2\right\} + (\gamma_L/\gamma_V)/\left\{1 + 16\left[(\omega - \omega_j)/\gamma_V\right]^2\right\} \ , \qquad (2.12a)$$

where Voigt half-width is expressed in terms of γ_L and γ_D as

$$\gamma_V = (\gamma_L/2) + \left[(\gamma_L^2/4) + \gamma_D^2\right]^{1/2} \ , \qquad (2.12b)$$

and

$$\kappa_{\omega o} = S_j/\left\{\gamma_V\left[1.065 + 0.447(\gamma_L/\gamma_V) + 0.058(\gamma_L/\gamma_V)^2\right]\right\} \ . \qquad (2.12c)$$

This form is very convenient for numerical computation and it

matches the Voigt profile within 5 percent under worst conditions. Generally the error is within 3 percent, with maximum errors occurring near zero pressures. A somewhat better approximation for the Voigt function is suggested by Kielkopf [52].

The radiative transmittance at a single wave number is given by the relation

$$\tau_{\omega j} = \exp\left(- \int_0^X \kappa_{\omega j} \, dX\right) , \tag{2.13}$$

where $X = \int_0^{\ell} \rho_a \, d\ell$ is the mass of the absorbing gas per unit area, $\kappa_{\omega j}$ is the mass absorption coefficient for the jth spectral line, ℓ is the length measured along the direction of the path which makes an angle θ with the vertical, and ρ_a is the density of the absorbing gas. For a homogeneous path, Eq. (2.13) becomes

$$\tau_{\omega j} = \exp\left(-\kappa_{\omega j} \, X\right) \tag{2.14}$$

The total absorption of a single line, in an infinite spectral interval, is given by

$$A_j = \int_{-\infty}^{\infty} \left(1 - \tau_{\omega j}\right) \, d\left(\omega - \omega_j\right) , \tag{2.15}$$

where ω_j represents the wave number at the line center of the jth spectral line. For a homogeneous path, this can be expressed as

$$A_j = \int_{-\infty}^{\infty} \left[1 - \exp\left(-\kappa_{\omega j} \, X\right)\right] \, d\left(\omega - \omega_j\right) . \tag{2.16}$$

For small values of the quantity $\left(\kappa_{\omega j} \, X\right)$, Eq. (2.16) reduces to an important limiting form which is independent of any spectral model used for $\kappa_{\omega j}$. This is the conventional optically thin (or linear) limit in radiative transfer. This limit is obtained by expanding the exponential in Eq. (2.16) and retaining only the

first two terms in the series such that

$$A_j = X \int_{-\infty}^{\infty} \kappa_{\omega j} \, d(\omega - \omega_j) = X \, S_j \ . \qquad (2.17)$$

Another limit, which does depend upon the particular model employed for $\kappa_{\omega j}$, is the square-root limit or the strong line approximation for which the total absorption occurs in the vicinity of the line center. To find expressions for absorptance in this limit, it is required that $(\kappa_{\omega j} \, x) >> 1$ for $\omega = \omega_j$.

The average absorption $\bar{A}$ of a single line, which is a member of a group of lines, is given by

$$\bar{A}_j = \frac{1}{d} \int_{-\infty}^{\infty} \left[1 - \exp(-\kappa_{\omega j} \, X)\right] d(\omega - \omega_j) \ , \qquad (2.18)$$

where d is the average spacing between lines. This is related to the so-called *equivalent width* of a line, $W_j(X)$, by $W_j(X) = \bar{A}_j d$, where the expression for $W_j(X)$ is exactly the same as given by Eq. (2.16). Thus,

$$W_j(X) = A_j(X) = \int_{-\infty}^{\infty} A_j(\kappa_{\omega j} \, X) \, d(\omega - \omega_j) = \bar{A}_j d \ . \qquad (2.19)$$

The equivalent width is interpreted as the width of a rectangular line (whose center is totally absorbed) having the same absorption area as that of the actual line.

The mean transmittance of a single line, in a finite wave number interval $D = 2\delta$, may be expressed as

$$\bar{\tau}_{j,D} = \frac{1}{2\delta} \int_{-\delta}^{+\delta} \exp(-\kappa_{\omega j} \, X) \, d(\omega - \omega_j) \ , \qquad (2.20)$$

where δ is the wave number interval from the center of the line. The mean absorption over this interval, therefore, becomes

$$\bar{A}_{j,D} = 1 - \bar{\tau}_{j,D} = \frac{1}{\delta}\int_0^{\delta} \left[1 - \exp\left(-\kappa_{\omega j}\, X\right)\right] d\left(\omega - \omega_j\right) . \qquad (2.21)$$

Note that $\bar{\tau}_{j,D}$ and $\bar{A}_{j,D}$ are in nondimensional form.

2.1. Radiative Transmittance by Spectral Lines

For a homogeneous atmosphere, the radiative transmittance of a line with Lorentz profile is obtained by combining Eqs. (2.4) and (2.14) as

$$\tau_{\omega j} = \tau_L(\omega) = \exp[-2x/(y^2 + 1)] = \tau_L(x,y) , \qquad (2.22)$$

where

$$x = S_j\, X/2\pi\gamma_L , \quad y = \left(\omega - \omega_j\right)/\gamma_L .$$

It should be noted that, for large y (i.e., away from the line center), Eq. (2.22) approaches to unity for all x while for small x it approaches to unity for all y.

The transmittance of a Doppler broadened line is obtained by combining Eqs. (2.11) and (2.14) as

$$\tau_{\omega j} = \tau_D(\omega) = \exp\left[-x_D \exp(-v^2)\right] = \tau_D\left(v,\, x_D\right) , \qquad (2.23a)$$

where

$$x_D = \kappa_o\, X = \left[\left(S_j/\gamma_D\right)\left(\ell n\ 2/\pi\right)^{1/2}\right] X$$

represents the optical path at the line center. For large v (i.e., away from the line center), the transmittance approaches a value of unity while in the vicinity of the line center, it may be expressed by

$$\tau_D(\omega) = \exp\left(-x_D\right) . \qquad (2.23b)$$

As in the case of the Lorentz line profile, $\tau_D(\omega)$ also approaches a value of unity in the linear limit.

The transmittance of a combined Lorentz-Doppler (Voigt) line profile is obtained by combining Eqs. (2.10) and (2.14) as

$$\tau_{\omega j} = \tau_V(\omega) = \exp\left[-x_D\ K(a,\ v)\right] = \tau_V(a,\ v,\ x_D)\ . \qquad (2.24)$$

Note that the transmittance of a Voigt line profile also approaches to unity in the linear limit. It can be shown that Eq. (2.24) reduces to the Lorentzian case for large a and to the Doppler case in the limit of small a.

The transmittance by the Lorentz line profile, Eq. (2.22), can be expressed in terms of the quantities x_D, a, and v as

$$\tau_L(\omega) = \exp\left\{-x_D\left[(a/\sqrt{\pi})/(v^2 + a^2)\right]\right\} = \tau_L\left(a,\ v,\ x_D\right)\ . \qquad (2.25)$$

For transmittance at the line center, this can be written as

$$\tau_L\left(a,\ x_D\right) = \exp\left(-x_D/a\sqrt{\pi}\right)\ . \qquad (2.26)$$

Equation (2.25) is a convenient expression for comparing the results with the transmittance of the Doppler and Voigt line profiles.

The transmittance of the three line profiles (Lorentz, Doppler, and Voigt) at the line center are illustrated in Figure (2.2) for various values of the parameter a. As would be expected, for $a = 0 \rightarrow 0.1$, the Voigt line transmittance is analogous to that given by the Doppler line profile. For values of $a \geq 5$, the transmittance by Lorentz and Voigt lines are identical for all path lengths.

Comparisons of the transmittance by the three line profiles are also shown in Figures (2.3) and (2.4) for $x_D = 10$, and for values of a equal to 0.1 and 1 respectively. It should again be noted that at $a = 0.1$, the transmittance of a Voigt line can be approximated quite accurately by the transmittance of a Doppler line. At $a = 1$, however, the transmittance by the Lorentz line provides a better approximation for the Voigt line transmittance.

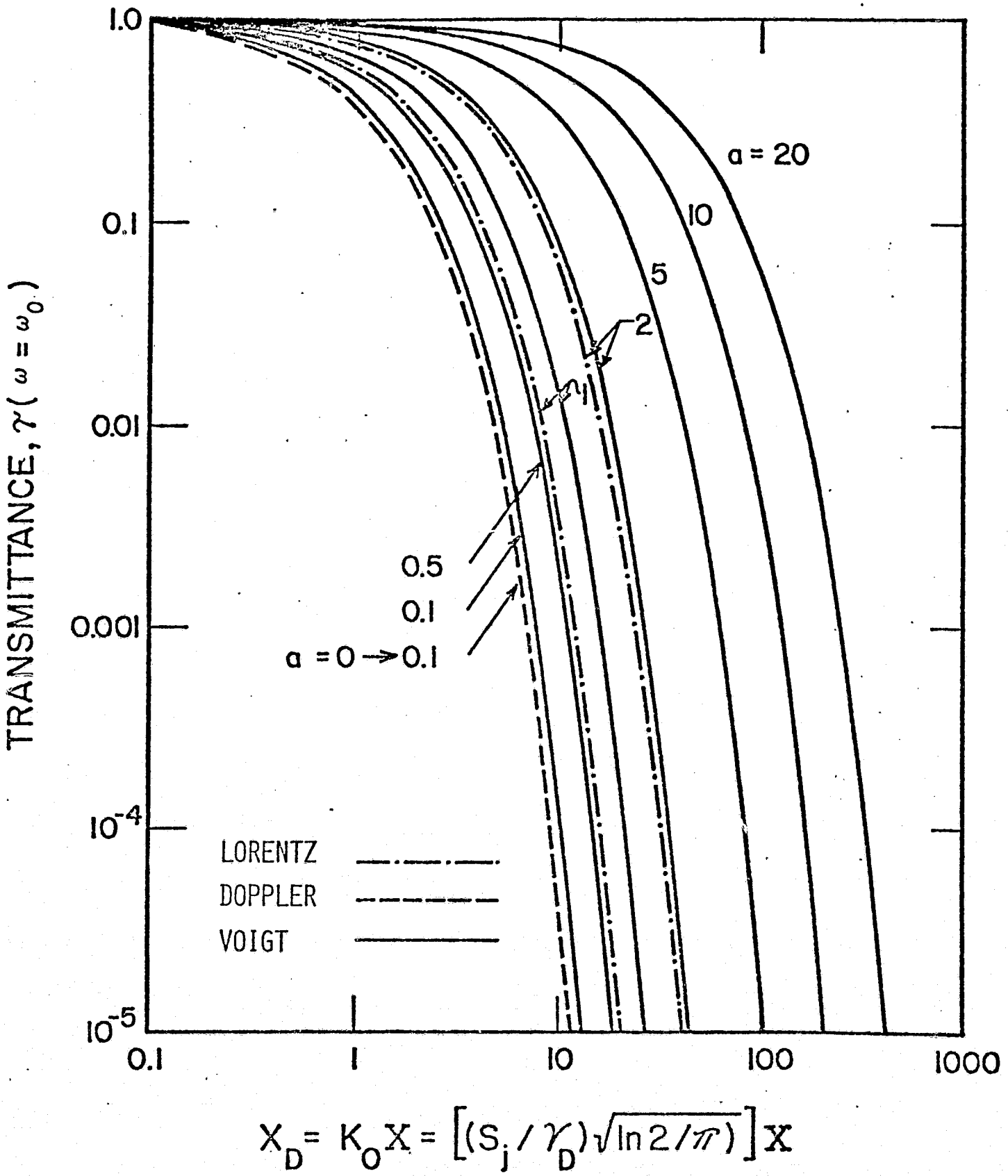

Fig. 2.2 Transmittance of Lorentz, Doppler, and Voigt lines evaluated at the line center.

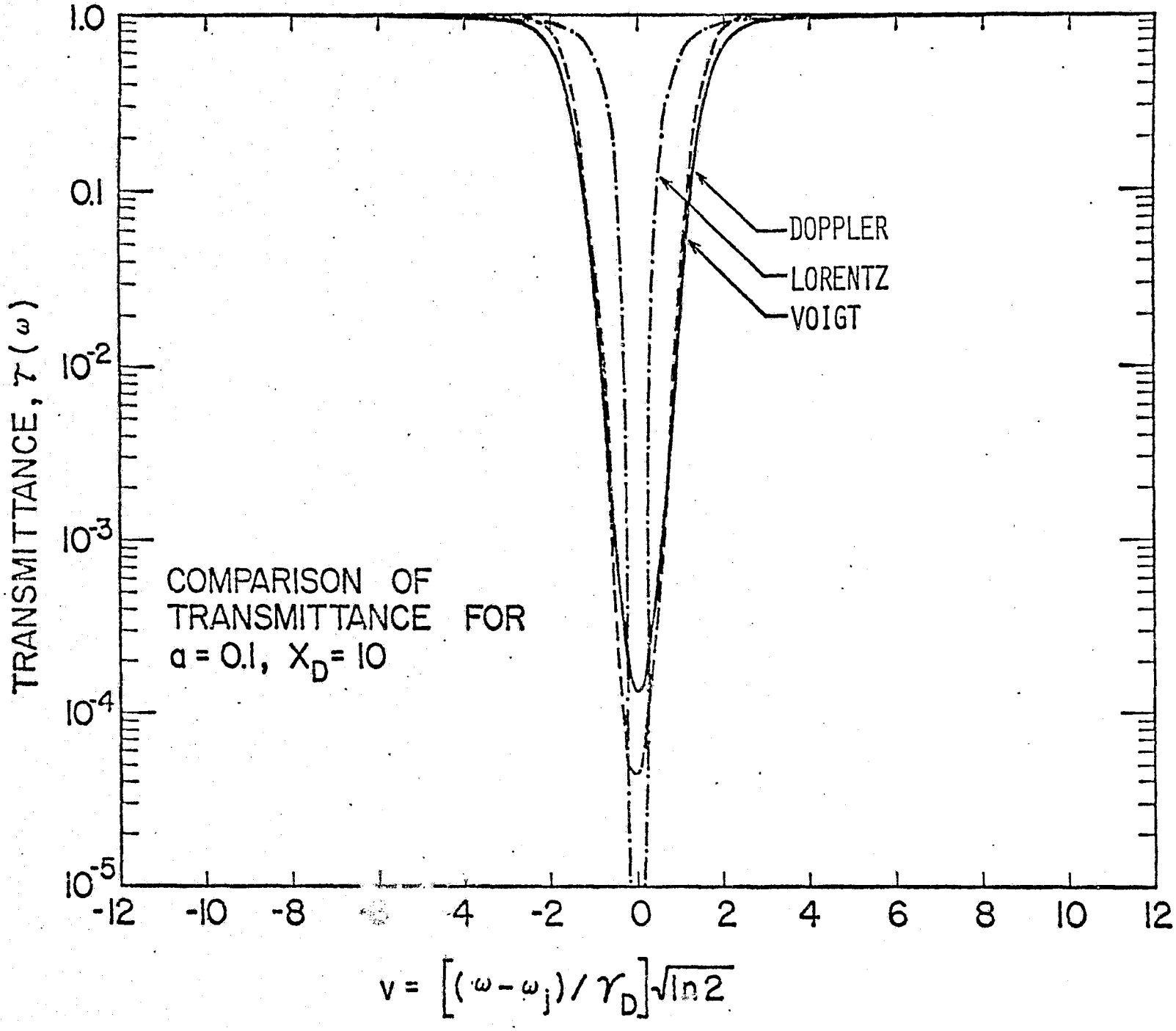

Fig. 2.3 Comparison of transmittance for a = 0.1 and x_D = 10.

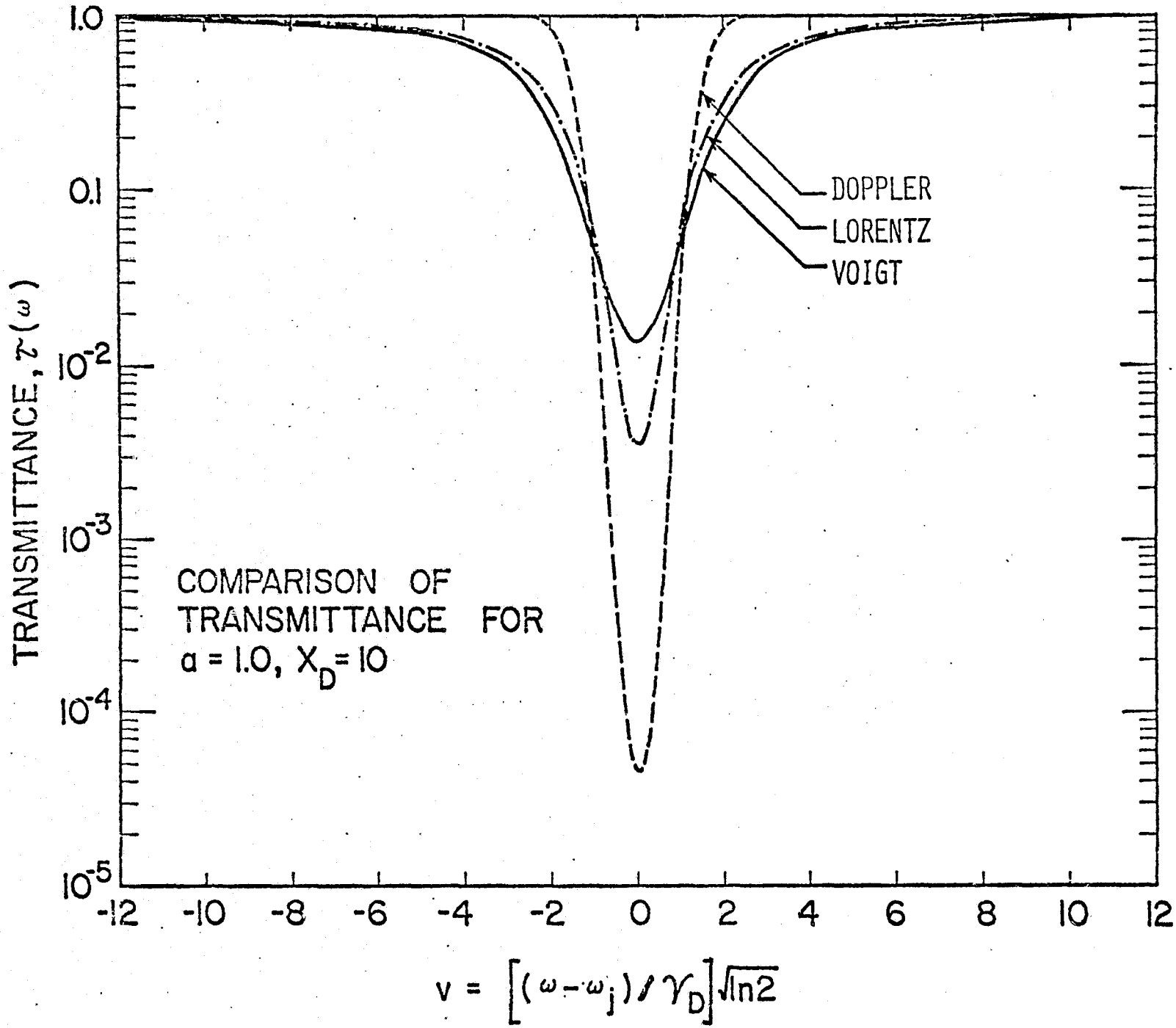

Fig. 2.4 Comparison of transmittance for a = 1.0 and x_D = 10

2.2. Absorption of an Isolated Spectral Line in an Infinite Spectral Interval

For homogeneous atmospheric path, the absorption of an isolated spectral line of Lorentz shape (in an infinite spectral interval), A_L, may be obtained by combining Eqs. (2.4) and (2.16) as

$$A_L = 2\gamma_L \int_0^\infty \{1 - \exp[-2x/(y^2 + 1)]\}\, dy , \qquad (2.27)$$

where x and y are defined in Eq. (2.22). An exact solution of this equation is found in terms of Ladenberg-Reiche function, $L(x)$, as [9, 13]

$$A_L/2\pi\gamma_L = L(x) = x \cdot \exp(-x)\, [I_0(x) + I_1(x)] , \qquad (2.28a)$$

where I_0 and I_1 are the Bessel functions of imaginary arguments. By multiplying Eq. (2.4) by the mass of the absorbing gas, X, it can be shown that the quantity x represents one-half the optical path at the line center. In the linear limit (small x), Eq. (2.16) reduces to

$$A_L = 2\pi\gamma_L x = S_j X , \qquad (2.28b)$$

while in the square-root limit (large x), it becomes

$$A_L = 2\gamma_L (2\pi x)^{1/2} = 2\left(S_j\, \gamma_L\, X\right)^{1/2} . \qquad (2.28c)$$

For further discussions on absorption by the Lorentz lines, one should refer to [6-8, 10, 13, 22]. For these lines, absorption calculations for non-isothermal paths have been carried out by Simmons [53], Yamamoto and Aida [54], and Cogley [55].

Several approximate solutions of Eq. (2.27) are suggested in the literature. These are,

$$A_L/2\pi\gamma_L = (2x/\pi)^{1/2} \left\{1 - \exp\left[-(\pi x/2)^{1/2}\right]\right\} , \quad \text{(TIEN [18, 56])} \qquad (2.29a)$$

$$A_L/2\pi\gamma_L = \{(2x/\pi)\ [1 - \exp(-\pi x/2)]\}^{1/2} , \qquad \text{(VARANASI [18,57])} \qquad (2.29b)$$

$$A_L/2\pi\gamma_L = 1/[1 + (\pi x/2)]^{1/2} , \qquad \text{(RODGERS [18])} \qquad (2.29c)$$

$$A_L/2\pi\gamma_L = x/[1 + (\pi x/2)]^{1/2} , \qquad \text{(GOLDMAN [58])} \qquad (2.29d)$$

$$A_L/2\pi\gamma_L = x/[1 + (\pi x/2)]^{1/2\alpha} \qquad \text{(GOLDMAN [58])} \qquad (2.29e)$$

The value of α in Eq. (2.29e) range between $1 < \alpha < 3/2$. For $\alpha = 1$, Eq. (2.29e) reduces to Eq. (2.29d). A value of $\alpha = 5/4$ is recommended by Goldman [58] for better approximation. Each equation in Eqs. (2.29) reduces to the correct asymptotic limits. Over the entire range of x, however, the approximations listed in Eqs. (2.29) agree with the exact solution, Eq. (2.28a), by a varying degree of accuracy. As discussed by Goldman, a maximum error of about 17% occurs in using Eq. (2.29a) while less than 8% errors are encountered in using Eqs. (2.29b) and (2.29d). Equation (2.29c) agrees with the exact solution within 3%, and for a value of $\alpha = 5/4$, Eq. (2.29e) gives accurate results within 1% over the entire range of x. In calculating the total absorptance over a band pass, by employing the line-by-line model, a tremendous amount of computational time is saved if an appropriate form of Eq. (2.29) is used.

The absorption of a Doppler broadened line, A_D, is obtained by combining Eqs. (2.15) and (2.23a) as

$$A_D^* = A_D/A_n = \int_0^\infty \left\{1 - \exp\left[-x_D \exp(-v^2)\right]\right\} dv , \qquad (2.30a)$$

where

$$A_n = 2\gamma_D/(\ell n\ 2)^{1/2} .$$

As $x_D \to 0$ (linear limit), Eq. (2.30a) reduces to

$$A_D^* = (\sqrt{\pi}/2)\ x_D \quad \text{or} \quad A_D = S_j\ \mathbf{X} , \qquad (2.30b)$$

and in the limit of large x_D , it yields

$$A_D^* = \left(\ell n\ x_D\right)^{1/2} . \tag{2.30c}$$

Equation (2.30b) is identical to the result for the Lorentz profile in the linear limit (Eq. 2.28b). Since the linear limit can be obtained from Eq. (2.15), independent of line shape, the absorption by any line profile should reduce to the same expression in this limit. From Eq. (2.30c), it should be noted that, in the limit of large x_D , the absorption increases very slowly with the amount of absorbing gas. For further discussions on absorption by the Doppler lines, references should be made to [6-8, 10, 13, 22, 59].

For conditions where both the Doppler and the Lorentz broadenings are important, the total absorption, A_V , is obtained by combining Eqs. (2.15) and (2.24) as

$$A_V^*\left(x_D, a\right) = A_V/A_n = \int_0^\infty \left\{1 - \exp\left[-x_D K(a, v)\right]\right\} dv \equiv A_{VE}^*\left(x_D, a\right) . \tag{2.31}$$

It can easily be shown that Eq. (2.31) reduces to the Lorentzian case for large values of a and to the Doppler case in the limit of small a.

By employing the numerical procedure described by Young [45, 46], Eq. (2.31) was solved for a range of parameter a , and the results are illustrated in Figure 2.5. Similar results were also obtained by Jansson and Korb [60], who employed a somewhat modified version of Armstrong's [47] computer program. As would be expected, for $a = 0$, the results correspond to the case of a pure Doppler profile while for $a > 0$, the results correspond to the case of a pure Doppler profile while for $a > 10$, they correspond to the Lorentzian shape. Kyle [61] has given results for Voigt line profiles in an isothermal atmosphere with an exponentially decreasing pressure.

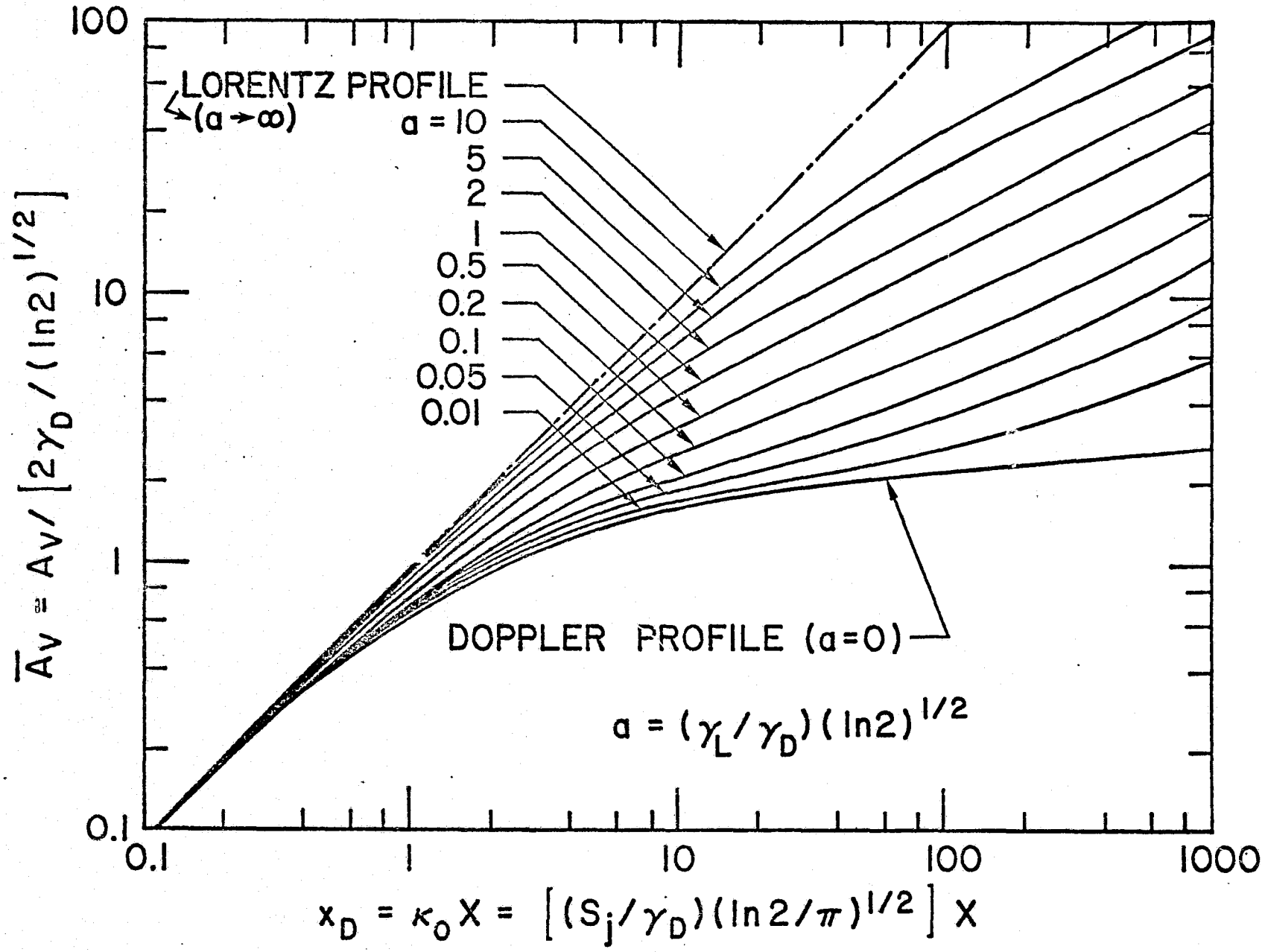

Fig. 2.5 Absorption of a single line of Voigt shape.

The errors, in the integrated line absorption, encountered in using the Lorentz shape to approximate the Voigt profile, are illustrated in Figure 2.6, for a range of the parameter a. The nondimensional form of the integrated absorption for Lorentz profile, A_L^*, is obtained by dividing Eq. (2.28) by A_n and by noting that $x = x_D/(2a\sqrt{\pi})$. As would be expected, maximum errors occur for intermediate path lengths and for lower values of a. The errors, however, are not significant in the two limiting cases of small and large path lengths. As discussed earlier, for small path lengths (linear limit), the line absorption is independent of the line shapes. In the limit of large path lengths, however, the central portion of the line becomes opaque and absorption occurs only in the wing regions. Since the Voigt profile is essentially Lorentzian in the line wings, the error encountered in the large path length limit becomes insignificant.

The errors resulting from using the Doppler line profile to approximate the absorption by the Voigt line profile are illustrated in Figure 2.6 by the solid lines. Since $a = 0$ corresponds to the case of pure Doppler absorption, the errors are expected to be higher for larger values of a. Maximum errors, in this case, are found in the large path length limit. This is because, in this limit, the absorption occurs essentially in the line wings and the Voigt profile in the wing regions is Lorentzian rather than of Doppler shape.

It should be emphasized that for cases of intermediate path lengths and for moderate values of a $(0.1 < a < 10)$ the use of the Voigt profile becomes almost essential. This situation corresponds to the radiative transmittance in the earth's troposphere and lower stratosphere. Consequently, for radiative modeling of the lower atmosphere, consideration must be given to the application of combined line profiles.

In Figures 2.7 and 2.8, comparisons of results for all three line profiles (Lorentz, Doppler, and Voigt) are made for $a = 0.01$ and 0.1. Comparison of results for other values of a is available in [6, 7, 62]. Figures 2.7 and 2.8 clearly illustrate

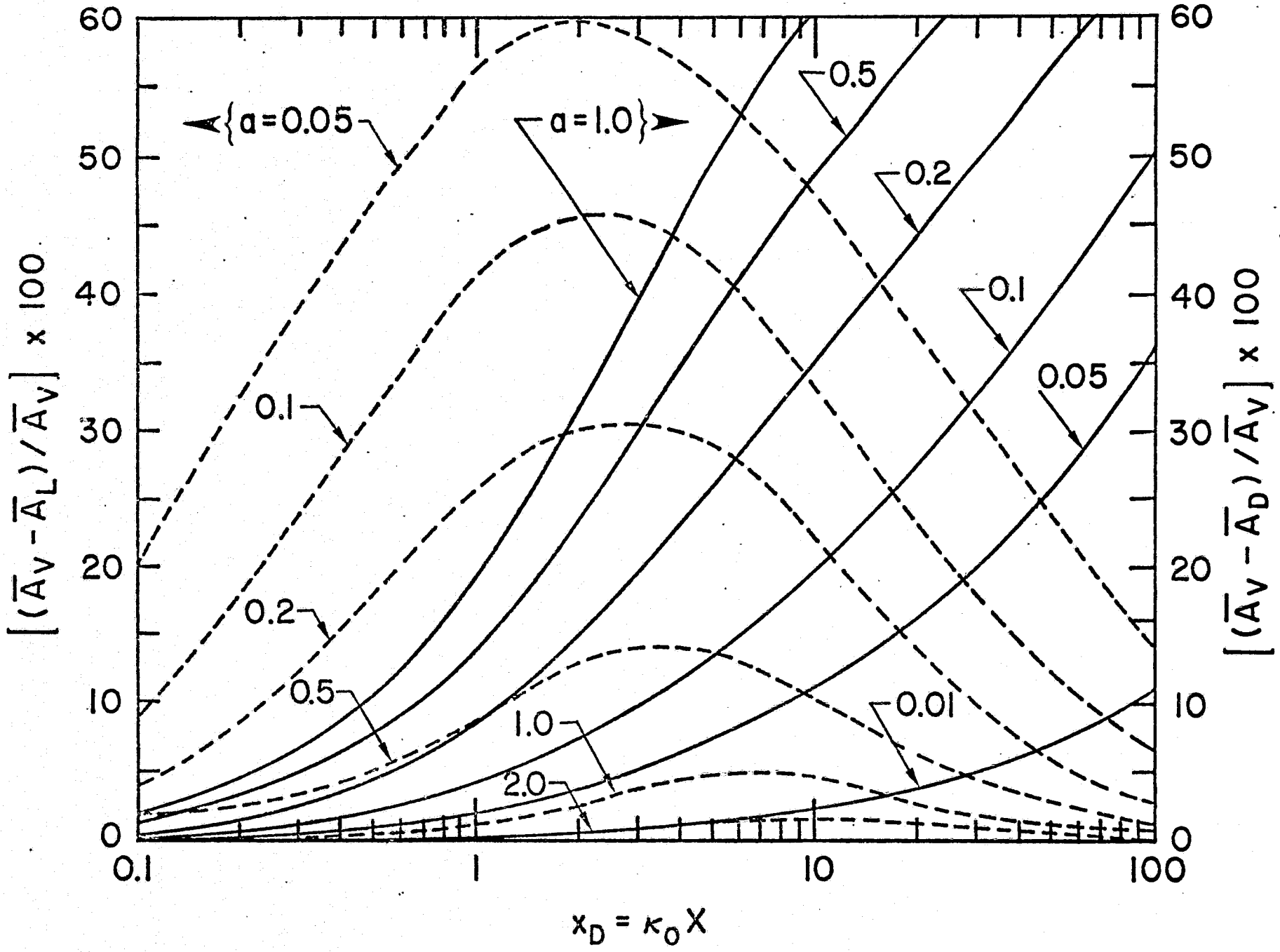

Fig. 2.6 Errors in the absorption by using the Lorentz and Doppler line shapes instead of the Voigt line profile.

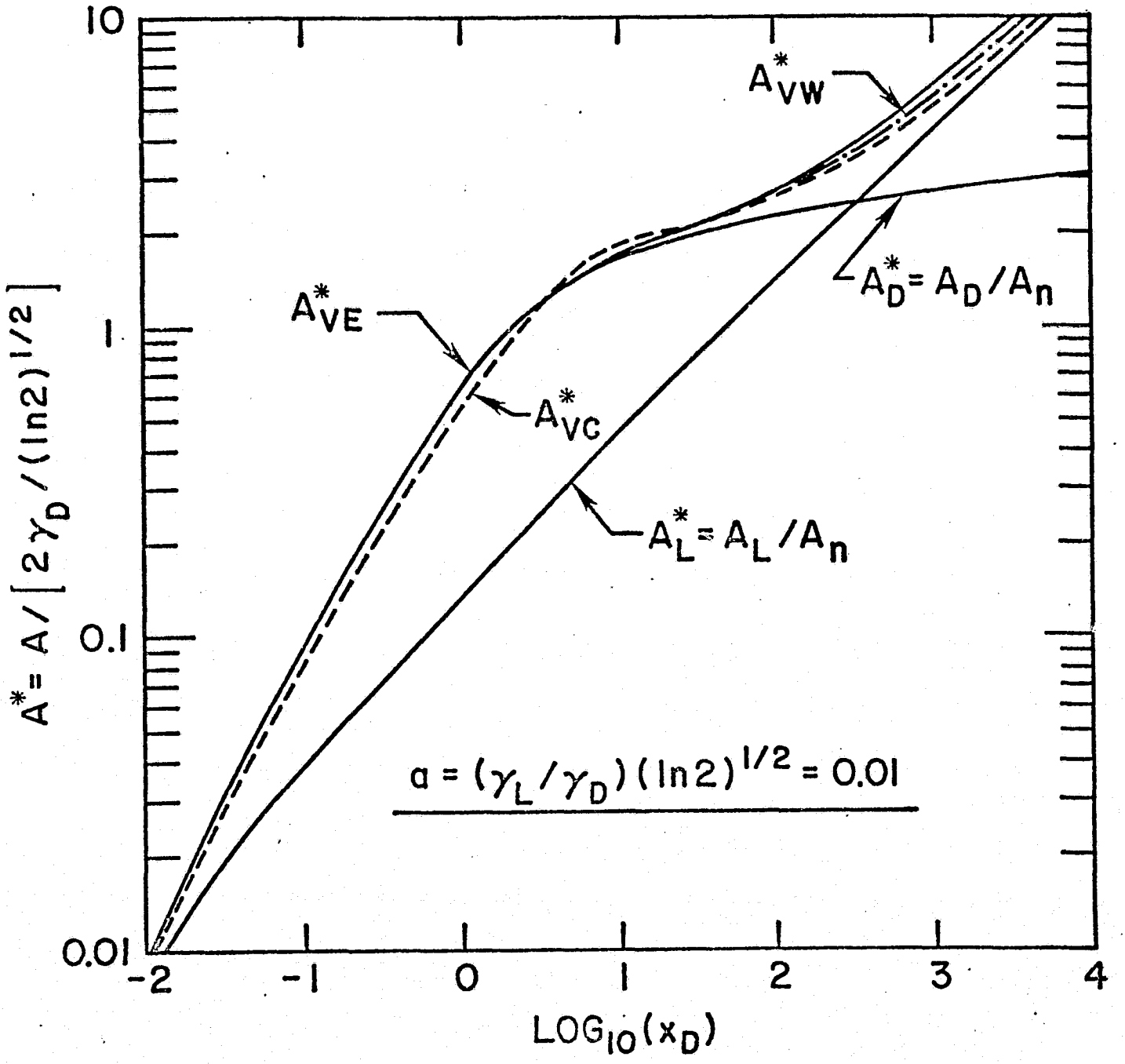

Fig. 2.7 Comparison of line absorption for a = 0.01.

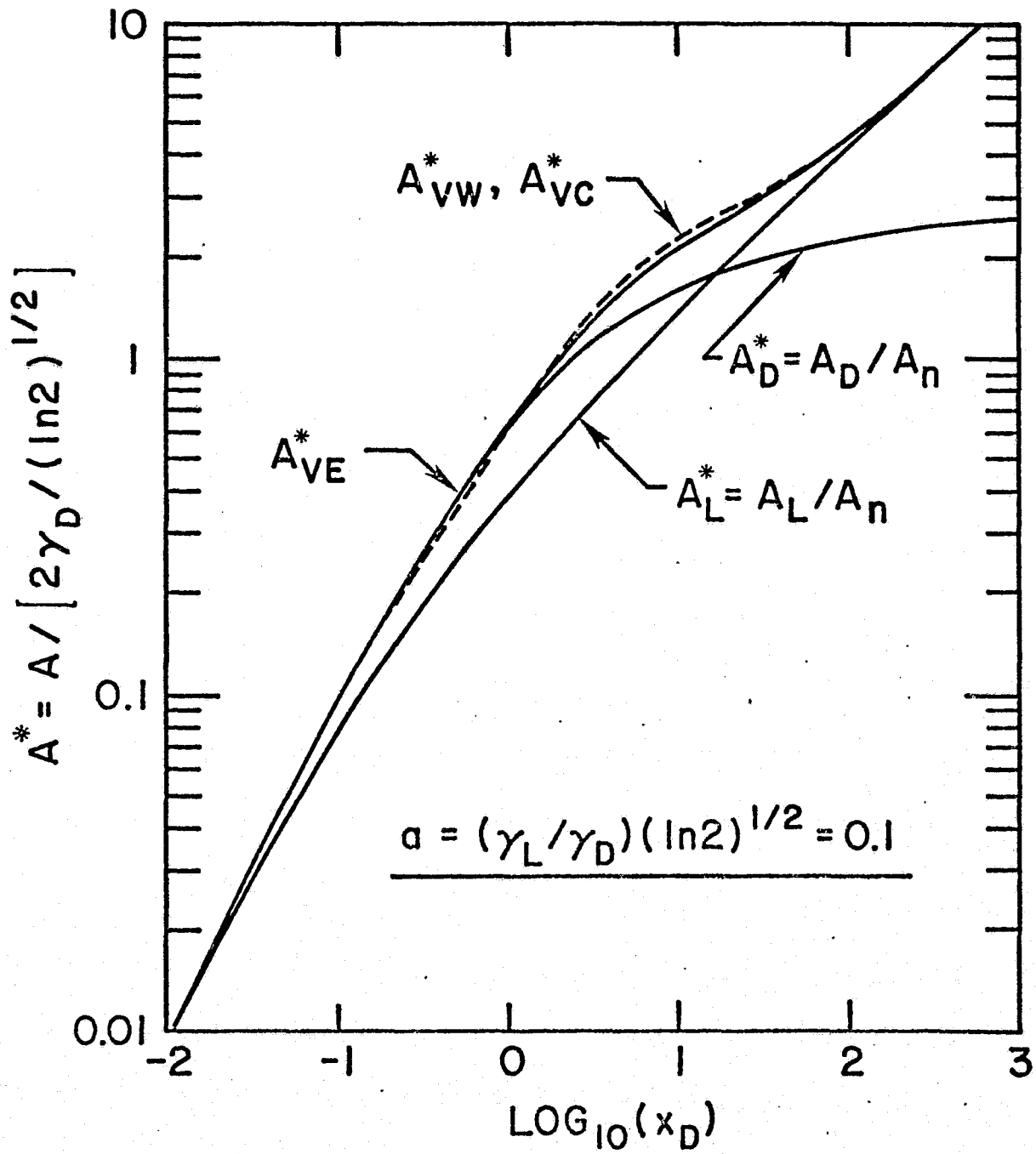

Fig. 2.8 Comparison of line absorption for a = 0.1.

the range of validity of the absorption by the three line profiles. The curves for A_L^* and A_D^* intersect at some point, the location of which increases with decreasing a. For $a > 2$, A_L^* and A_V^* (or A_{VE}^*) curves become identical for all path lengths.

In atmospheric problems involving conduction, convection and radiation, one ends up with an integro-differential form of the energy equation. If use of the Voigt line profile is made in formulating the expression for absorptance, then the divergence of the radiative flux in the energy equation will involve an equation with triple integrals even for the simple case of energy transfer between plane-parallel atmosphere. The number of integrals appearing in the governing equations remain the same even if one is only concerned with the problem of purely radiative equilibrium. In order to reduce the mathematical complexities and save computational time, it often becomes necessary to express the absorptance of the Voigt line profile by fairly accurate approximate forms. A few such forms have been suggested in the literature.

Curtis [63] has suggested a simple form in terms of the absorptance by Lorentz and Doppler lines as

$$A_V \simeq A_L + A_D - A_L A_D/A_S \ , \tag{2.32}$$

where $A_S = S_j X$ is the absorptance in the linear limit and is independent of any line shape. This is a convenient form for mathematical operations (especially differentiation) and it reduces to the correct limiting forms. According to Gille and Ellingson [64], however, this form overestimates the absorption (as compared with the exact solution of Eq. (2.31)), especially when $A_L \simeq A_D$, with errors up to fifty percent. Rodgers and Williams [65] have suggested a modified form of the Curtis approximation as

$$A_V = \left[A_L^2 + A_D^2 - \left(A_L A_D/A_S\right)^2\right]^{1/2} \ . \tag{2.33}$$

This also reduces to the correct limiting forms, is easily differentiable, and is accurate within eight percent. In final calculation of A_V, however, approximate forms of A_L and A_D (expressed

in terms of series coefficients) are employed which makes this form somewhat cumbersome. If the approximate relation suggested by Whiting, Eq. (2.12), is employed, then the absorption of a Voigt line can be expressed as [6]

$$A^*_{VW} = A_{VW}/A_n = \int_0^\infty \left\{1 - \exp\left[-x_D\, W(a, v)\right]\right\} dv \,,$$

where

$$\left.\begin{aligned} W(a, v)/[\ell n\ 2/\sqrt{\pi})\ F(a)] &= \left(1 - \gamma_{LV}\right) \exp\left\{-11.088\left[(v/a)\ \gamma_{LV}{}^2\right]\right\} \\ &\quad + \gamma_{LV}/\left\{1 + 16\left[(v/a)\ \gamma_{LV}\right]^2\right\} \,, \\ F(a) &= \left[a\left(1.065/\gamma_{LV} + 0.447 + 0.058\gamma_{LV}\right)\right]^{-1} \,, \\ \gamma_{LV} &= \gamma_L/\gamma_V = \left\{0.5 + [0.25 + \ell n\ 2/a^2)]^{1/2}\right\}^{-1} \,. \end{aligned}\right\} \quad (2.34)$$

The results of this equation are found to be accurate within five percent [6]. Use of this equation has been made in radiative transfer models for detection of atmospheric pollutants [4, 5]. The drawback of this form is that it involves integration over one variable and its use in the final form of the energy equation requires a considerably long computational time. Another accurate approximation to the absorption by a Voigt line profile can be obtained by employing the expression for Voigt function suggested by Kielkopf [52]. However, as with the Whiting's approximation, this form will also involve integration over one variable (while calculating the total line absorption) and consequently would require long computational time.

While Eqs. (2.33) and (2.34) provide quite accurate approximations to the integrated absorption of a Voigt line profile, a relatively simple (and equally accurate) form can be obtained by employing the approximate formulations for A_L (as given by Goldman [58]) and A_D (cf Tiwari [6], Penner [22]) into Eq. (2.33) to yield

$$
\left.
\begin{aligned}
A^*_{VC} &= (\sqrt{\pi}/2)\left\{F(L)\left[1 - \exp\left(-\sqrt{x_D}\right) + x_D^{\,2}\exp\left(-\sqrt{x}\right)\right]\right\}^{1/2}, \\
&\quad 0.1 \le x_D \le 20 \\
A^*_{VC} &= \left\{(\pi/4)\,F(L) + \ell n\, x_D\left[1 - F(L)/x_D^{\,2}\right]\right\}^{1/2}, \\
&\quad x_D \ge 20
\end{aligned}
\right\} \quad (2.35)
$$

where

$$
F(L) = x_D^{\,2}\Big/\left[1 + \left(x_D\sqrt{\pi}/4a\right)^{\alpha}\right]^{1/\alpha}, \quad \alpha = 5/4 .
$$

This equation possesses the mathematical simplicity offered by Eqs. (2.32) and (2.33), and reduces to the correct limiting forms.

The solutions of Eq. (2.35) are compared with the exact solution, A^*_{VE}, in Figures (2.7) and (2.8) for values of the parameter a equal to 0.01 and 0.1. The solutions of Whiting's approximation are also illustrated in these figures. It should be noted that while the agreement between the results is not very good for $a = 0.01$, it is excellent for $a = 0.1$. Depending on the nature of a particular problem, use of the correlation, as given by Eq. (2.35), in radiative flux equations could result in significant saving of computational time.

2.3. Absorption of a Spectral Line in a Finite Spectral Interval

Expressions for absorption by nonoverlapping spectral lines, in finite spectral intervals, are important in obtaining meaningful formulations for narrow and wide band models. For brevity, attention is directed only to the Lorentzian line profiles in the subsequent formulations. The procedure, however, can easily be extended to obtain formulations for other line profiles.

The average transmission of a Lorentz line, in a finite spectral interval may be obtained by combining Eqs. (2.4) and (2.20) as

$$\bar{\tau}_{L,\delta} = \frac{1}{\delta}\int_0^{\delta} \exp\left\{-\left(S_j X\ \gamma_L\right)/\pi\left[\left(\omega - \omega_j\right)^2 + \gamma_L{}^2\right]\right\} d\left(\omega - \omega_j\right) . \qquad (2.36)$$

By defining nondimensional quantities

$$\eta = \gamma_L/\delta \ , \quad \xi = \left(\omega - \omega_j\right)/\delta \ ,$$

Eq. (2.36) can be transformed into

$$\bar{\tau}_{L,\delta} = \int_0^1 \exp\{-2x/[(\xi/\eta)^2 + 1]\}\, d\xi . \qquad (2.37)$$

The relation for the mean absorption over the interval can, in turn, be expressed by

$$\bar{A}_{L\delta} = 1 - \bar{\tau}_{L,\delta} = \int_0^1 \left(1 - \exp\{-2x/[1 + (\xi/\eta)^2]\}\right) d\xi \ , \qquad (2.38)$$

It is important to note that the parameter η in Eqs. (2.37) and (2.38) represents the ratio of the line half-width and the wave number interval from the line center. If required, the limiting forms of Eq. (2.38) can easily be obtained.

Upon introducing a new variable

$$\omega - \omega_j = \gamma_L(1 + \cos t)^{1/2}/(1 + 2\eta^2 - \cos t)^{1/2} \ , \qquad (2.39a)$$

and a new dimensionless path length

$$\bar{x} = S_j X/2\pi\ \gamma_L\ (1 + \eta^2) \ , \qquad (2.39b)$$

Eq. (2.36) is transformed to give

$$\bar{\tau}_{L,\delta} = \eta(1 + \eta^2)\ \exp[-\bar{x}(1 + 2\eta^2)] \int_0^{\pi} \exp(\bar{x}\cos t)\ f(t)\ dt \ , \qquad (2.40a)$$

where

$$f(t) = \sin t/\left[(1 + \cos t)^{1/2}\ (1 + 2\eta^2 - \cos t)^{3/2}\right] . \qquad (2.40b)$$

Several limiting and approximate forms of this equation have been obtained by Yamamoto and Aida [66]. As in the previous case, the expression for the mean absorption over the interval can be expressed by $\bar{A}_{L\delta} = 1 - \bar{\tau}_{L,\delta}$.

The total absorption (not the average absorption) of a single line over the wave number interval $D = 2\delta$ can be obtained from the expression

$$A_{L,D} = 2D \int_0^{1/2} (1 - \exp\{-2x/[1 + (\bar{\xi}/\bar{\eta})^2]\})\, d\bar{\xi} , \qquad (2.41)$$

where $\eta = \gamma_L/D$, and $\bar{\xi} = (\omega - \omega_j)/D$.

Equations (2.38), and (2.40), and (2.41) are useful in calculating the absorption over a band pass of nonoverlapping spectral lines.

If there are n nonoverlapping lines in a finite wave number interval $\Delta\omega$ (with an average spacing between the lines of d), then the absorption of a single line over the interval $D = \Delta\omega = nd$ can be expressed by

$$A_{L,D} = \int_{-D/2}^{D/2} \left[1 - \exp\left(-\kappa_{\omega j}\, X\right)\right] d\left(\omega - \omega_j\right) . \qquad (2.42)$$

For a line with Lorentz shape, this becomes

$$A_{L,D} = (d/\pi) \int_0^{n\pi} (1 - \exp\{-2x/[1 + (z/\beta)^2]\})\, dz , \qquad (2.43)$$

where $\beta = 2\pi\gamma_L/d$, and $z = 2\pi(\omega - \omega_j)/d$. It can easily be shown that, in the linear limit, Eq. (2.43) reduces to

$$A_{L,D} = (2d\beta x/\pi)\, \tan^{-1}(n\pi/\beta) = 4\gamma_L\, x\, \tan^{-1}(n\pi/\beta) , \qquad (2.44)$$

while for large x, it becomes

$$A_{L,D} = \zeta\sqrt{\pi}[1 - \mathrm{erf}(\zeta)] + 1 - \exp(-\zeta^2) , \qquad (2.45)$$

where

$$\zeta^2 = 2x(\beta/n\pi)^2 \ , \quad \mathrm{erf}(\zeta) = (2/\sqrt{\pi}) \int_0^{\zeta} \exp(-t^2)\, dt \ .$$

The quantity β , which expresses the ratio of line width to line spacing, is called the line structure parameter. Since $\gamma_L \sim P$, the limit of large pressure correspond to $\beta \to \infty$.

Expressions for the average absorption can be obtained by dividing Eqs. (2.43) - (2.45) by the wave number interval nd .

The average absorption of a single line, in the spectral interval equal to the average spacing between the lines, can be given by

$$\bar{A}_{L,d} = (1/\pi) \int_0^{\pi} \left(1 - \exp\{-2x/[1 + (z/\beta)^2]\}\right) dz \ . \qquad (2.46)$$

The limiting forms of Eq. (2.46) are obtained from Eqs. (2.44) and (2.45) simply by replacing n with unity.

Since the solution of a single line of Lorentz shape (in an infinite spectral interval) is known from Eq. (2.28a), one can obtain an alternate form for the average absorption over the wave number interval $\Delta\omega = d$ as

$$\bar{A}_{L,d} = (1/d)\, A_{L,\infty} - (1/\pi) \int_{\pi}^{\infty} \left(1 - \exp\{-2x/[1 + (z/\beta)^2]\}\right) dz \ , \qquad (2.47)$$

where

$$A_{L,\infty}/d = \beta x \exp(-x) \left[I_0(x) + I_1(x)\right] \ .$$

The absorption model expressed by Eq. (2.47), is called the Schnaidt's model and is often employed for calculating the total absorptance of a band of overlapping lines. The effect of the overlap is accounted for by cutting off each line at displacements $\pm(d/2)$ from its center. Under normal atmospheric conditions, the line spacing greatly exceeds the line half-width (i.e., $(z/\beta) >> 1$) , and Eq. (2.47) can be approximated by

$$\bar{A}_{L,d} = (1/d)\, A_{L,\infty} + 1 - \exp(-u^2) - u\sqrt{\pi}\, \mathrm{erf}(u) \ , \qquad (2.48)$$

where

$$u^2 = 2x(\beta/\pi)^2 \ .$$

All expressions for absorptance in this section are written in non-dimensional form. It should be noted that the expressions for absorption over finite spectral interval do not reduce to the correct linear limit, Eq. (2.28b).

The solutions of Eq. (2.46), along with the limiting solutions, are illustrated in Figure 2.9 for various values of the line structure parameter β . As discussed earlier, the line structure parameter, which expresses the ratio of line half-width to line spacing, is essentially a pressure parameter. It is obvious from Figure 2.9 that the total absorption increases with the path length. This is physically realistic because at a fixed pressure, if the path length is increased then more molecules become available to interact with the radiative processes of emission and absorption. For any particular path length, however, the total absorption increases as the pressure is increased (i.e., $\bar{A}_{L,d}$ increases with β). This increase in absorption with β continues until the large β limit is achieved. At this point, lines become saturated (completely pressure broadened) and a further increase in pressure does not contribute to the absorption.

2.4. Absorption of an Overlapping Line in a Finite Spectral Interval

Spectral lines of an infrared band, in general, have different line intensities, half-widths, and spacing. At moderately high pressures, these lines overlap (especially in the wing regions). While calculating the transmittance of a single line in a finite spectral interval $D = 2\delta$, one must account for the contribution of the overlapping lines which occur outside the interval δ .

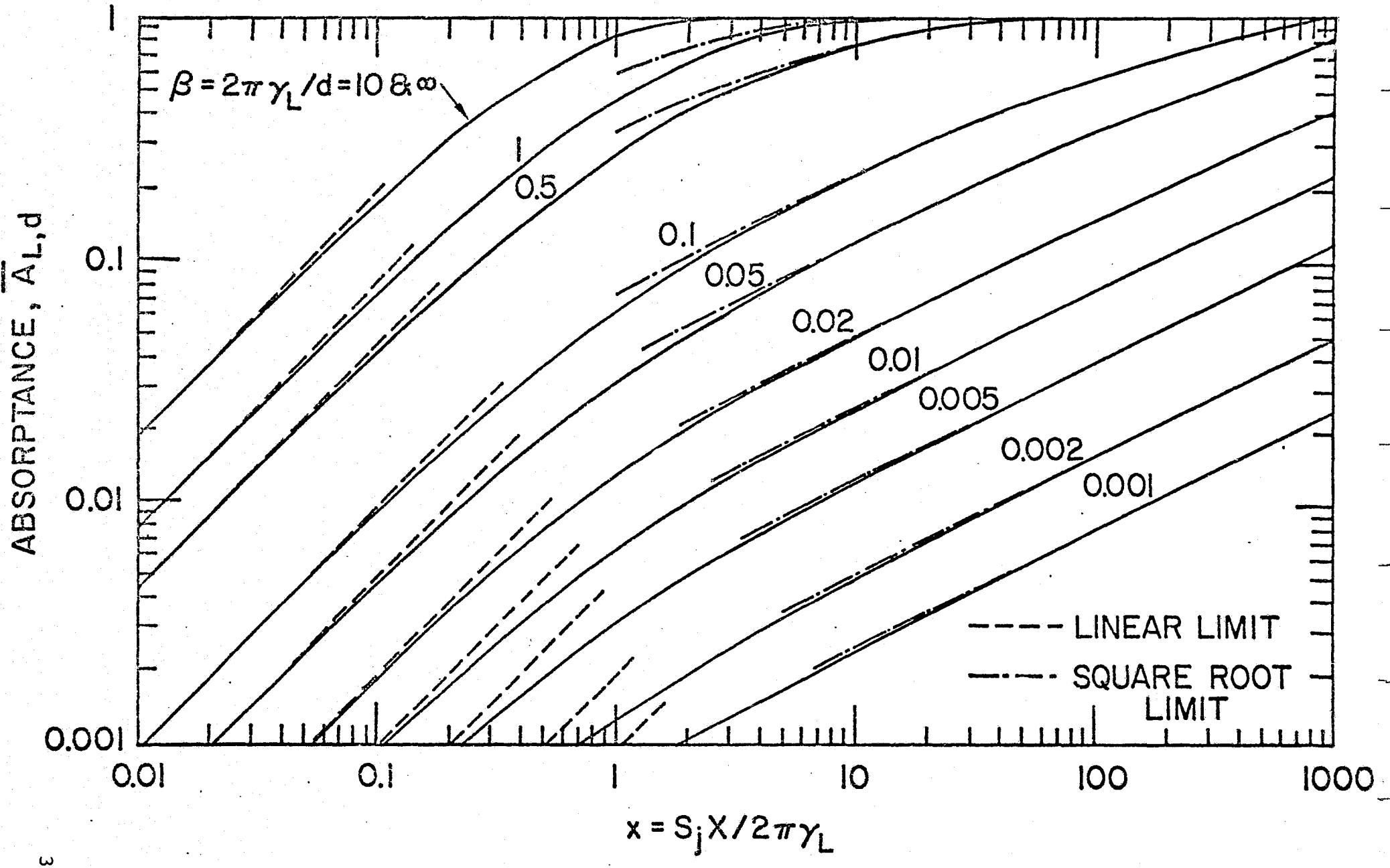

Fig. 2.9 Absorption of a single line of Lorentz profile in the spectral interval equal to the average spacing between the lines.

The absorption coefficient of a Lorentz line, in such cases, may by expressed by

$$\kappa_{\omega j} = S_j \gamma_{Lj}/\pi\left[(\omega - \delta_j)^2 + \gamma_{Lj}^2\right] , \quad j = 0, 1, 2, \ldots , \tag{2.49}$$

where $j = 0$ refers to the main line under consideration and δ_j's are the wave number locations (of center of jth lines) measured from the center of the main line. The expression for the spectral transmittance, therefore, becomes

$$\tau_{\omega j} = \exp\left[-\left(\kappa_{\omega o} + \sum_{j=1}^{n} \kappa_{\omega j}\right) X\right] , \tag{2.50}$$

and the average absorption over the interval $D = 2\delta$ is given by

$$\bar{A}_{L,\delta} = \frac{1}{2\delta} \int_{-\delta}^{+\delta} \left(1 - \tau_{\omega o} \exp\left\{-\sum_{j=1}^{n} S_j \gamma_{Lj} X/\pi\left[(\omega - \delta_j)^2 + \gamma_{Lj}^2\right]\right\}\right) d(\omega - \omega_o) . \tag{2.51}$$

Note that $\omega_o = \delta_o$ denotes the center of the main line.

By introducing quantities

$$n_j = \gamma_{Lj}/\delta , \quad \xi = (\omega - \omega_o)/\delta , \quad x_j = S_j X/2\pi\gamma_{Lj} ,$$

Eq. (2.51) can be written as

$$\bar{A}_{L,\delta} = (1/2) \int_{-1}^{1} \left(1 - \exp\left(-\sum_{j=o}^{n} 2x_j/\left\{1 + \left[(\xi/n_j) + (\omega_o - \delta_j)/\gamma_{Lj}\right]^2\right\}\right)\right) d\xi . \tag{2.52a}$$

For a particular atmospheric condition, evaluation of this equation requires the knowledge of δ_j , γ_{Lj} , and S_j for each interfering line. If in the interval δ , there are no contributions from the lines whose centers lie outside the interval, then Eq. (2.52a) directly reduces to Eq. (2.38).

By defining a new dimensionless quantity

$$\varepsilon_j = \left(\omega_o - \delta_j\right)/\gamma_{Lj} \ ,$$

Eq. (2.52a) can be written as

$$\left.\begin{aligned} \bar{A}_{L,\delta} &= A_{L,\delta}\left(x_j,\ \eta_j,\ \varepsilon_j\right) \\ &= (1/2)\int_{-1}^{1}\left(1 - \exp\left(\sum_{j=o}^{n} - 2x_j/\left\{1 + \left[\left(\xi/\eta_j\right) + \varepsilon_j\right]^2\right\}\right)\right) d\xi \ . \end{aligned}\right\} \quad (2.52b)$$

Since for $\varepsilon_j = o$, the mean absorption of a line is independent of the influence of neighboring lines, then ε_j may be treated as an overlapping parameter.

Expressions, similar to Eq. (2.52), can easily be written for the total absorption of a line over any spectral interval. The absorption of an overlapping line, in a finite spectral interval equal to the mean line spacing d , is given by

$$A_{L,d} = (d/2\pi)\int_{-\pi}^{\pi}\left(1 - \exp\left(\sum_{j=o}^{n} - 2x_j/\left\{1 + \left[\left(z/\beta_j\right) + \varepsilon_j\right]^2\right\}\right)\right) dz \quad (2.53)$$

where $\beta_j = 2\pi\gamma_{Lj}/d$, and $z = 2\pi\left(\omega - \omega_o\right)/d$.

For a fixed value of β_j (i.e., same value of β for all lines), the effect of overlapping can be studied simply by assigning different values to ε_j and completing the indicated summation in the exponential. For a fixed average spacing between the lines, it should be obvious from the definitions of the parameters ε_j and β_j that while ε_j varies inversely with pressure, β_j is a direct function of pressure such that the product $\varepsilon_j\beta_j$ becomes a constant. This, of course, will not be the case if one considers the variation in spacing between the lines. Since the quantity $\varepsilon_j\beta_j$ solely depends on the locations of the main and interfering lines and on the average spacing between the lines, then more realistic parameters for this problem will be β_j and $\varepsilon_j\beta_j$ rather than ε_j and β_j . In terms of these new parameters, Eq. (2.53) can be expressed as

$$A_{L,d} = A_{L,d}(x_j,\ \beta_j,\ \zeta_j)$$
$$= (d/2\pi) \int_{-\pi}^{\pi} \left(1 - \exp\left(\sum_{j=o}^{n} - 2x_j/\left\{1 + \left[(z + \zeta_j)/\beta_j\right]^2\right\}\right)\right) dz \ , \qquad (2.54)$$

where

$$\zeta_j = \varepsilon_j\ \beta_j = 2\pi(\omega_o - \delta_j)/d \ .$$

For a fixed average spacing between the lines, a large ζ_j value physically means that the line centers of the interfering lines are at larger wave number from the main line center and, therefore, their influence on the absorption of the main line will be smaller.

If all lines in a spectral interval are equally intense and have the same half-widths, then Eq. (2.54) can be written as

$$A_{L,d} = (d/2\pi) \int_{-\pi}^{\pi} \left(1 - \exp\left(-2x \sum_{j=o}^{n} \left\{1 + \left[(z + \zeta_j)/\beta_j\right]^2\right\}^{-1}\right)\right) \ . \qquad (2.55)$$

If there is significant interference only due to one neighboring line, then Eq. (2.55) is written, for average absorption, as

$$\bar{A}_{L,d} = \bar{A}_{L,d}(x,\ \beta,\ \zeta_1) \qquad (2.56)$$
$$= (1/2\pi) \int_{-\pi}^{\pi} \left(1 - \exp(-2x/\{1 + [(z + \zeta_1)/\beta]^2\})\right) dz \ .$$

This is a convenient form to study the effect of overlapping in a spectral interval equal to the mean line spacing. It should be noted that for $\zeta_1 = 0$, Eq. (2.56) directly reduces to Eq. (2.46). It should further be noted that, in general, the integrands in Eqs. (2.52) through (2.56) are not symmetric because lines on either side of the main line may have different line intensities and half-widths. Therefore, one cannot simply integrate these equations between the limit of zero to π and multiply the results by two. This, however, is possible for the special case considered in Eq. (2.56).

The results of Eq. (2.56) are illustrated in Figure 2.10 for $\beta = 0.1$. For a fixed β (i.e., at a constant pressure), the

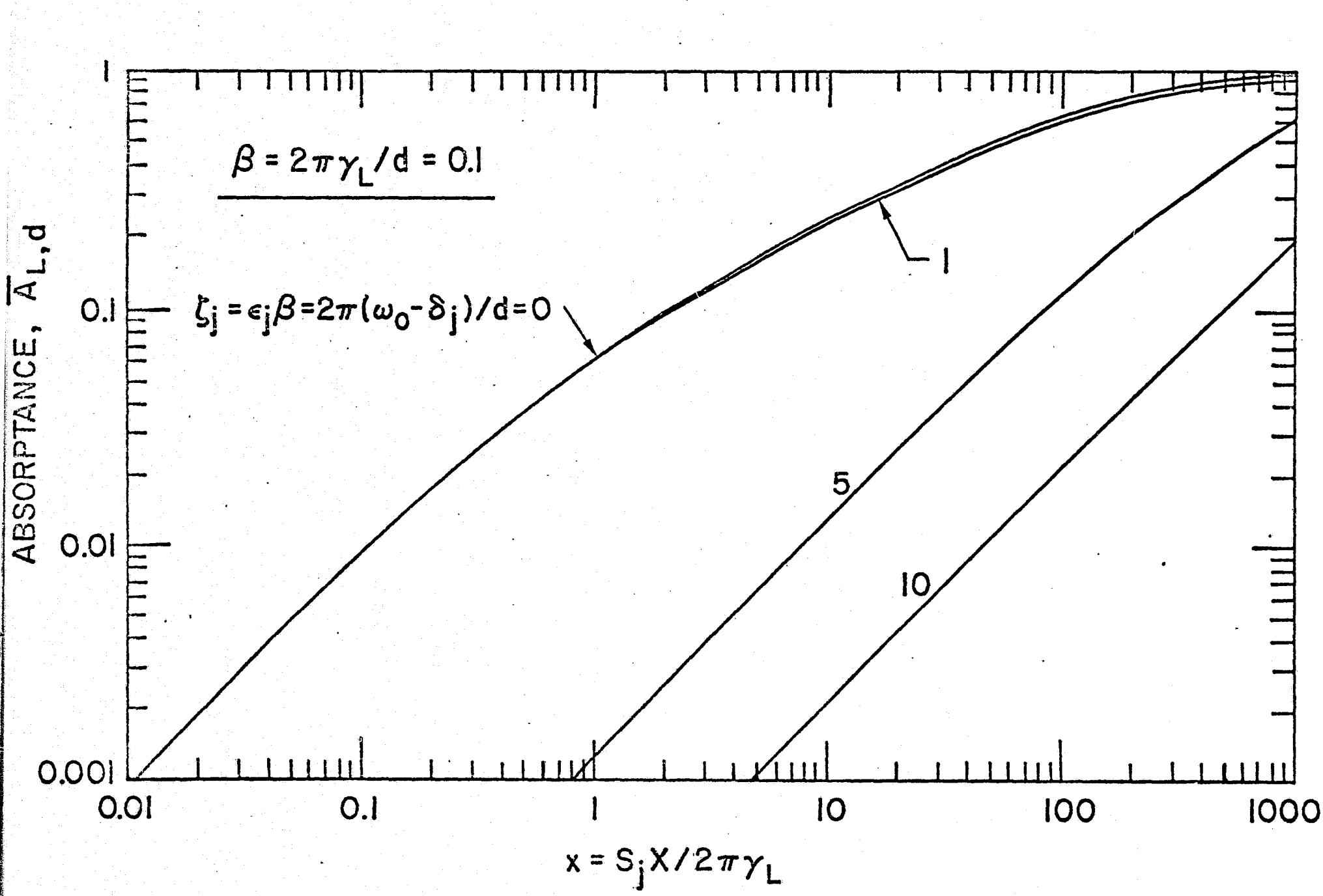

Fig. 2.10 Effect of interference of a neighboring line on the absorption of the main line for β = 0.1.

absorption of the main line is influenced solely due to the wave number location of the interfering lines. The influence is stronger if the neighboring line centers are closer to the main line center. Thus, absorption will be higher for smaller values of the parameter ζ_1 . This is clearly evident from the results presented in Figure 2.10.

Other results of absorption (and transmission) by a spectral line, in various spectral intervals, are available in [6-8].

3. BAND ABSORPTION

The absorptions by atmospheric gases, under certain atmospheric conditions, result in overlapping spectral lines. Thus, the total absorption within certain frequency interval cannot accurately be represented simply by summing the absorption by individual lines. This is because the absorption in a region of overlapped lines is always less than the absorption calculated by considering the contributions of individual non-overlapping lines.

The total absorption of a band of overlapping lines strongly depends upon the line intensity, the line half-width, and the spacing between the lines. In a particular band, the absorption coefficient varies very rapidly with the frequency and, therefore, it becomes a very difficult and time-consuming task to evaluate the total band absorptance by numerical integration over the actual band contour. Consequently, several approximate band models have been proposed which represent absorption from an actual band with reasonable accuracy. These are discussed in some detail in this section.

The spectral absorptance of a narrow band (consisting of sufficiently large number of spectral lines) may be expressed by

$$\alpha_\omega = 1 - \tau_\omega = 1 - \exp\left(-\int_0^X \kappa_\omega \, dX\right) , \qquad (3.1)$$

where κ_ω is the mass absorption coefficient for the band. The physical interpretation of α_ω is that it is the fraction of energy which is absorbed when a beam of radiant energy passes

through a slab of gas of thickness ℓ . For a homogeneous path, the total absorptance of a narrow band is given by

$$A = \int_{\Delta\omega} \alpha_\omega \, d\omega = \int_{\Delta\omega} \left[1 - \exp\left(-\kappa_\omega X\right)\right] d\omega \ , \tag{3.2}$$

where limits of integration are over the narrow band pass considered.

The total band absorptance of a wide band may, in turn, be expressed by

$$A = \int_{-\infty}^{\infty} \left[1 - \exp\left(-\kappa_\omega X\right)\right] d\left(\omega - \omega_o\right) \ , \tag{3.3}$$

where the limits of integration are over the entire band pass and ω_o is the wave number at the center of the wide band.

In subsequent sections, various band models are considered to illustrate the basic features of the total band absorptance. There are, however, specific situations where absorption of a band may be represented quite accurately by one of the limiting forms of the total band absorptance discussed in the next subsection.

3.1. Limiting Forms of the Total Band Absorptance

Various limiting forms of the total band absorptance are: Nonoverlapping Line Approximation, Linear Approximation, Weak Line Approximation, Strong Line Approximation, Square-Root Limit, Limit of Large Pressure, and the Large Path Length Limit. Physically realistic expressions for band absorptance in these limits depend upon the specific band model employed. Certain characteristics of band absorption, however, can be discussed in general terms independent of any band model.

3.1.1. Nonoverlapping Line Approximation

For this approximation, it is assumed that the spectral lines in a given interval $\Delta\omega$ do not overlap appreciably. The total absorptance due to n lines, in the interval, is obtained by summing

the contributions of individual lines, i.e., $A = \sum_{j=1}^{n} A_j$, where A_j is given by Eq. (2.16).

As long as the criteria of nonoverlapping lines are satisfied, this approximation is valid regardless of the value of the absorption at the line centers. Since there is no influence of overlapping in this approximation, the absorption is independent of whether the spacing between the lines is regular or random. The absorption may, however, depend slightly on the distribution of line intensities in the band. The expressions of band absorptance for this approximation, therefore, depend on the particular band model employed.

For this approximation to be valid, it is required that the integrand in Eq. (2.16) approach zero for $(\omega - \omega_j) = 0(d)$, where d is the line spacing. For lines with Lorentz profile, the nonoverlapping limit will be satisfied if

$$\kappa_{\omega j} X = \left(S_j X/\pi\right) \left[\gamma_j/\left(\gamma_j^2 + d^2\right)\right] << 1 , \qquad (3.4)$$

and if, in addition, $\gamma_j << d$ [19]. The conditions for achieving the nonoverlapping limit can, therefore, be stated as

$$\left(\gamma_j/d\right) << 1 , \quad \left(S_j X \gamma_j/\pi d^2\right) << 1 . \qquad (3.5a)$$

Alternately, this can be expressed by

$$\beta << 1 , \quad \beta^2 x << 1 . \qquad (3.5b)$$

The nonoverlapping approximation is specially useful in extrapolating the absorption to small values of pressure and path lengths.

3.1.2. Linear Approximation (Linear Limit)

One of the important limiting form of the band absorptance, which is completely independent of the band model, is the linear limit (or linear approximation). This approximation is valid when the total absorption due to all of the spectral lines is small at

every frequency within the interval (i.e., $\kappa_\omega X << 1$ at all wave numbers). As pointed out earlier, this is the conventional optically thin limit in radiative transfer. Upon expanding the exponential in Eq. (3.3) and retaining only the first two terms in the series, the expression for band absorptance in the linear limit is found to be

$$A = X \int_{-\infty}^{\infty} \kappa_\omega \, d(\omega - \omega_o) = X \, S \, , \tag{3.6a}$$

where S is the band intensity. The total band absorptance in this limit increases linearly with the path length and the line intensity but is independent of the rotational line structure. Since all of the absorption from spectral lines (whose centers are within the wave number interval considered) occurs within $\Delta\omega$, this approximation is valid only when there is no overlapping of the spectral lines. In essence, therefore, the linear approximation is valid when this is an appropriate approximation for a single line and when in addition there is no appreciable overlapping of lines in the spectral range of interest. Equation (3.6a), therefore, is a consequence of summing the absorption from individual lines, i.e.,

$$A = \sum A_j = X \sum_j \int_{\Delta\omega j} \kappa_{\omega j} \, d(\omega - \omega_j) = X \sum_j S_j = S \, X \, . \tag{3.6b}$$

The linear approximation fails if the spectral lines begin to overlap strongly.

3.1.3. Weak Line Approximation

The weak line approximation is valid when the absorption is sufficiently small at all frequencies in the band (i.e., the absorption is small for each line in the wave number interval considered). Thus, the effect of different spectral lines is additive even if these are strong overlapping of lines. Note the difference between this and the linear approximation which is valid only for the case of nonoverlapping lines.

When weak line approximation is valid, the amount of radiation absorbed by each line is always a small fraction of the incident flux [10, 11]. If, however, many such weak lines overlap in a given spectral interval, then almost all of the radiation can be absorbed in that interval. The absorption coefficient is no longer a rapidly varying function of the wave number (i.e., it is almost constant) and, therefore, the particular arrangement of the spectral lines in the band (regular or random) does not influence the band absorptance significantly.

Physically, the weak line approximation is valid when the path length is small and the pressure is sufficiently large such that the absorption at the line centers is small. As will be shown later, the mean absorption in this case is a function of a single variable, $\beta x = S_j X/d$, and is given by the relation

$$\bar{A} = 1 - \exp\left(-S_j X/d\right) = 1 - \exp(-\beta x) \ . \qquad (3.7)$$

It should be noted that the linear limit, Eq. (3.6), is a special case of the weak line approximation, Eq. (3.7).

3.1.4. Strong Line Approximation

The strong line approximation is valid when the incident radiation is completely absorbed near the centers of the strongest spectral lines in the band and when these lines are primarily responsible for the total band absorption. In this approximation, therefore, the centers of the main absorbing lines are opaque and further radiative contributions are primarily from the wing regions. The physical conditions for this approximation to be valid occurs either at large optical path lengths or for low pressure values. The approximation is valid for overlapping as well as nonoverlapping lines in the band. The expressions for band absorption, however, do depend on the particular arrangement of the spectral lines (regular or random) in the band.

The strong line approximation requires that $\kappa_\omega X >> 1$ for $\omega = \omega_j$. For spectral lines of Lorentz shape, the strong line condition is obtained from Eq. (2.4) as

$$S_j \, X/\pi \, \gamma_j >> 1 \, . \qquad (3.8)$$

As will be shown later, the band absorptance in this case is a function of a single variable, $\beta^2 \, x = 2\pi \, \gamma \, S_j \, X/d^2$.

The strong line approximation should not be confused with the square root approximation (discussed in the next subsection) which is valid only when the spectral lines do not overlap. The strong line approximation results are useful for extrapolating the absorption to small pressure and large path length values.

3.1.5. Square Root Limit (Strong Nonoverlapping Line Limit)

For line radiation, the square root limit (square root law, or square root absorption, or square root approximation) is achieved at relatively large optical path lengths. In this limit the central portion of the line is completely absorbed and the mean absorptance of the line is proportional to the square-root of the optical path length [13].

For band radiation, the square-root approximation is valid when this is a suitable approximation for a single line and when in addition, there is no overlapping of the spectral lines. Consequently, the square-root limit is a special case of the strong line approximation. This is also referred to as the strong nonoverlapping line limit. As the name implies, the limit requires that two separate conditions (strong lines and nonoverlapping lines) be satisfied. These conditions are described by Eqs. (3.8) and (3.5) respectively.

3.1.6. Limit of Large Pressure (Large β Limit)

Pressure plays a dual role in gaseous radiation. It appears in the path length as well as in the line structure parameter β . Its appearance in the pressure path length, py (or pℓ), is due simply to the fact that absorption is dependent upon the number of molecules which are present along a line of sight. Pressure enters in the line structure parameter because the line half-widths are directly dependent on pressure. For sufficiently high pressures,

the discrete line structure is smeared out, and in this limit (large pressure limit) pressure enters solely through the pressure path length py (or through ρy). The absorption coefficient in this limit is given by the expression $\kappa_\omega = S_j/d$. The average absorption in this case, therefore, is a function of a single variable S_j X/d and is given by the Eq. (3.7). As such, the weak line approximation may be considered as a special case of the large β limit.

3.1.7. Large Path Length Limit (Logarithmic Limit)

If, in addition to high pressure (large pressure limit), the pressure path length is sufficiently large, then the total band absorptance reaches a logarithmic asymptote (i.e., A ∿ ℓn (path length)). In this limit the central portion of the band becomes opaque, and radiation transfer within the gas takes place solely in the wing regions of the band. As such, the strong line approximation may be considered as a special case of the large path length limit. The large path length limit is an appropriate limit for a wide rather than a narrow band model.

3.2. Narrow Band Models

The absorption within a narrow frequency interval of a vibration rotation band can be represented quite accurately by so-called "narrow band models." Four commonly used narrow band models are, Elsasser, statistical, Random Elsasser, and Quasi Random. The application of any model to a particular case depends upon the nature of the absorbing-emitting molecule. For example, one model may provide an excellent agreement with experimental results for linear molecules but it may fail completely for asymmetric and spherical top molecules.

3.2.1. Elsasser (Regular) Band Model

The absorption of some vibration-rotation band, in a sufficient narrow frequency range, may be represented quite accurately by the regular Elsasser band model [9], which consists of equally-spaced

Lorentz lines of equal half-width and intensity. This is an appropriate model to use for most diatomic gases and some linear triatomic molecules such as CO_2 and N_2O (if the path length is not too large).

In an Elsasser band, the absorption coefficient is a periodic function (with the period of the line spacing), and is given by Eq. (2.8) which is rewritten in a slightly different form as

$$\kappa_\omega = \sum_{n=-\infty}^{\infty} \left\{ S_j \, \gamma_L / \pi \left[(\omega - nd)^2 + \gamma_L^2 \right] \right\} , \tag{3.9}$$

where ω is the distance from the center of any line and d is the distance between adjacent lines. Elsasser [9] showed that Eq. (3.9) can be expressed in an alternate form as

$$\kappa_\omega = \left(S_j / d \right) \sinh \beta / (\cosh \beta - \cos z) , \tag{3.10}$$

where β and z are same as defined in Eq. (2.43).

The average absorptance of the periodic line pattern over the line spacing d is obtained by combining Eqs. (3.2) and (3.10) as

$$\bar{A}_N(x, \beta) = 1 - (1/2\pi) \int_{-\pi}^{\pi} \exp[-\beta x \sinh \beta / (\cosh \beta - \cos z)] \, dz , \tag{3.11}$$

where A_n represents the absorptance of a narrow Elsasser band, and the quantity x is defined in Eq. (2.27). Elsasser [9] expressed this equation in the form

$$\bar{A}_N(x, \beta) = \sinh \beta \int_0^y I_0(t) [\exp(-t \cos \beta)] \, dt , \tag{3.12}$$

where $y = S_j \, X / (d \sinh \beta) = \beta x / \sinh \beta$, and $I_0(t)$ is the modified Bessel function of order zero. Solutions of Eq. (3.12) are tabulated in [67] for $\beta = 0.0001$ to 1.0 , and for $y = 0.02$ to $1.5(10)^5$. Equation (3.12) can be written in terms of the tabulated Schwarz function $I_e(k, v)$ as

$$\bar{A}_N(x, \beta) = \tanh \beta \left[I_e(\operatorname{sech} \beta, \beta x \coth \beta) \right] , \qquad (3.13)$$

where

$$I_e(k, v) = \int_0^v I_0(kt) \exp(-t)\, dt .$$

Although the numerical solution of Eq. (3.11) can be easily obtained, several attempts have been made [67-71] to find the exact solution of this equation by employing either form (3.12) or (3.13). For exact solutions particularly applicable to the problems of atmospheric radiation, references should be made to [67, 70].

Numerical solutions of Eq. (3.11) are illustrated in Figures 3.1-3.4 in four different ways. Figure 3.1 is simply a plot of band absorption versus path length for different β-values and illustrates that absorption increases with pressure and path lengths. The results illustrated in Figures 3.2-3.4 are convenient for comparison with the approximate solutions discussed below.

Several useful forms of Eqs. (3.11) through (3.13) can be obtained in the various limits and some of these are discussed here.

For large β (i.e., high pressure), $\sinh \beta \to \cosh \beta \to \infty$ such that $\sinh \beta/(\cosh \beta - \cos z) \to 1$ and Eq. (3.11) reduces to

$$\bar{A}_N(x, \beta) = 1 - \exp(-\beta x) . \qquad (3.14)$$

In this limit, the mean absorption is a function of a single variable $\beta s = S_j X/d$, the lines overlap and there is no fine structure (i.e., absorption is independent of the line structure parameter β). As would be expected, Eq. (3.14) is the same as the Beer's law (i.e., the absorption of a band is given by a simple exponential law and the transmittance is independent of pressure).

An important form of the band absorptance is obtained in the limit of weak line approximation which is valid when the path length is small and the pressure is sufficiently high. For small

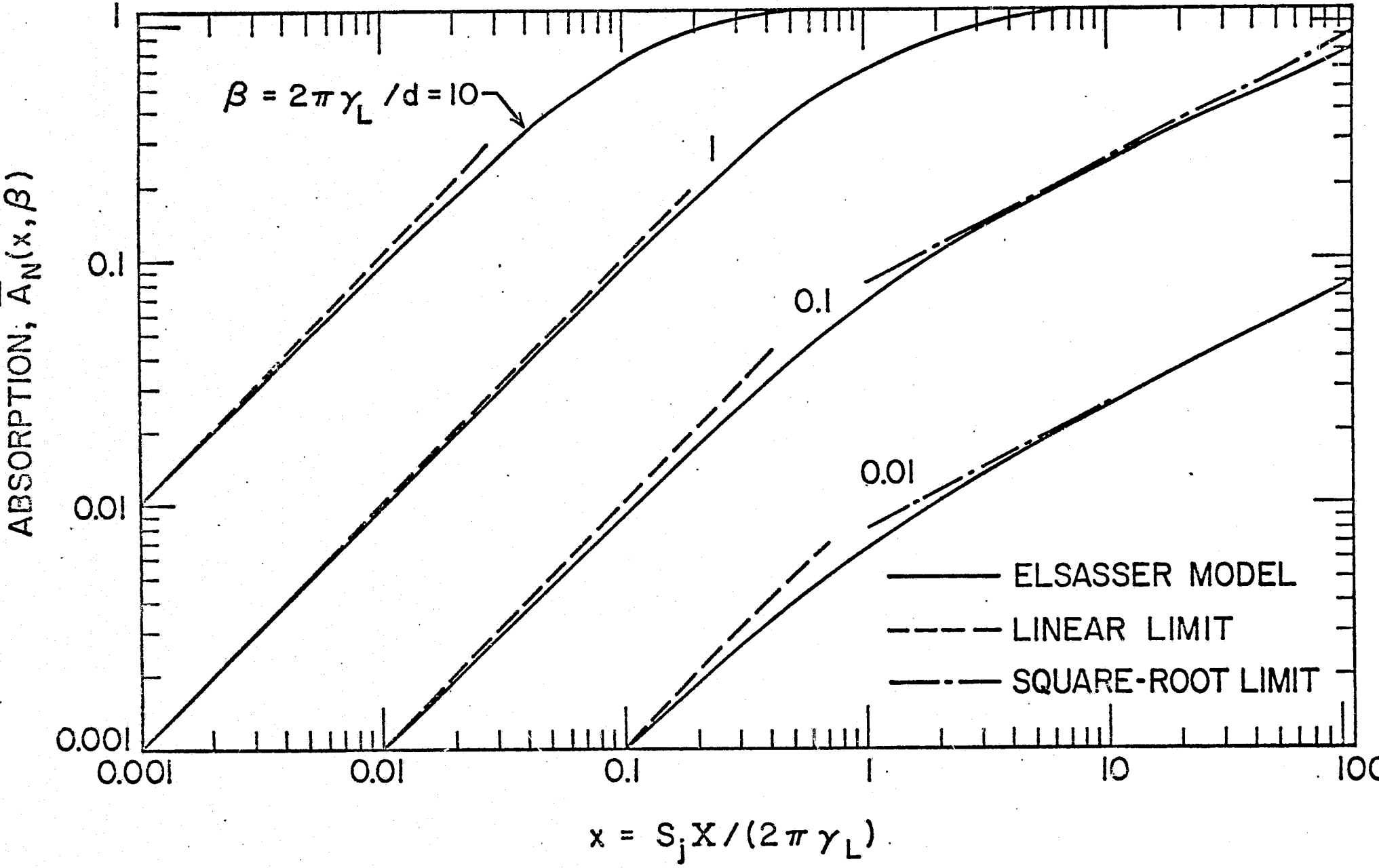

Fig. 3.1 Absorption by narrow Elsasser band.

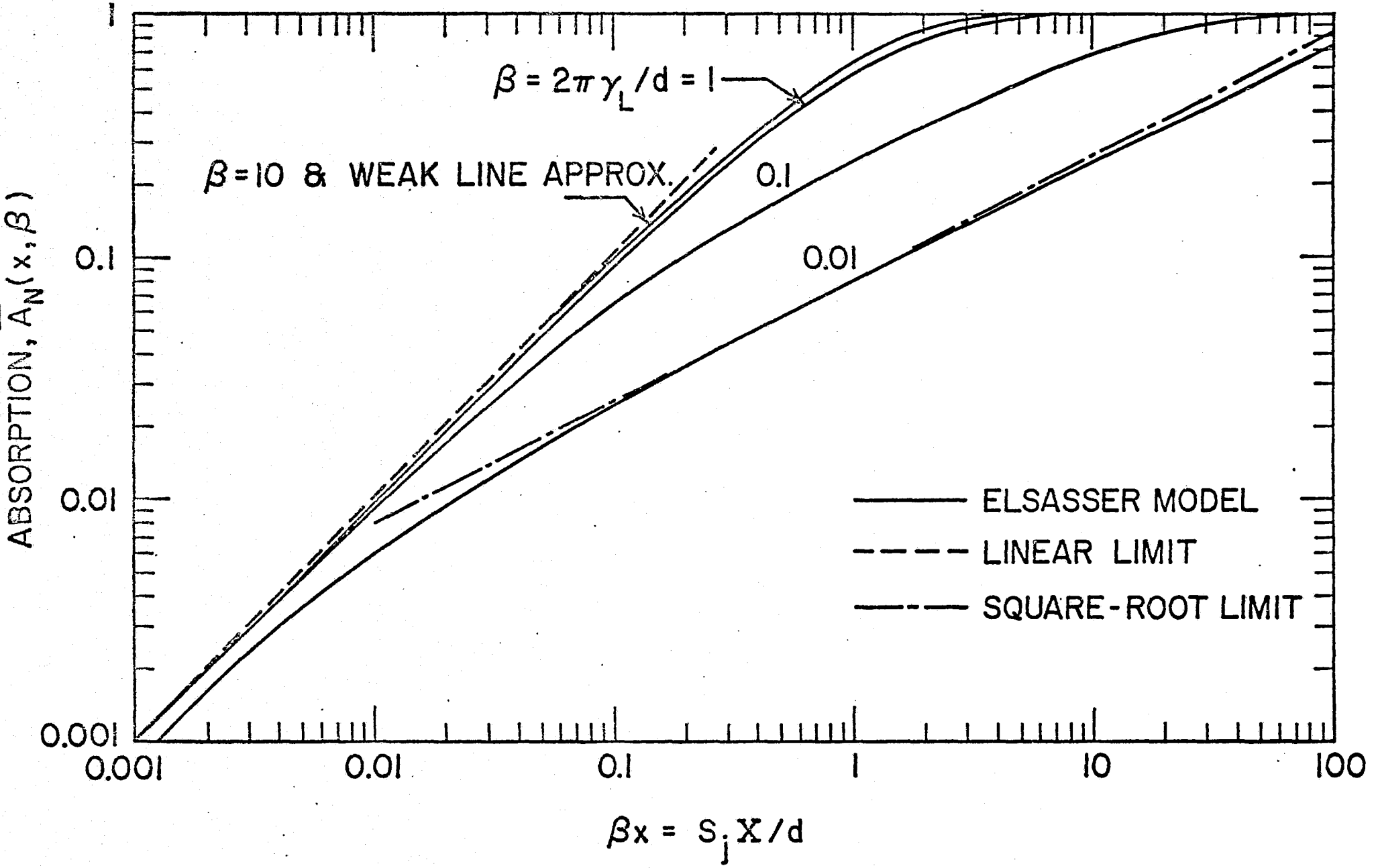

Fig. 3.2 Absorption as a function of βx for the Elsasser model.

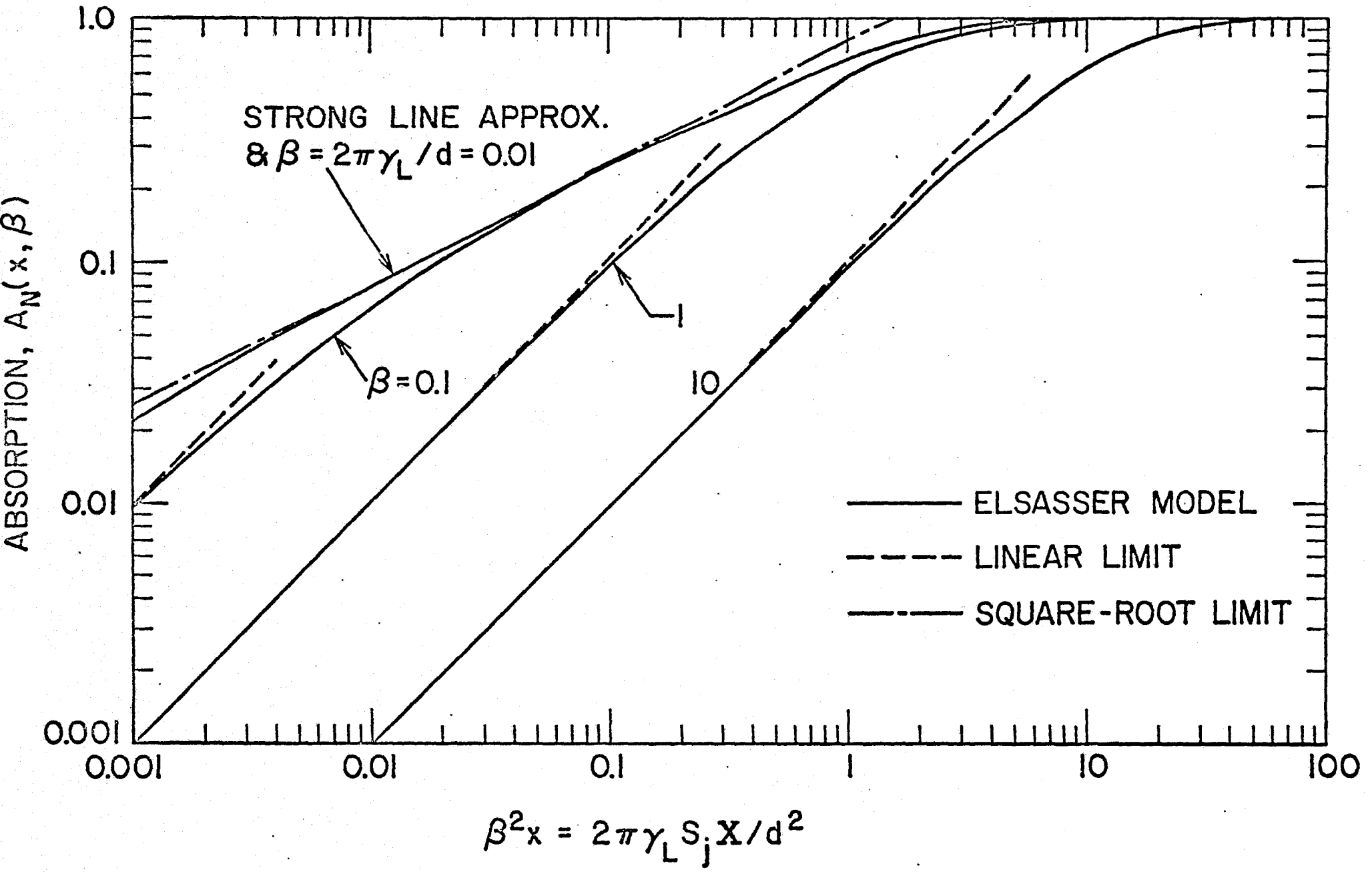

Fig. 3.3 Absorption as a function of $\beta^2 x$ for the Elsasser model.

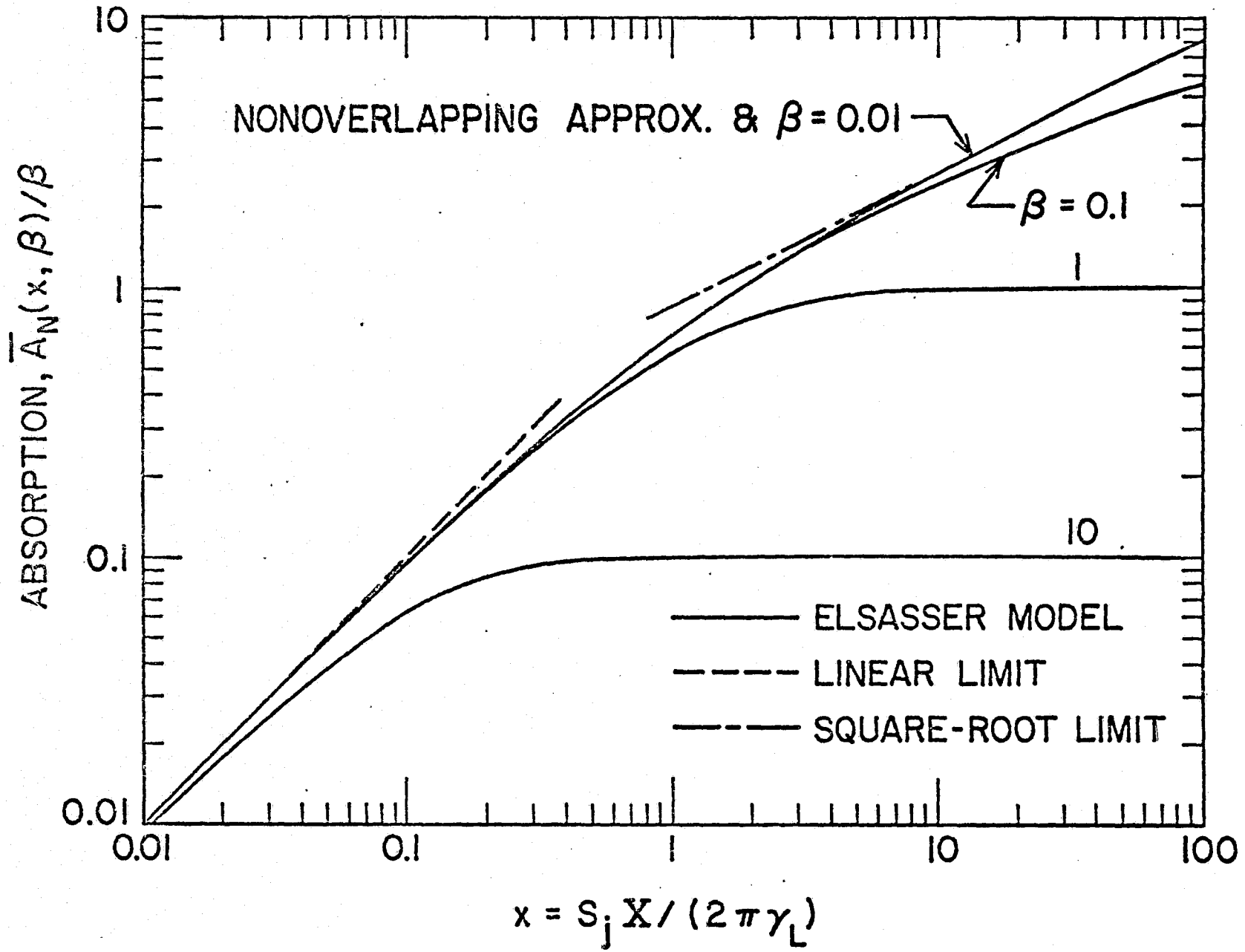

Fig. 3.4 Absorption divided by β as a function of x for the Elsasser model.

x , therefore, Eq. (3.14) represents the weak line approximation. Note that Eq. (3.14) is exactly the same as Eq. (3.7).

The results of Eqs. (3.11) and (3.14), as a function of βx , are illustrated in Figure 3.2. The uppermost curve is the solution of Eq. (3.14). Note that the absorption can never be greater than that given by Eq. (3.14). For $x < 0.2$ and $\beta < 0.1$, the results of Eq. (3.14) are within 10% of the exact solution of Eq. (3.11). For a particular β value, better accuracies are obtained at lower x-values. For $\beta \geq 1$, the results of Eq. (3.14) are in good agreement with the exact solution for all x-values [11].

For $x << 1$, Eq. (3.14) reduces to the linear limit as given by Eq. (3.6). This is illustrated in Figure 3.2 by the broken line. As noted earlier, this limit is independent of the spectral model for band absorptance.

Another important form of Eq. (3.11) is obtained when the strong line approximation is justified. With reference to Eq. (3.8), the condition for the strong line approximation is that $x >> 1$, and following Goody [13], Eq. (3.3) may be reduced to

$$\left.\begin{aligned} \bar{A}_N(x, \beta) &= \operatorname{erf}\left[\left(\tfrac{1}{2}\,\beta^2\, x\right)^{1/2}\right] , \quad x >> 1 , \\ \text{where} \qquad & \\ \operatorname{erf}(t) &= (2/\sqrt{\pi}) \int_0^t \exp(-t^2)\, dt . \end{aligned}\right\} \tag{3.15}$$

As mentioned earlier, the mean absorption, in this case, is a function of a single variable $\beta^2 x$. The expansion of Eq. (3.15) in powers of $\beta^2 x$ results in

$$\bar{A}_N(x, \beta) \doteq \beta (2x/\pi)^{1/2} \left[1 - (\beta^2 x/6) + \text{---}\right] . \tag{3.16}$$

Note that the first term in this equation is identical with the strong line approximation for a single line (provided $\Delta\omega = d$).

The results of Eqs. (3.11) and (3.15), as a function of $\beta^2 x$, are illustrated in Figure 3.3. The uppermost curve is the

solution of Eq. (3.15). Note that the absorption can never be greater than this limiting solution. For $x > 1.6$, the results of Eq. (3.15) are within 10% of the results of Eq. (3.11) for all β values [11]. For $\beta > 1$, the results compare well even for smaller x-values. As discussed by Plass [11], the influence of Doppler broadening on the absorption can be determined from the results illustrated in the form of Figure 3.3.

Another important form for the band absorptance is obtained in the limit of nonoverlapping lines. The conditions for achieving this approximation are given by Eq. (3.5). The mean absorption of an Elsasser band, in this case, may be expressed by

$$\left.\begin{aligned} &\bar{A}_N(x, \beta) = n\,\bar{A}_j/\Delta\omega = A_j/d = \beta\, L(x) \ , \quad \beta << 1 \ , \\ &\beta^2 x << 1 \ , \\ &\text{and} \\ &\bar{A}_N/\beta = L(x) = x\, e^{-x}\left[I_0(x) + I_1(x)\right] \ . \end{aligned}\right\} \quad (3.17)$$

Thus, in this limit the expression for mean absorption of the Elsasser band is the same as that of a single Lorentz line.

The results of Eqs. (3.11) and (3.17) are illustrated in Figure 3.4. The uppermost curve represents the nonoverlapping line approximation. For lower x-values, this curve has a slope of unity indicating the region where the weak line approximation is valid. For large x-values, the curve has a slope of one-half which is the region where the strong line approximation is valid. For $\beta < 1$, the nonoverlapping line approximation accurately represents the absorption in the transitional region near $x = 1$.

A final form for the narrow band absorptance is obtained in the limit of strong nonoverlapping lines (the square root limit). For Elsasser band, the expression for absorptance in this limit can be obtained from either Eq. (3.16) or Eq. (3.17). While this will be given by the first term of Eq. (3.16), it will be the limiting form

of Eq. (3.17) for large x (as given by Eq. (2.28c)). For this limit, therefore, one can write

$$\bar{A}_N(x, \beta) = \beta(2x/\pi)^{1/2} , \quad x >> 1 , \quad \beta << 1 , \quad \beta^2 x << 1 . \quad (3.18)$$

The results of Eq. (3.18) are illustrated in Figures 3.1-3.4 and they clearly reveal the fact that the square root limit is the limiting solution for low pressure and large path lengths.

The Elsasser band model was originally developed for the pressure broadened Lorentz line profiles. Recently, the model has been extended to the Doppler line shape by Kyle [72], Golden [73, 74], and Young [75, 76], and to the Voigt profile by Golden [77].

3.2.2. Statistical (Mayer-Goody) Model

The statistical band model is based upon the assumption that, in a given wave number interval, the spectral lines are spaced randomly, and the intensity of these lines can be specified by some distribution function [10, 13]. The model is useful in describing the absorption characteristics of CO_2 (especially at larger path lengths), H_2O, and other relatively complex polyatomic molecules.

The model considers a spectral interval of width $\Delta\omega = D = nd$ containing n total lines with each individual line having intensity S_j and wave number ω_j occurring within $\Delta\omega$. Let $N(\omega_j)\, d\omega_j$ represent the probability that the jth line has an intensity between S_j and $S_j + dS_j$. If ω_j's and S_j's are mutally independent, then the probability of finding the set of n lines with the distribution ω_1 --- ω_n, S_1 --- S_n is

$$\sum_{j=1}^{n} N(\omega_j)\, P(S_j)\, d\omega_j\, dS_j . \quad (3.19)$$

The average transmittance at wave number ω is obtained by averaging the transmittance at ω over the probability distribution of the set of n lines as

$$\bar{\tau}(\omega) = \int_{\Delta\omega} \cdots \int_{\Delta\omega} \int_0^\infty \cdots \int_0^\infty \sum_{j=1}^{n} N(\omega_j) \exp\left[-S_j X f_j(\omega, \omega_j)\right] d\omega_j \, dS_j \, . \tag{3.20}$$

By assuming that the line positions are distributed at random in $\Delta\omega$ and that all the lines in $\Delta\omega$ have the same intensity, Eq. (3.20) can be expressed as

$$\bar{\tau}(\omega) = \left\{(1/D) \int_{\Delta\omega} \exp\left[-S_j X f_j(\omega, \omega_j)\right] d\omega_j\right\}^n \, . \tag{3.21}$$

The absorptance over the wave number interval $\Delta\omega = D = nd$ may, in general, be expressed by [10, 13]

$$\bar{A}_N = 1 - \left[1 - (\tilde{A}_{j,D}/D)\right]^n \, , \tag{3.22a}$$

where

$$\tilde{A}_{j,D}(S_o, X, p) = \int_0^\infty A_{j,D}(S_j, X, p) \, P(S_j, S_o) \, dS_j \, . \tag{3.22b}$$

In these equations, $A_{j,D}$ is the absorptance of a single line over the entire wave number interval D, $P(S_j, S_o)$ is the normalized probability of finding a spectral line with the intensity S_j and $S_j + dS_j$, and S_o is the parametric mean line intensity that occurs in the intensity distribution function.

For a large number of lines in the interval D, the term nd may be considered to approach infinity even if the mean spacing d is held constant. By employing one definition of the exponential, it may be shown that, for large number of lines, Eqs. (3.22) becomes

$$\bar{A}_N = 1 - \exp(-\tilde{A}_j/d) \, , \quad n >> 10 \, , \tag{3.23}$$

where $\tilde{A}_j$ without the subscript D represents the absorptance of a single line for an infinite spectral interval. Physically, this assumes that there is no appreciable absorption by the single line outside the interval D. If this is not the case, then a more

accurate expression for the absorption of a single line in the finite spectral interval (as given in subsections 2.3 and 2.4) should be employed.

Since the lines are assumed to be distributed randomly in the statistical model, the absorption by this model is always less than that by the Elsasser model. The advantage of the statistical model is that it can easily be applied to any line shape. Depending upon the variation in the intensity of individual spectral lines in a particular band, the statistical model is usually divided into two subclasses: uniform statistical model (equally intense lines), and general statistical model (exponential distribution of line intensity).

3.2.2.1. Uniform Statistical Model - Equally Intense Lines. If in a narrow spectral interval all spectral lines are assumed to be equally intense such that $P(S_j) = \delta(S_j - S_o)$, then in Eq. (3.22)

$$\bar{A}_{j,D}(S_o, X, p) = A_{j,D}(S_o, X, p) , \tag{3.24}$$

and one can now write

$$\bar{A}_N = 1 - \left[1 - \left(A_{j,D}/D\right)\right]^n . \tag{3.25}$$

An appropriate relation for the absorption by a specific line profile (such as Lorentz, Doppler, or Voigt), over a specified spectral interval, should be used in Eq. (3.25). At this point, it should be pointed out that Eq. (3.25) could have been obtained directly by combining Eqs. (3.1), (3.2), and (3.21).

In a special case, if all spectral lines are equally intense, the use of the Lorentz line shape is justified, the absorption in a narrow band is due to a large number of spectral lines (with an average spacing d), and if there is no absorption by a single line outside the interval D , then Eq. (3.24) can be expressed as

$$\bar{A}_j/d = A_j/d = \beta\, L(x) = \beta\, x\, e^{-x}\left[I_o(x) + I_1(x)\right] . \tag{3.26}$$

The expression for the narrow band absorptance can be obtained now by combining Eqs. (3.23) and (3.26) as

$$\bar{A}_N(x, \beta) = 1 - \exp\left\{-\beta\, x\, e^{-x}\left[I_0(x) + I_1(x)\right]\right\} , \quad n >> 10 \qquad (3.27)$$

By employing the approximate form of the Ladenberg-Reiche function (see Eqs. (2.27), (2.28a), and (2.29e)), Eq. (3.27) can be expressed in an alternate form as

$$\bar{A}_N(x, \beta) = 1 - \exp\left\{-\beta\, x \Big/ \left[1 + (\pi\, x/2)^{\alpha}\right]^{1/2\alpha}\right\} . \qquad (3.28)$$

With $\alpha = 5/4$, results of Eq. (3.28) are within 1% of the results of Eq. (3.27). In atmospheric radiance calculations, use of Eq. (3.28) results in considerable savings of computational time.

The weak line approximation for this model can be obtained by substituting the appropriate value for $(A_{j,D}/D)$ in Eq. (3.25). For small x , the absorption by a Lorentz line, in an infinite spectral interval, is given by Eq. (2.28b) and, therefore, one can write

$$A_j/D = \left(2\pi\, \gamma_L\, x\right)/d = \beta x \qquad (3.29a)$$

$$A_j/D = A_j/(nd) = \beta\, x/n \qquad (3.29b)$$

Upon substituting Eq. (3.29) into Eqs. (3.25) and (3.26), the expressions for the weak line approximation are obtained as

$$\bar{A}_N(x, \beta) = 1 - [1 - (\beta x/n)]^n , \qquad (3.30a)$$

or

$$\bar{A}_N(x, \beta) = 1 - \exp(-\beta x) . \qquad (3.30b)$$

Note that Eq. (3.30b) could have been obtained directly from Eq. (3.27) by using the linear form of $L(x) = x$ for small x . Eq. (3.30b) is exactly the same as Eqs. (3.7) and (3.14). This, however, should be expected because the particular arrangement of

the spectral lines in the band does not influence the absorption when the weak line approximation is valid.

The strong line approximation for this model can be obtained from the asymptotic form of $(A_{j,D}/D)$ in Eq. (3.25) for large x. For large x, the absorption by a Lorentz line in an infinite spectral interval is given by Eq. (2.28c) such that

$$A_j/d = \left[2\gamma_L(2\pi x)^{1/2}\right]/d = \beta(2x/\pi)^{1/2} \quad . \tag{3.31}$$

By substituting this in Eqs. (3.25) and (3.26), the expressions for the strong line approximation are found to be

$$\bar{A}_N(x, \beta) = 1 - \left[1 - (2\beta^2 x/\pi)^{1/2}\right]^n \tag{3.32a}$$

or

$$\bar{A}_N(x, \beta) = 1 - \exp\left[-(2\beta^2 x/\pi)^{1/2}\right] \quad , \quad n >> 10 \quad . \tag{3.32b}$$

Note that Eq. (3.32b) could have been obtained directly from Eq. (3.27) by using the asymptotic form of $L(x) = (2x/\pi)^{1/2}$ for large x. Furthermore, in calculating the results for the strong line approximation from Eq. (3.32), an appropriately defined average value of the line intensity should be used for finding the value of x. Otherwise, the term in the square bracket of (3.32a) should be evaluated for each of the n spectral lines and the results multiplied together.

The nonoverlapping approximation for the statistical model, in general, can be obtained from Eq. (3.23) by expanding the exponential and only retaining the first term, such that

$$\bar{A}_N = \bar{A}_j/d = \int_0^\infty \left(A_j/d\right) P\left(S_j, S_o\right) dS_j \quad , \tag{3.33}$$

where again A_j represents the absorption of a single line in an infinite spectral interval. For spectral lines of Lorentz shape, Eq. (3.33) can be expressed as

$$\bar{A}_N/\beta = \int_0^\infty L(x)\, P(S_j, S_o)\, dS_j \ , \qquad (3.34)$$

where the right hand side is only a function of x .

For the present case of equally intense lines, Eq. (3.34) yields

$$\bar{A}_N/\beta = L(x) = x\, e^{-x}\left[I_0(x) + I_1(x)\right] \ . \qquad (3.35)$$

Note that this expression could have been obtained directly from Eq. (3.27) by expanding the exponential and retaining only the first term. Furthermore, it should be noted that Eq. (3.35) exactly the same as the nonoverlapping approximation for the Elsasser model (Eq. (3.17)). This, however, should be expected because it is the intensity distribution function (and not the regular or random spacing of spectral lines) that influences the absorption in this approximation.

The square-root limit (strong nonoverlapping line approximation) of Eq. (3.27) can be obtained by expanding the exponential in Eq. (3.32b) and retaining only the first term (because for this limit $\beta^2 x << 1$). This will be exactly the same expression as given by Eq. (3.18) or Eq. (3.31).

Various results (general and limiting) or the uniform statistical model are discussed in detail in [16].

3.2.2.2. General Statistical Model - Exponential Distribution of Line Intensities. If an exponential distribution of line intensities is assumed (i.e., in a band, the probability of finding a spectral line of intensity S_j in a given intensity range decreases exponentially), then

$$P(S_j, S_o) = \left[\exp\left(-S_j/S_o\right)\right]/S_o \ . \qquad (3.36)$$

For a particular line shape, the line absorptance in Eq. (3.22b) is calculated by using this line intensity distribution.

The absorption by the general statistical band model consisting of Lorentz lines is obtained by combining Eqs. (3.36), (3.22) and

(3.23) as [10]

$$\bar{A}_N(x_o, \beta) = 1 - \left\{1 - \left[\beta x_o / n\left(1 + 2x_o\right)^{1/2}\right]\right\}^n , \qquad (3.37a)$$

and

$$\bar{A}_N(x_o, \beta) = 1 - \exp\left[-\beta x_o / \left(1 + 2x_o\right)^{1/2}\right] , \quad n >> 10 , \qquad (3.37b)$$

where

$$x_o = S_o X / 2\pi\gamma_L .$$

It should be emphasized here that the expression for absorption by a single line in an infinite spectral interval as given by Eq. (2.28a) was used in obtaining Eq. (3.37). Expressions similar to Eq. (3.37) can be obtained for lines in a band having Doppler or Voigt line profiles [10, 72-77].

The results of Eq. (3.37b) are illustrated in Figures 3.5-3.7 along with the limiting solutions which are discussed below.

The weak line approximation for the general statistical model is also given by Eqs. (3.7), (3.14), or (3.30) but x is replaced by x_o. The results of this approximation are shown in Figure 3.5 along with the solution of Eq. (3.37b). The weak line approximation is always valid within 10% for $x_o < 0.1$.

The strong-line approximation for this case is given by Eq. (3.32) where again x is replaced by x_o. The results are shown in Figure 3.6 along with the solution of Eq. (3.37b). For $x_o > 2.4$, the strong line approximation results are within 10% of the exact solution for all β values. For $\beta \geq 1$, the results compare well even for smaller x-values [11].

The nonoverlapping line approximation for this case is obtained by combining Eqs. (3.34) and (3.36) as

$$\bar{A}_N / \beta = x_o \left(1 + 2x_o\right)^{-1/2} . \qquad (3.38)$$

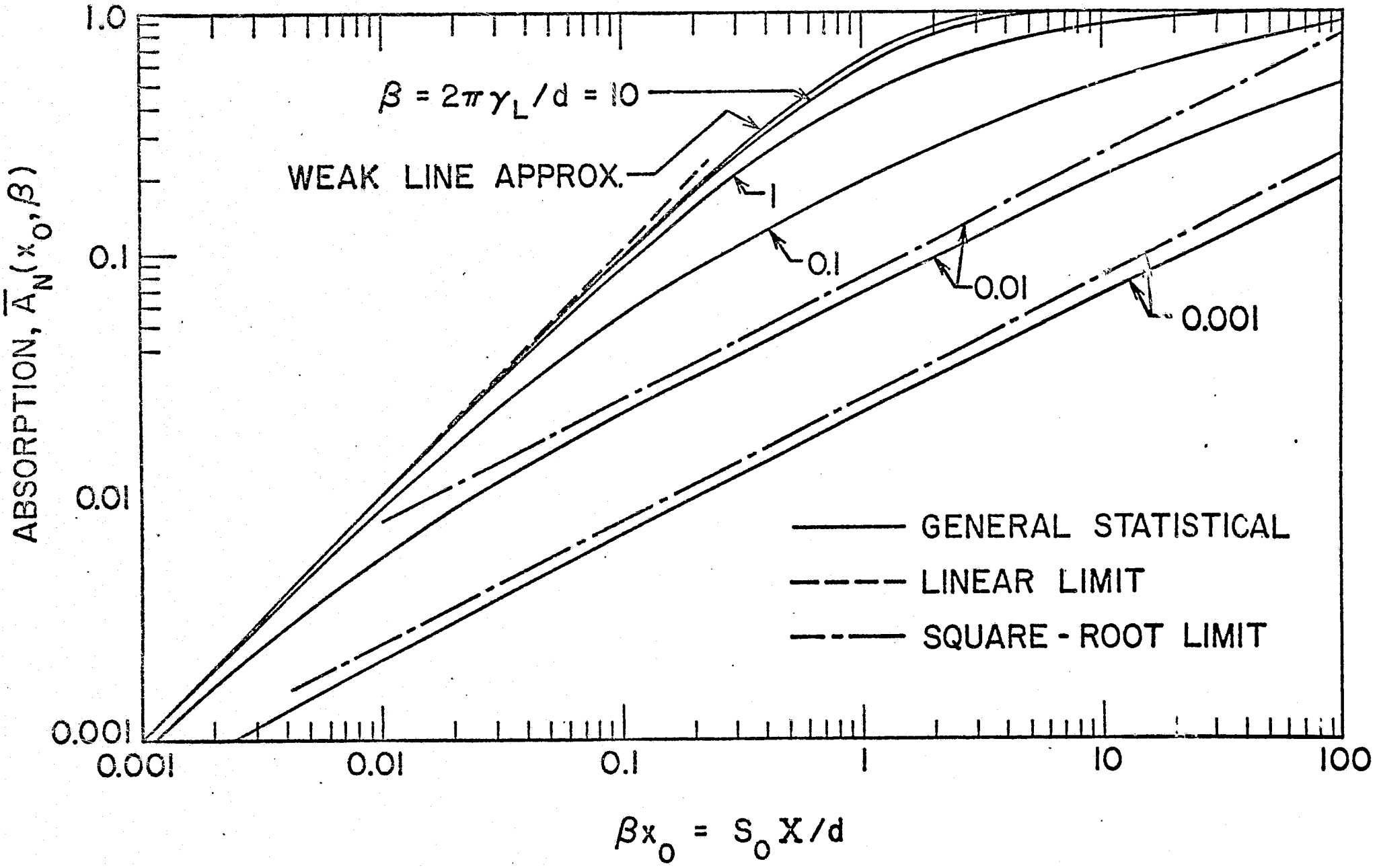

Fig. 3.5 Absorption as a function of βx for the general statistical model.

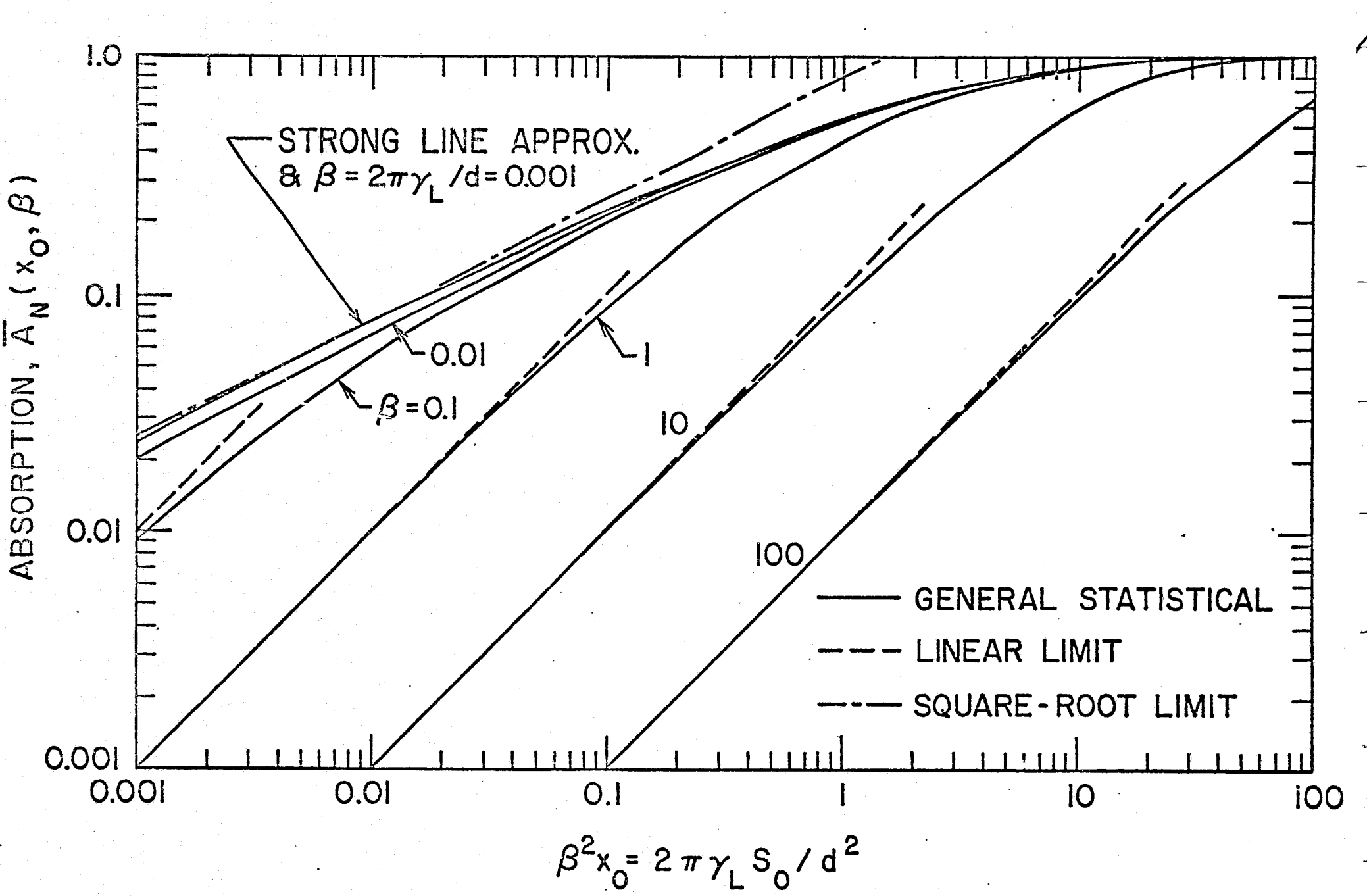

Fig. 3.6 Absorption as a function of $\beta^2 x$ for the general statistical model.

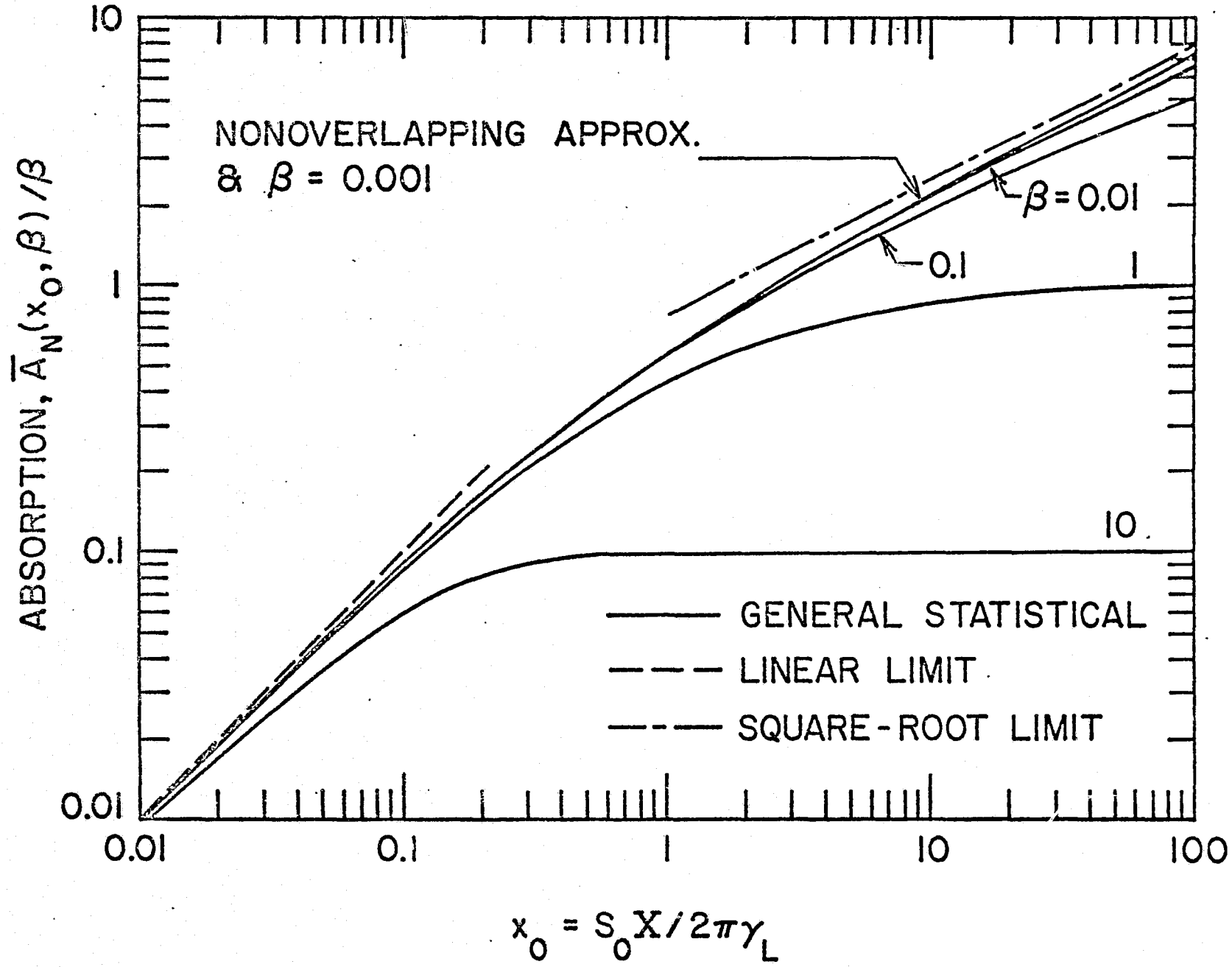

Fig. 3.7 Absorption divided by β as a function of x for the general model.

The results of Eqs. (3.37b) and (3.38) are illustrated in Figure 3.7 where the uppermost curve is the solution of Eq. (3.38).

The square root limit for this case is given by Eq. (3.18) or (3.31) where again x is replaced by x_0. The results are illustrated in Figures 3.5-3.7. It should be noted that the region of validity of the square root limit as illustrated in Figures 3.5-3.7 is different than those for the Elsasser model Figures 3.2-3.4.

For the sake of brevity, it is often deisrable to express the results of statistical models (uniform and general) on a single graph. According to Plass [10, 11], this is possible if one employs the relation $x = (\pi/4)x_0 = \left(S_0 X/8\gamma_L\right)$ in plotting the results.

From the comparison of results presented in Figures 3.2 and 3.5, it is noted that the absorption curve for $\beta = 1$ is much closer to the weak line approximation for the Elsasser model than for the statistical model. This is because the absorption saturates at a smaller value of βx for the Elsasser model.

A comparison of results illustrated in Figures 3.4 and 3.7 indicates that the spectral lines begin to overlap at considerably larger path lengths for the Elsasser model than for the statistical model. Thus, the nonoverlapping line approximation has a considerably larger region of validity for the Elsasser model than for the statistical model.

Another line intensity distribution sometimes employed in the statistical band formulation is the inverse-first-power model which is given by [13].

$$P\left(S_j\right) = k\, S_j^{-1} \,, \tag{3.39}$$

where k is a normalization constant. For proper normalization, the above distribution must be cut off at some upper limit S_j' on S_j. Depending upon its application, a lower cutoff limit for S_j might also be essential in determining the correct value of k. For Lorentz lines, the expression for $\left(\bar{A}_j/d\right)$ in Eq. (3.23) is found to be

$$\bar{A}_j/d = \beta\left\{e^{-x}\, I_0(x) + 2x\, e^{-x}\left[I_0(x) + I_1(x)\right] - 1\right\} . \qquad (3.40)$$

Substitution of this into Eq. (3.23) will result in another expression for absorption by a narrow statistical model. Different solutions of this model can also be obtained in the manner discussed for the previous two cases.

Malkmus [78, 79] and Rodgers [80] have suggested yet another distribution of line intensity in a band. This constitutes a superposition of the exponential and the inverse-first-power distribution of line intensity. For detailed discussion of this model references should be made to [78-80].

3.2.3. Random Elsasser Band Model

In actual vibration-rotation bands, lines are arranged neither completely at random nor at regular intervals. Within a band, there may be a number of strong lines in certain narrow spectral region, whereas in other regions only very weak lines may be present. There also may occur a superposition of equally intense lines in another spectral region of the band. In cases like this, a more accurate representation of band absorption is provided by the random Elsasser model, which assumes the random superposition of several different Elsasser bands. Each of the superposed bands may have different line intensities, half-widths, and spacing. As many different Elsasser bands as necessary may be superimposed in this model. Thus, all the weak spectral lines that contribute to the absorption for the path lengths and pressure considered can be included in the absorption calculations. As the number of superposed Elsasser bands becomes large, the absorption by the entire band approaches that given by the statistical band model. For N randomly superposed Elsasser bands, the absorption is given by the relation [10, 13, 71]

$$\bar{A}_N(x, \beta) = 1 - \prod_{i=1}^{N}\left[1 - \bar{A}_{E,i}\left(x_i, \beta_i\right)/\delta_i\right] \qquad (3.41)$$

where $\bar{A}_{E,i}\left(x_i, \beta_i\right)$ is the absorptance of the ith Elsasser band and

is given by

$$\bar{A}_{E,i}/\delta_i = \int_0^\infty \bar{A}_{E,i}(x_i, \beta_i)\, P_E(S_i, S_{oi})\, dS_i \,. \tag{3.42}$$

With known intensity relations between individual sub-bands (e.g., two Elsasser bands with one having five times more intensity than the other, etc.), the general result for the absorption from a random superposition of N Elsasser band can be obtained from the preceding equations.

As a special case, if exponential distribution of intensity for narrow Elsasser band is assumed, then

$$P_E(S_i, S_{oi}) = (1/S_{oi}) \exp(-S_i/S_{oi}) \,, \tag{3.43}$$

and Eq. (3.42) becomes

$$\bar{A}_{E,i}/\delta_i = (\beta_i x_{oi} \sinh \beta_i)\Big/\left[(\beta_i x_{oi} \sinh \beta_i + \cosh \beta_i)^2 - 1\right]^{1/2} \,. \tag{3.44}$$

A combination of Eqs. (3.41) and (3.44) yields the expression for absorptance by a modified random Elsasser band model as

$$\bar{A}_N(x_o, \beta) = (\beta x_o \sinh \beta)\Big/\left[(\beta x_o \sinh \beta + \cosh \beta)^2 - 1\right]^{1/2} \,. \tag{3.45}$$

The weak-line approximation for the random Elsasser model, in general, can easily be found to be

$$\bar{A}_N(x, \beta) = 1 - \prod_{i=1}^{N}\left[\exp(-\beta_i x_i)\right] \,. \tag{3.46}$$

The weak line approximation corresponding to Eq. (3.45) will be the same as for the general statistical model. The strong-line approximation for the random Elsasser model, in general, is given by

$$\bar{A}_N(x, \beta) = 1 - \prod_{i=1}^{N}\left\{1 - \operatorname{erf}\left[\left(\tfrac{1}{2}\beta_i^2 x_i\right)^{1/2}\right]\right\} \,. \tag{3.47}$$

For the modified random Elsasser model the strong-line approximation is given by Eq. (3.32b) where x is replaced by x_o .

The nonoverlapping line approximation and the square root limit for the modified random Elsasser model are given by the analogous expressions for the general statistical model.

The results of Eq. (3.45), along with the limiting solutions, are discussed in detail in [16].

3.2.4. Quasi-Random Band Model

Quasirandom model is probably the best model to represent the absorption of a vibration-rotation band quite accurately. It assumes neither a regular nor a random spacing of the spectral lines. The essential feature of this model is to divide the wider frequency interval of the actual band into much narrower subintervals. In each of these subintervals, the spectral lines are assumed to have random spacing. In this manner, the model accounts for the actual intensity distribution of strong as well as weak spectral lines. The absorption of the narrow spectral interval is calculated from the relation of a single-line absorption over a finite interval. The absorption of each of the n lines in the narrow interval is calculated separately and the results are combined by assuming a random position for the lines within the interval. The total band absorptance is calculated by averaging the results from the smaller intervals.

The fundamental features of the quasi-random band model are discussed, in detail, in references [12, 14, 15]. The procedure for calculating the atmospheric transmittance by employing the quasi-random band model is discussed, in detail, in [15] where a listing of the computer program is also provided. Since, in the final analysis, the quasi-random band model requires detailed spectroscopic information on the specific molecule under consideration, it has not been included in the present general parametric study.

The absorption by four narrow band models (Elsasser, general statistical, uniform statistical, and modified random Elsasser) are compared in Figure 3.8 for three different values of β .

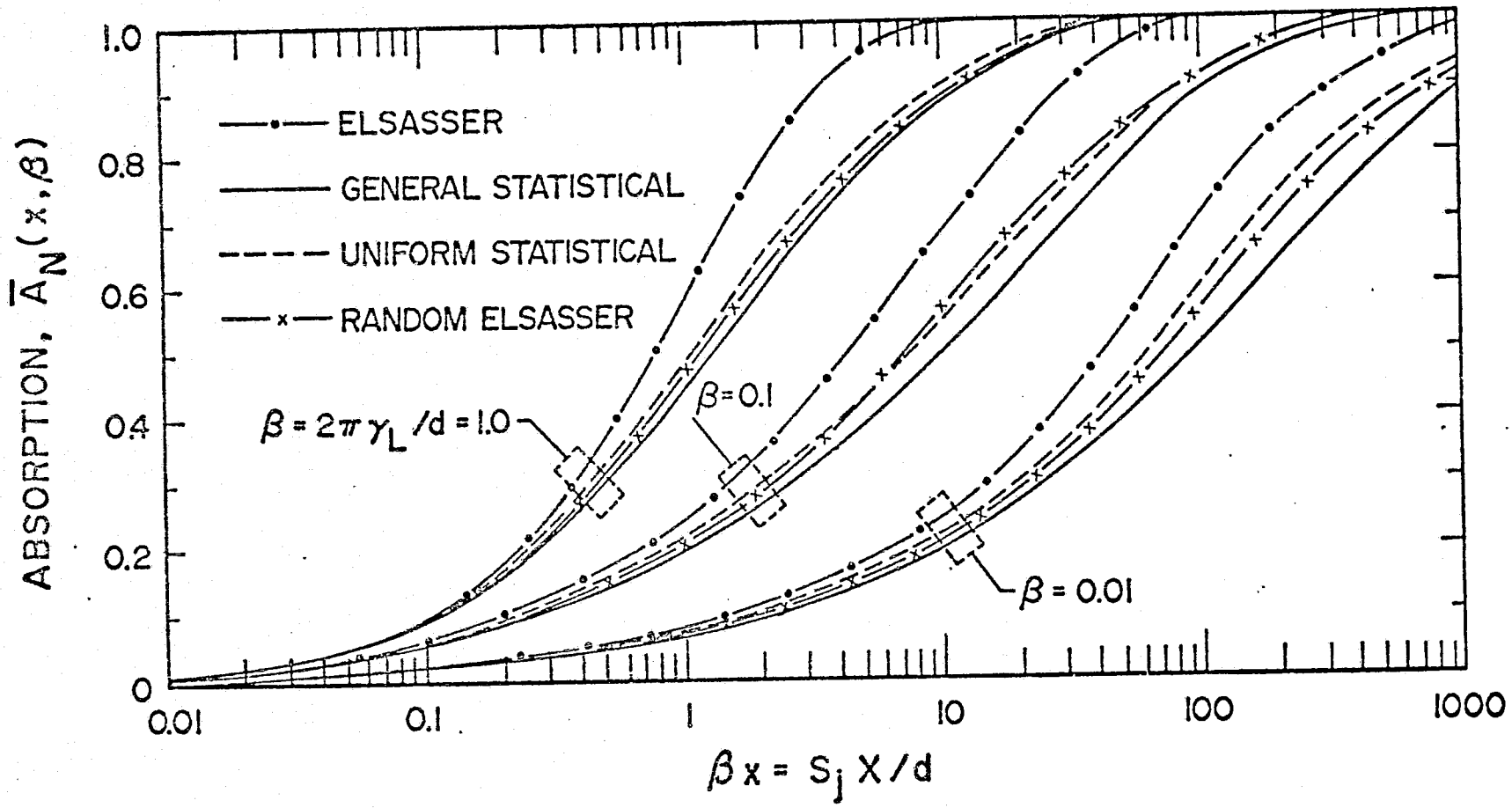

Fig. 3.8 Comparison of absorption by narrow band models.

Since the absorption at small path lengths is a function solely of the total intensity of absorbing lines, the results by all models agree well in this region. At larger path lengths, however, the Elsasser theory predicts higher absorption than the general or uniform statistical model. As pointed out earlier, this is because there is always more overlapping of the spectral lines in the statistical models than in the regular Elsasser band.

The narrow band model formulations discussed thus far represent absorptions of gases under homogeneous conditions. They can be extended to nonisothermal nonhomogeneous optical paths by employing various scaling approximations available in the literature. The original Curtis-Godson approximation [81, 82] for computing atmospheric transmission along an inhomogeneous path has been updated and several improved approximations are now available in the literature [13, 75, 76, 83-90]. In infrared signature work, it becomes essential to use an absorption model for a single highly inhomogeneous optical path [75]. For many atmospheric applications, however, the atmosphere can be divided into an appropriate number of homogeneous layers and the models discussed in this report can be divided into an appropriate number of homogeneous layers and the models discussed in this report can be employed directly [4, 14, 15, 88, 90]. In most cases this gives better results than any scaling technique employed to treat the entire atmosphere as a single layer.

3.3. Wide Band Models

Aside from the narrow band models discussed in the previous section, there are also available in literature the so-called wide band models, which provide correlations that are valid over the entire band pass [16-20, 91-94]. Besides possessing the conventional linear and square root limits, these models also possess another asymptotic limit, which is called the logarithmic limit. Even though the use of these models may be restricted for atmospheric applications, they do provide a quick and accurate information regarding transmittance of gases at moderately high temperatures. As such,

these models are quite useful in many engineering applications (for some recent applications, see [19, 95-102]).

3.3.1. Box (or Coffin) Model

The simplest of the wide band models is the box model which was introduced first by Penner [22]. For this model, it is assumed that the absorption coefficient, κ_ω, is constant over an effective band width $\Delta\omega$. The expression for the total absorptance by this model is given as

$$A = \int_{\Delta\omega} \left[1 - \exp\left(-\kappa_\omega X\right)\right] d\omega = (\Delta\omega)_e \left[1 - e^{-\bar{\kappa}X}\right] \tag{3.48}$$

where $(\Delta\omega)_e$ is the effective band width, and $\bar{\kappa}$ is the mean absorption coefficient for the interval $(\Delta\omega)_e$. At relatively high temperatures, the spectral intervals between fundamental bands of infrared active gases are filled by the combination and overtone bands. Under these conditions, modified forms of the box model become useful in radiative transfer calculations [103]. Further discussion and application of the box model is available in references [16, 22, 104].

3.3.2. Exponential Wide Band Model

Edwards et al. [91, 92] have considered various wide band models (rigid rotator, non-rigid rotator, and arbitrary) and have concluded that three parameters (the mean line intensity to spacing ratio, the mean line-width to spacing ratio, and the effective broadening pressure) are necessary for a complete description of the band absorption. For complete discussions of these models and their limiting forms, one should refer to [16-20, 91-94]. The final form of the total band absorptance relation presented by Edwards et al. [91, 99] is based on the formulation of the narrow statistical band model. The expression for the transmissivity employed in this model is given by

$$\tau_j = \prod_{j=1}^{N} \tau_{\omega j} = (1/\Delta\omega) \int_{\omega-(\Delta\omega/2)}^{\omega+(\Delta\omega/2)} \left[\exp\left(-\kappa_\omega X\right)\right] d\omega \qquad (3.49a)$$

$$\simeq \exp\left(-\left(S_j/d\right) X/\left\{1 + \left[\left(S_j/d\right) X/B\, P_e\right]\right\}^{1/2}\right) , \qquad (3.49b)$$

where B is π times the mean line width to spacing ratio for a dilute mixture at one atmospheric pressure, and P_e is an equivalent broadening pressure. Use of Eq. (3.49b) also was made by Felske and Tien [94] to develop relations for the wide band absorptance from the general statistical band model.

In the present study, four different formulations for the total band absorptance are presented. These are based on various narrow band model relation for absorption. For an exponential wide band if one assumes that the line intensity is an exponential decaying function of the wave number [92, 99], then

$$S_j/d = \left(S/A_o\right) \left(\exp\left\{\left[-b_o|\omega - \omega_o|\right]/A_o\right\}\right) = \left(S/A_o\right) \zeta , \qquad (3.50)$$

where S is the integrated intensity of a wide band, $A_o = nd$, $b_o = 2$ for a symmetrical band and $b_o = 1$ for bands with upper and lower wave number heads at ω_o. Equation (3.50) is used in the relation for absorption of a narrow band model and the resulting expression is integrated over the entire band pass to obtain the total absorptance of a wide band as

$$\left.\begin{aligned} \bar{A}(u, \beta) = A(u, \beta)/A_o &= \int_{\substack{\text{wide}\\ \text{band}}} \bar{A}_N(u, \beta)\, d\left(\omega - \omega_o\right) \\ &= b_o \int_o^\infty \bar{A}_N(u, \beta, \zeta)\, d\zeta , \end{aligned}\right\} \qquad (3.51)$$

where $u = S\, X/A_o = S\, P\, \ell/A_o$. The second form of Eq. (3.51) incorporates the relation given by Eq. (3.50).

3.3.2.1. Exponential Wide Band Absorptance from the Elsasser Model. By substituting Eq. (3.50) into Eq. (3.11), the expression for absorptance by the Elsasser band can be written as

$$\bar{A}_N(u, \beta) = 1 - (1/2\pi) \int_{-\pi}^{\pi} \exp[-F_1(u, \beta, z, \zeta)]\, dz \qquad (3.52)$$

where $F_1 = u\zeta \sinh \beta/(\cosh \beta - \cos z)$ and ζ is defined in Eq. (3.50). It should be emphasized here that within a narrow Elsasser band the line intensities are constant but over a wide spectral interval the line intensity variation is given by the Eq. (3.50). A combination of Eqs. (3.51) and (3.52) results in

$$\bar{A}(u, \beta) = (1/\pi) \int_0^{\pi} \left\{ \int_0^1 \zeta^{-1} \left[F_2(u, \beta, z, \zeta)\right] d\zeta \right\} dz \ , \qquad (3.53)$$

where $F_2 = 1 - \exp(-F_1)$. The inner integral in Eq. (3.53) can be evaluated in closed form as

$$\int_0^v \{[1 - \exp(-\psi\zeta)]/\zeta\}\, d\zeta = \gamma + \ell n(\psi v) + E_1(\psi v) \ , \qquad (3.54)$$

where $\psi = F_1/\zeta$, $v = 1$, $\gamma = 0.5772156$ is the Euler's constant, and $E_1(t)$ is the exponential integral of the first order. The final form of the exponential wide band absorptance (based on the narrow Elsasser model) is obtained by combining Eqs. (3.53) and (3.54) as

$$\bar{A}(u, \beta) = \gamma + (1/\pi) \int_0^{\pi} [\ell n\ \psi + E_1(\psi)]\, dz \ . \qquad (3.55)$$

Equation (3.55) can be reduced to several useful limiting forms. One of the important forms is obtained when the weak line approximation for the Elsasser model is valid. Since this approximation is valid for large pressures, the limiting form of the total band absorptance in this case is obtained by letting $\beta \to \infty$ in Eq. (3.55). Alternately, this form can be obtained by combining Eqs. (3.14), (3.50), and (3.51) as

$$\left.\begin{aligned} \bar{A}(u) &= \int_0^1 \zeta^{-1}[1 - \exp(-u\zeta)]d\zeta \\ &= \gamma + \ell n(u) + E_1(u) \ . \end{aligned}\right\} (3.56)$$

Note that in this limit the absorptance is independent of the line structure parameter β. For $u > 10$, $E_1(u) < 10^{-5}$, and Eq. (3.56) reduces to $\bar{A}(u) = \gamma + \ell n(u)$, and for $u \leq 0.005$, it is approximately equal to u. Thus, one can write

$$\left.\begin{aligned} \bar{A} &= u , && (u << 1 , \ \beta > 1) \\ \bar{A} &= \gamma + \ell n(u) , && (u >> 1 , \ \beta > 1) \end{aligned}\right\} \tag{3.57}$$

which are the appropriate linear and logarithmic limits of Eqs. (3.55) and (3.56).

When strong line approximation is justified, then the absorption of a narrow Elsasser band is given by the Eq. (3.15). By combining Eqs. (3.15), (3.50) and (3.51), the relation for the strong line approximation for the wide band is obtained as

$$\bar{A}(u, \beta) = \int_0^1 \zeta^{-1} \left\{ \operatorname{erf} \left[(u\beta\zeta/2)^{1/2} \right] \right\} d\zeta . \tag{3.58}$$

By introducing a new variable $t^2 = u\beta\zeta/2$, Eq. (3.58) can be written as

$$\bar{A}(u, \beta) = 2 \int_0^{\sqrt{(u\beta/2)}} t^{-1} \operatorname{erf}(t) \, dt . \tag{3.59}$$

For all values of t, the series expansion for the error function is given by

$$\operatorname{erf}(t) = (2/\sqrt{\pi}) \sum_{n=0}^{\infty} \left\{ (-1)^n \, t^{(2n+1)} / [n!(2n+1)] \right\} . \tag{3.60}$$

Upon substituting (3.60) into (3.59), interchanging the summation and integration, and integrating the resulting expression, there is obtained

$$\bar{A}(u, \beta) = (4/\sqrt{\pi}) \sum_{n=0}^{\infty} \left\{ (-1)^n \, (u\beta/2)^{(2n+1)/2} / [n!(2n+1)^2] \right\} , \tag{3.61}$$

This can be considered a closed form expression for the strong line approximation.

According to the requirements of the square root limit (see Eq. (3.18)), retaining only the first term in Eq. (3.61) results in

$$\bar{A}(u, \beta) = (4/\sqrt{\pi})\ (u\beta/2)^{1/2} = 2(2\beta u/\pi)^{1/2} , \quad \beta << 1 ,$$

$$u/\beta >> 1 , \quad \beta u << 1 , \tag{3.62}$$

which is the correct square root limit for the wide band absorption [19, 105]. Thus, Eq. (3.55) is seen to reduce to correct limiting forms in the linear, square root and logarithmic limits.

Since Eq. (3.55) involves double integration, its application in some radiative transfer analyses may require considerably long computational time. This, sometimes, can be avoided by expressing the equation in a series form. In order to do this, Eq. (3.53) is first written as

$$\bar{A}(u, \beta) = \int_0^1 \left(\frac{1}{\pi} \int_0^{\pi} \{1 - \exp[A\zeta/(1 - B \cos z)]\}\, dz\right) \zeta^{-1}\, d\zeta , \tag{3.63}$$

where $A = -u \tanh \beta$, and $B = 1/\cosh \beta$. The inner integral in this equation can be evaluated in a series form such that

$$\bar{A}(u, \beta) = \int_0^1 \left\{ \sum_{n=1}^{\infty} - (A)^n \zeta^n [SUM(mn)] \Big/ \left[(B + 1)^n\, n!\, (n - 1)!\right] \right\} \zeta^{-1}\, d\zeta , \tag{3.64}$$

where

$$SUM(mn) = \sum_{m=0}^{\infty} \left[(n + m - 1)!\ (2m - 1)!\ C^m\right] \Big/ \left[2^m (m!)^2\right] ,$$

$$C = 2/(1 + \cosh \beta) = 2B/(B + 1) .$$

Integration over ζ in this equation gives a value of $(1/n)$. Thus, the solution of Eq. (3.53) or (3.55) in the series representation (which converges rapidly) is given by

$$\bar{A}(u, \beta) = \sum_{n=1}^{\infty} \left\{ -(A)^n \, [SUM(mn)] \Big/ \left[n(B + 1)^n \, n! (n - 1)! \right] \right\} . \qquad (3.65)$$

The solutions of Eqs. (3.55), (3.56), (3.61), and (3.65) are illustrated in Figure 3.9 along with the limiting solutions for four different values of the line structure parameter $t = \beta/2 = \pi\gamma/d$. No difference in the results of Eqs. (3.55) and (3.65) were noticed. As such, the solution given by Eq. (3.65) is treated as the "exact" solution. The uppermost curve in the figure represents the solution of Eq. (3.56). For $t \geq 1$, the results of Eqs. (3.55) and (3.56) are identical. For comparison, the theoretical results obtained by Hsieh and Greif [105] are shown also in Figure 3.9. As would be expected, the comparison is not very good at large path lengths.

3.3.2.2. Exponential Wide Band Absorptance from the Uniform Statistical Model. Upon combining Eqs. (3.27) and (3.50) an expression for absorption by the uniform statistical model is obtained which, in turn, is used in Eq. (4.4) to find the relation for the wide band absorptance as

$$\bar{A}(u, \beta) = \int_0^1 \{1 - \exp[-\beta \, L(\eta)]\} \, \zeta^{-1} \, d\zeta , \qquad (3.66)$$

where $\eta = u\zeta/\beta$, ζ is defined in Eq. (3.50), and $L(\eta)$ is defined in Eq. (2.28a). Equation (3.66) requires considerably long time for numerical solution. To save the computational time, function $L(\eta)$ can be replaced by Goldman's approximation (see Eqs. (2.29e) and (3.28)) and this results in

$$\bar{A}(u, \beta) = \int_0^1 \left(1 - \exp\left\{ -\beta\eta \Big/ \left[1 + (\pi\eta/2)^{5/4} \right]^{2/5} \right\} \right) \zeta^{-1} \, d\zeta . \qquad (3.67)$$

Numerical results of Eqs. (3.66) and (3.67) are identical and are in good agreement with the theoretical results of Hsieh and Greif [105] over the entire range of u and β (see Ref. [16]).

For sufficiently small η (i.e., for small u/β), function $L(\eta)$ reduces to η and Eq. (3.66) yields the result for the weak line approximation as

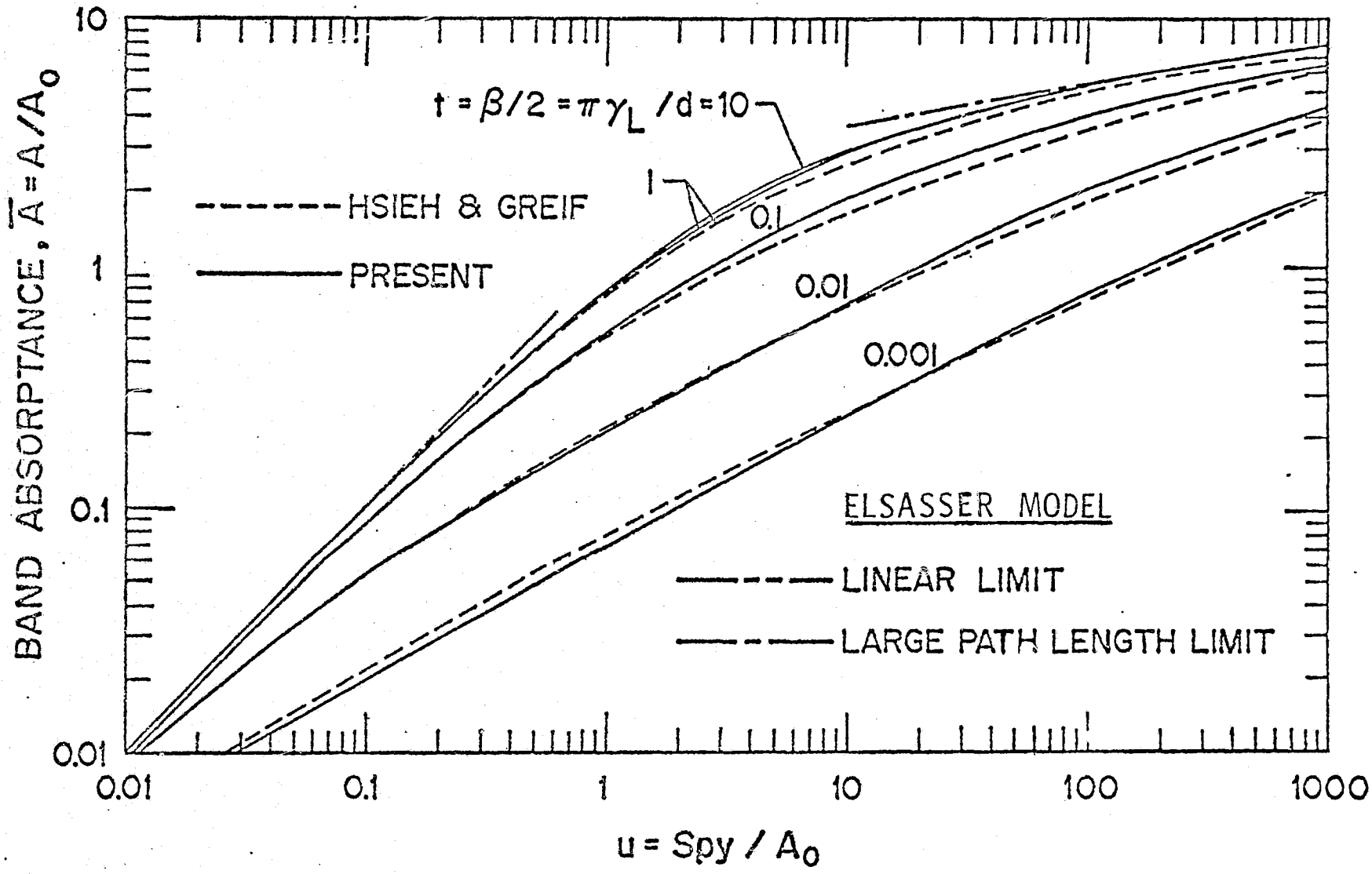

Fig. 3.9 Wide band absorptance based on narrow Elsasser model.

$$\bar{A}(u) = \int_0^1 [1 - \exp(-u\,\zeta)]\,\zeta^{-1}\,d\zeta$$
$$= \gamma + \ell n(u) + E_1(u) \ .$$

This is exactly the same as Eq. (3.56) and is independent of the line structure parameter β . The linear and logarithmic limits of Eq. (3.66), therefore, are given by the Eq. (3.57).

For large η , $L(\eta) \simeq (2\eta/\pi)^{1/2}$, and Eq. (3.66) reduces to the strong line approximation as

$$\bar{A}(u,\ \beta) = \int_0^1 \left\{1 - \exp\left[-(2\beta u\zeta/\pi)^{1/2}\right]\right\}\zeta^{-1}\,d\zeta$$
$$= 2\left\{\gamma + \frac{1}{2}\,\ell n(2\beta u/\pi) + E_1\left[(2\beta u/\pi)^{1/2}\right]\right\} \ . \qquad (3.68)$$

For $\beta u << 1$, this reduces to the correct square root limit as given by Eq. (3.62).

It should be emphasized here that the absorptance of a wide band, as obtained from both the narrow Elsasser and uniform statistical models, is the same at sufficiently high pressures. As such, for gases whose spectral behavior could be described either by a narrow Elsasser or a uniform statistical model, the use of Eq. (3.56) should be made in radiative transfer calculations at moderately high pressures ($P \geq 1$ atm).

3.3.2.3. Exponential Wide Band Absorptance from the General Statistical Model. For the sake of completeness and comparison of results, the relation for the wide band absorptance formulated by Felske and Tien [94] is presented here. This may be obtained by combining Eqs. (2.16), (3.49b) and (3.50) as

$$\left.\begin{aligned}\bar{A}(u,\ \beta) = \int_0^1 \left\{[1 - \exp(-\rho t)]/[\xi^2 + (2\rho_u)^2]^{1/2}\right\} d\xi \\ + \int_0^1 \{[1 - \exp(-\rho t)]/\xi\}\,d\xi \ ,\end{aligned}\right\} \qquad (3.69)$$

where

$$\rho = [1 - (u\zeta/t)] - 1/[1 + (u\zeta/t)] ,$$

$$\rho_u = \{(t/u)\ [1 + (t/u)]\}^{-1/2} ,$$

$$\xi = \rho/\rho_u , \quad t = \beta/2 = \pi\gamma_L/d ,$$

(3.69 cont'd)

In the linear and logarithmic limits, Eq. (3.69) reduces to the expressions given by Eq. (3.57), and in the square root limit it reduces to Eq. (3.62). The solutions of Eq. (3.69) are illustrated in Figure 3.10 along with the limiting solutions.

3.3.2.4. Exponential Wide Band Absorptance from the Random Elsasser Model. By combining Eqs. (3.42), (3.44), (3.50), and (3.51), the expression for the total band absorptance for this case can be written as

$$\bar{A}(u, \beta) = \int_0^1 \left(1 - \sum_{i=1}^{N} \left\{1 - \left[u_i\zeta \sinh \beta_i / G_1(u_i, \beta_i)\right]\right\}\right) \frac{d\zeta}{\zeta} , \qquad (3.70)$$

where

$$G_1(u_i, \beta_i) = \left[(u_i\zeta \sinh \beta_i + \cosh \beta_i)^2 - 1\right] .$$

This is the general result for absorptance derived from the narrow random Elsasser model. The special form of this equation is obtained for $N = 1$ as

$$\bar{A}(u, \beta) = \int_0^1 [u \sinh \beta / G_1(u, \beta)]\, d\zeta . \qquad (3.71)$$

Note that Eq. (3.71) could have also been obtained by combining Eqs. (3.46), (3.50), and (3.51). The solution of Eq. (3.71) is found to be

$$\bar{A}(u, \beta) = \ln\{[G_2(u, \beta) + u \sinh \beta + \cosh \beta]/(\sinh \beta + \cosh \beta)\} , \qquad (3.72)$$

where

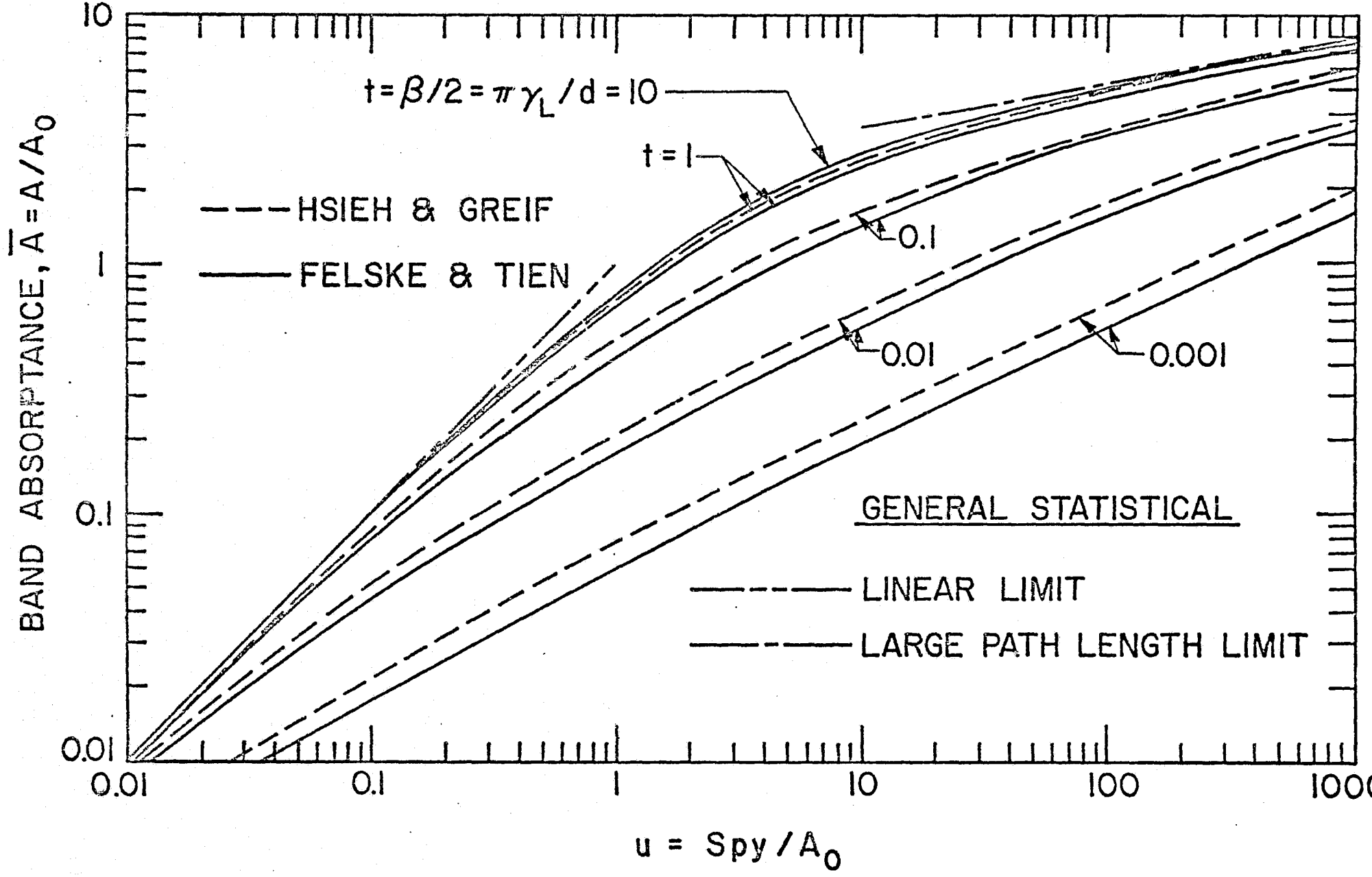

Fig. 3.10 Wide band absorptance based on narrow general statistical model.

$$G(u, \beta) = [(u^2 + 1) \sinh^2 \beta + 2u \sinh \beta \cosh \beta]^{1/2} .$$

It can be shown easily that Eq. (3.72) reduces to the correct limiting forms in the linear, square root, and logarithmic limits.

The relations for the exponential wide band absorptance given by Eqs. (3.55), (3.66), (3.69), and (3.72) are referred to as the exact relations and the numerical solutions of these equations are termed as the "exact" solutions. These solutions are compared for three different values of the line structure parameter in Figure 3.11. It is seen that the absorptance by wide band models follow the same general trend as by narrow band models illustrated in Figure 3.8. Once again it should be emphasized that, at larger path lengths, the Elsasser theory predicts higher absorption than the general or uniform statistical model. This fact is clearly evident from the results of Figures 3.8 and 3.11. For $t = \beta/2 = 1$, the absorption by the random Elsasser model in Figure 3.11 is seen to be lower than the general statistical model. This does not appear to be physically realistic because the results of random Elsasser model must fall between the results of Elsasser and general statistical models.

3.3.3. Axial or Slab Band Absorptance Model

The primary reason for employing the band absorptance models is to represent accurately the absorption-emission characteristics of a vibration-rotation band and consequently eliminate the spectral integration in the radiative flux equations. The angular dependency of radiation usually is not included in the molecular band models. In recent years, however, attempts have been made to incorporate the angular integration of the equation of radiative transfer by introducing the so-called axial or slab band absorptance models [93, 99, 100, 106]. By use of these models, in certain cases, the spectral as well as angular integration in the radiative flux equations can be avoided. The expression for the slab band absorptance can, in general be written as

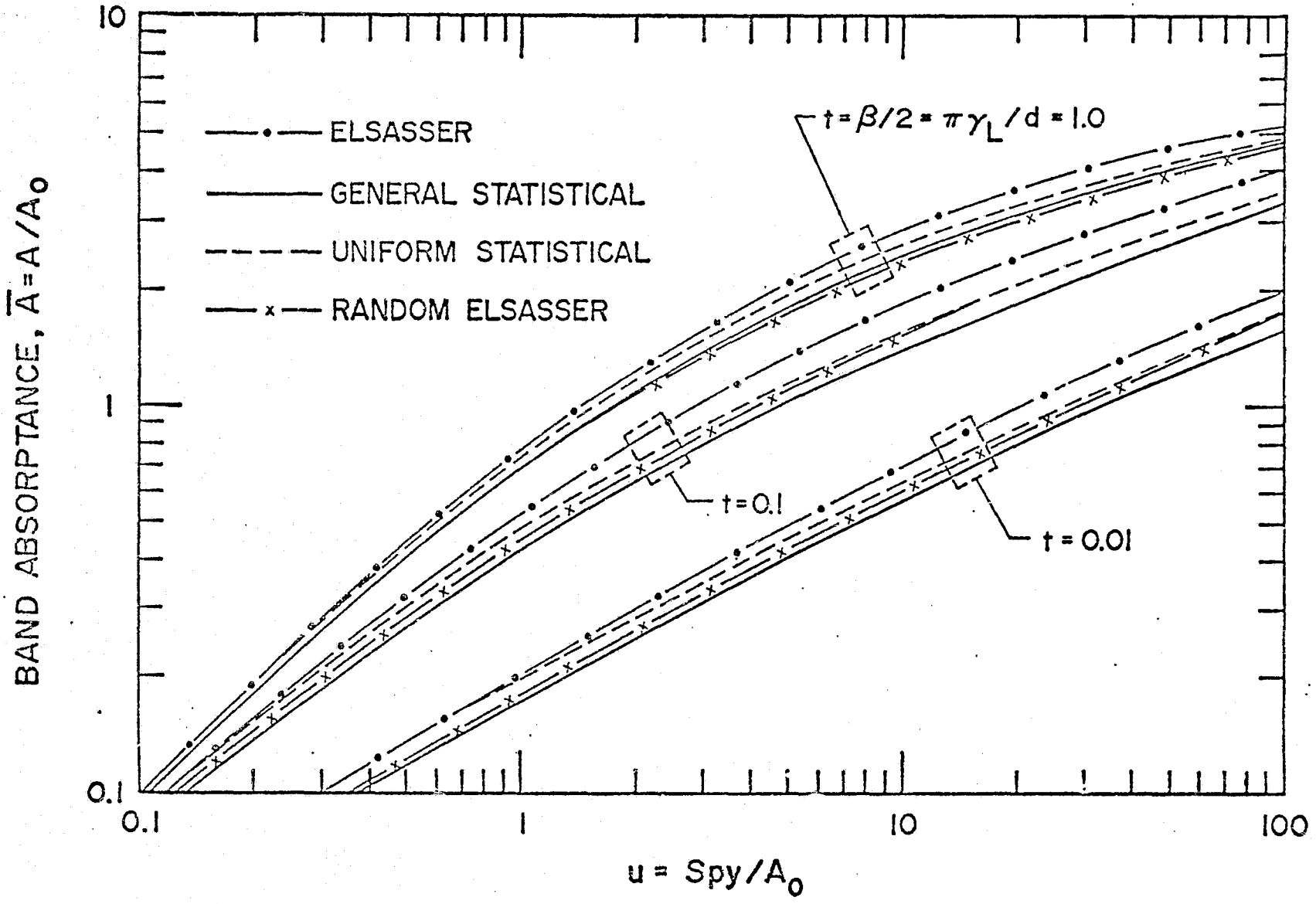

Fig. 3.11 Comparison of absorptance by wide band models.

$$\bar{A}_s(u, \beta) = 2 \int_0^1 \mu \, \bar{A}(u/\mu) \, d\mu \, , \tag{3.73}$$

where $\mu = \cos \theta$, and $\bar{A}(u/\mu)$ is the nondimensional total band absorptance. By introducing different relations for the total band absorptance in Eq. (3.73), various expressions for the slab band absorptance can be obtained.

Edwards and Balakrishnan [93] have proposed that when the pressure is high (i.e., when rotational line structure has smeared out), then the spectral absorption coefficient of many molecular gases can be represented by the exponential-winged band model and this results in an expression for the slab band absorptance as

$$\bar{A}(u) = \ell n(u) + E_1(u) + \gamma + \frac{1}{2} - E_3(u) \, , \tag{3.74}$$

where $E_n(u)$ are the exponential integral functions. As will be shown in the next section, the use of Eq. (3.74) is justified for relatively large path length values.

3.4. Band Absorptance Correlations

The divergence of radiative flux usually involves multiple integrals even for the simple case of energy transfer between a plane-parallel geometry. In order to reduce the mathematical complexities and save the computational time, it often becomes essential to express the integral form of the total band absorptance by fairly accurate continuous correlations. Several continuous relations for total absorptance of a wide band, which are valid over different values of path length and line structure parameter, are available in literature. A brief description of these correlations is given here in the sequence that they became available in the literature.

The first band absorptance correlation, satisfying the linear, square root, square root logarithmic, and logarithmic limits of a wide band absorptance, was proposed by Edwards and Menard [91]. By comparing the results of correlations in various limits with experimental data over a large range of pressure and temperature,

Edwards and co-workers have determined empirically the necessary correlation quantities $S(T)$, $A_o(T)$, and $\beta(T, P_e)$ for the important bands of CO, CO_2, H_2O, and CH_4. These results are summarized by Edwards et al. in [92].

A continuous band absorptance correlation has been proposed by Tien and Lowder [18, 107], and this is of the form

$$\bar{A} = \ell n(uf(t)\{(u + 2)/[u + 2f(t)]\} + 1) , \qquad (3.75)$$

where

$$f(t) = 2.94[1 - \exp(-2.60t)] , \quad t = \beta/2 .$$

The choice of Eq. (3.75) was based on the specification of five conditions, and the form of $f(t)$ was chosen so as to give agreement with the correlation of Edwards and Menard. This correlation does not reduce to the correct limiting form in the square root limit [19]. Extensive use of this correlation has been made in various radiative transfer analyses in the past ten years (see, for example, [19, 96, 97, 104]). The results of this correlation are compared with other correlations in Figure 3.12 for $t = \beta/2 = 0.01$ and 1. Comparative results for other t-values are available in [16, 17]. From these results it is concluded that the use of Eq. (3.75) should be restricted to relatively large β values.

Another continuous correlation for band absorptance has been proposed by Goody and Belton [108], and in terms of the present nomenclature this may be written as

$$\bar{A} = 2 \ell n\left\{1 + u/[4 + (\pi u/4t)]^{1/2}\right\} . \qquad (3.76)$$

Although this correlation satisfies the linear, square root, and logarithmic limits, its use is restricted to relatively small β values [19].

Tien and Ling [109] have proposed a simple two parameter correlation for $\bar{A}(u, \beta)$ applicable under certain thermodynamic

conditions, and this is of the form

$$\bar{A}(u) = \sinh^{-1}(u) \ . \tag{3.77}$$

This equation is valid only for the limit of large β . By obtaining the large β limit of Eq. (3.75) as

$$\bar{A}(u) = \ell n\{2.94\, u[(u + 2)/(u + 5.88)] + 1\} \ , \tag{3.78}$$

Tien and Ling have shown that throughout the whole range of u , the maximum deviation of Eq. (3.77) from Eq. (3.78) never exceeds seven percent.

A relatively simple continuous correlation for band absorptance, which was introduced first by Cess and Tiwari [19] and later applied by Cess and Ramanathan [110], is given by

$$\bar{A}(u, \beta) = 2\, \ell n\left(1 + u/\left\{2 + [u(1 + 1/\bar{\beta})]^{1/2}\right\}\right) \ , \tag{3.79}$$

where $\bar{\beta} = 4t/\pi = 2\beta/\pi$. It is seen from Figure 3.12 (number 3 curves) that this correlation yields lower absorptance than other correlations over the entire range of path length. As such, use of this correlation is justified, at relatively high pressures, to gases whose spectral behavior can be described by the general statistical model.

In the limit of large pressures (i.e., large β limit), the relation for the slab band absorptance proposed by Edwards and Balakrishnan, Eq. (3.74), can be treated as another correlation for the total band absorptance. The results of this correlation are found to be valid only at large path lengths. [16, 17].

Based upon the formulation of the total band absorptance from the general statistical model, as given by Eq. (3.69), Felske and Tien [94] have proposed a continuous correlation for $\bar{A}(u, \beta)$ as

$$\bar{A}(u, \beta) = 2E_1(t\rho_u) + E_1(\rho_u/2) - E_1[(\rho_u/2)\ (1 + 2t)] + \ell n[(t\rho_u)^2/(1 + 2t)] + 2\gamma \ . \tag{3.80}$$

This correlation is valid for the entire range of the governing parameters. Further discussion of the validity of this correlation is given in the next section.

Another form of the band absorptance correlation is obtained by slightly modifying the original correlation proposed by Cess and Tiwari as

$$\bar{A}(u, \beta) = 2 \ln\left(1 + u/\left\{2 + [u(C + \pi/2\beta)]^{1/2}\right\}\right), \qquad (3.81)$$

where $C \leq 1$. A value of $C = 1$ was suggested in [19]. For $\beta \leq 1$, $C = 0.1$ gives an accurate fit for all path lengths. For $\beta > 1$ and $u \leq 1$, C again is equal to 0.1, but for $\beta > 1$ and $u > 1$ a value of $C = 0.25$ should be used. If it is desired to use only one value of C for all β and path lengths, the value of $C = 0.1$ is recommended. It should be pointed out here that both Eqs. (3.79) and (3.80) reduce to the correct limiting forms suggested in [19, 91]. The results of this correlation (number 6 curves) are in general agreement with the results of Eq. (3.80) for all u and β values.

The form of the absorptance given by Eq. (3.56) can be treated as another correlation for the total band absorptance. It should be emphasized here that the only restriction in the use of Eq. (3.56) is that the pressure must be sufficiently high. Thus, use of Eq. (3.56) is justified at all path lengths for $t = \beta/2 \geq 1$ [16, 17].

For gases whose spectral characteristics warrant use of the Elsasser model, the series form solution given by Eq. (3.65) can be regarded as another correlation for the total band absorptance. As pointed out earlier, the series in Eq. (3.65) converges very rapidly and the results obtained by this are in excellent agreement with the numerical solution of Eq. (3.55). Thus, use of this correlation in actual radiative transfer problems will provide mathematical flexibilities as well as will result in saving of computational time.

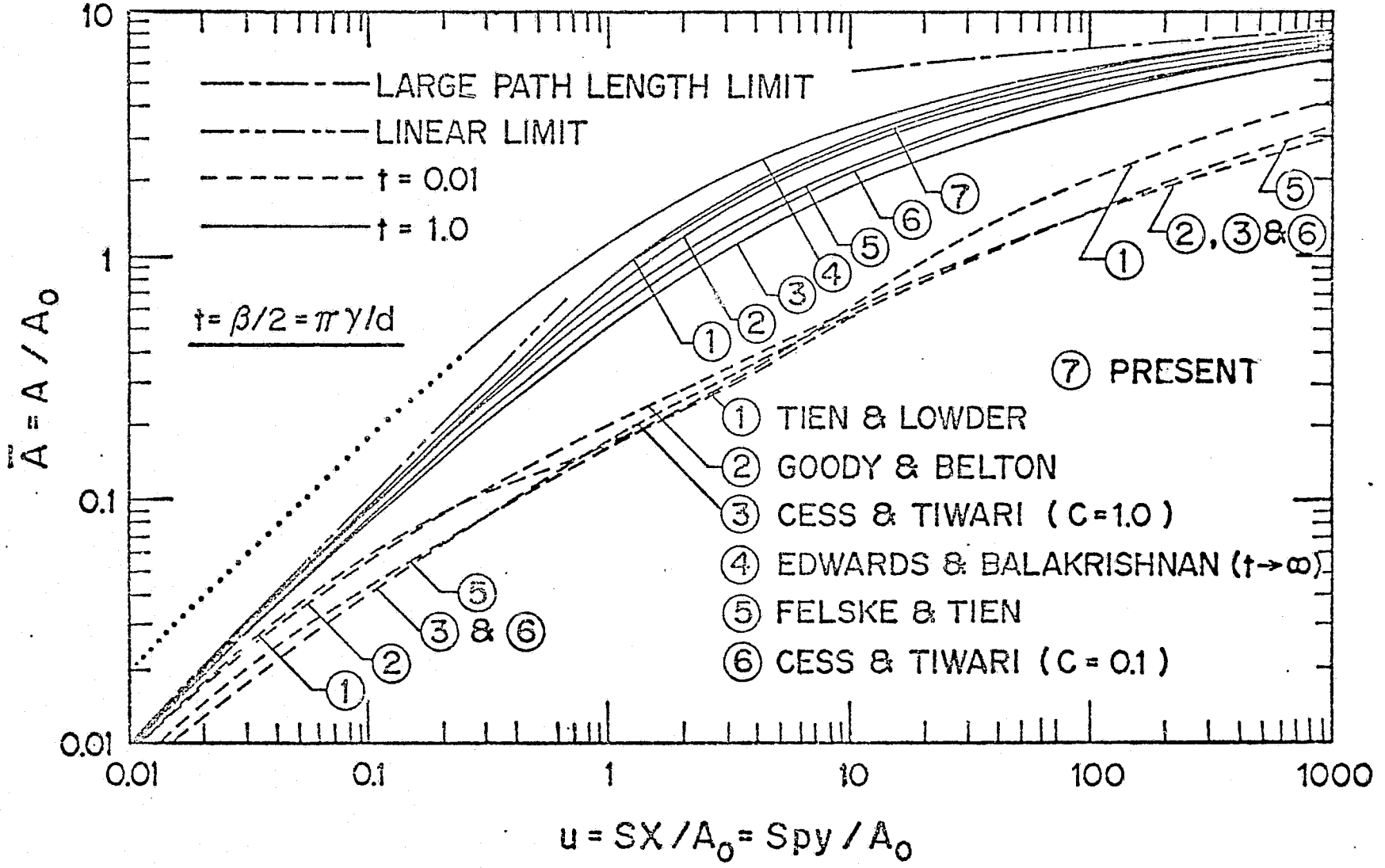

Fig. 3.12 Comparison of results of band absorptance correlations.

3.5. Comparison of Wide Band Absorptance Results

The results of different correlations have been compared with each "exact" solution of the wide band absorptance in this section. In comparing the results of a correlation with an "exact" solution, the limitations of both the particular correlation and the exact solution must be noted. A correlation developed from the general statistical model should not be expected to give good agreement when compared with the exact solution based on the Elsasser model, or vice versa.

The wide band absorptance results of various correlations are compared with the wide band "exact" solutions based on the Elsasser and general statistical models in Figures 3.13-3.16 for different values of the line structure parameter $t = \beta/2$. Comparative results based on the uniform statistical and random Elsasser models are given in [16, 17]. As would be expected, maximum errors (in most cases) occur in the intermediate path lengths. This is because most correlations are developed to satisfy at least the linear and logarithmic limits. As discussed earlier, the correlation presented by Edwards and Balakrishnan for large β is seen to be valid only for relatively large u values. In general, the correlation by Tien and Lowder appears to give maximum errors for low β values. The correlation by Goody and Belton gives maximum errors for large u and large β values (because its use is restricted to relatively small values of β [19]).

The maximum error by Felske and Tien's correlation is +25% (at $t = 0.1$, $u = 0.5$) for the case when it is compared with the exact solution based on the Elsasser model (see Figure 3.13). The maximum error by Cess and Tiwari's correlation is +30% (at $t = 0.1$, $u = 10$) and it is also for the case compared with the exact solution based on the Elsasser model (Figure 3.13, curve 6). The advantage in using Eq. (3.81) is that it does not involve any exponential integral and therefore requires significantly less computational time for radiative transfer analyses.

For $t = 1$, the results of correlation given by Eq. (3.56) are within 0.6% of the exact solution based on the Elsasser model

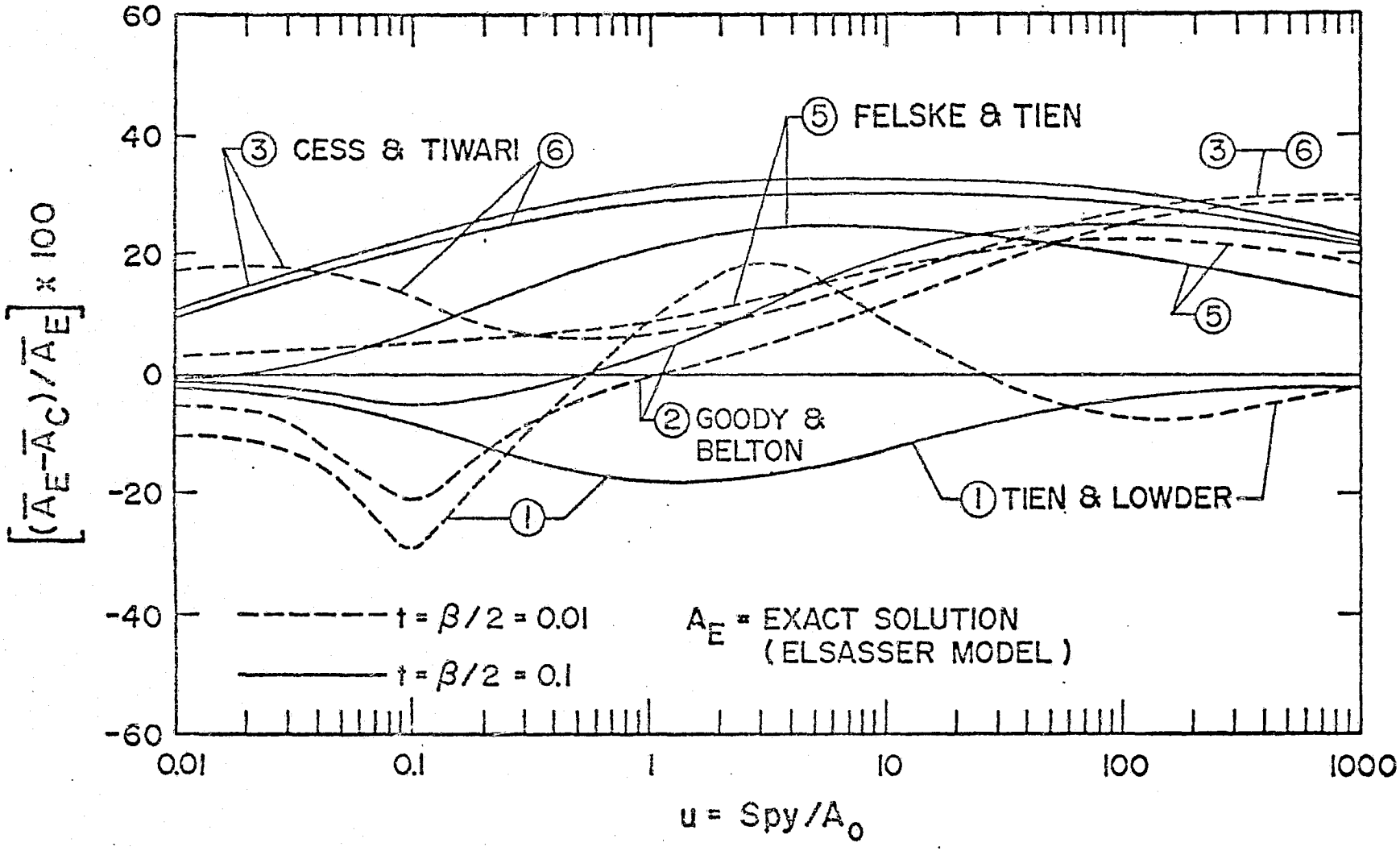

Fig. 3.13 Errors in the band absorptance correlations when compared with the exact solution (Elsasser Model) for t = 0.01 and 0.1.

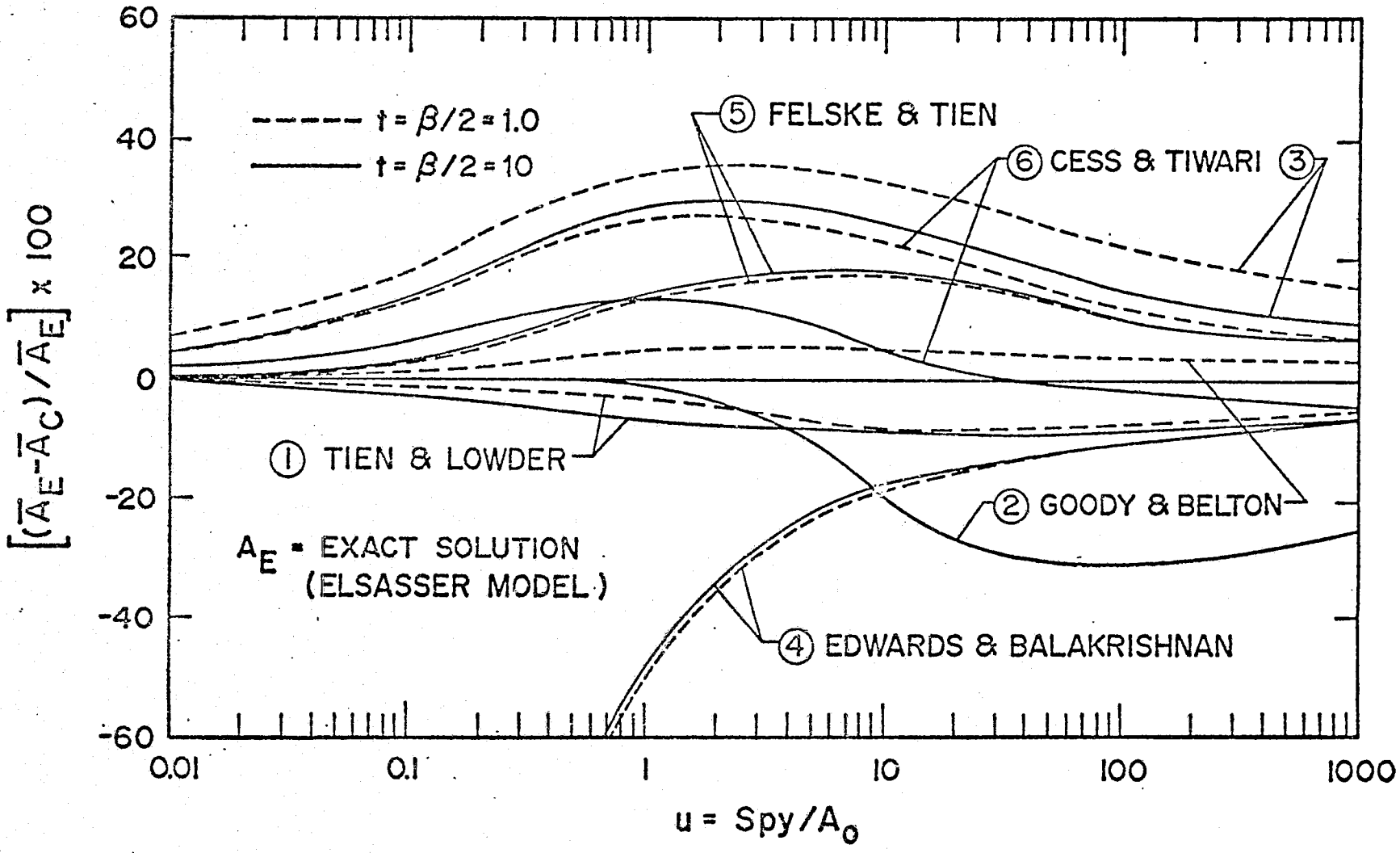

Fig. 3.14 Errors in the band absorptance correlations when compared with the exact solution (Elsasser Model) for t = 1 and 10.

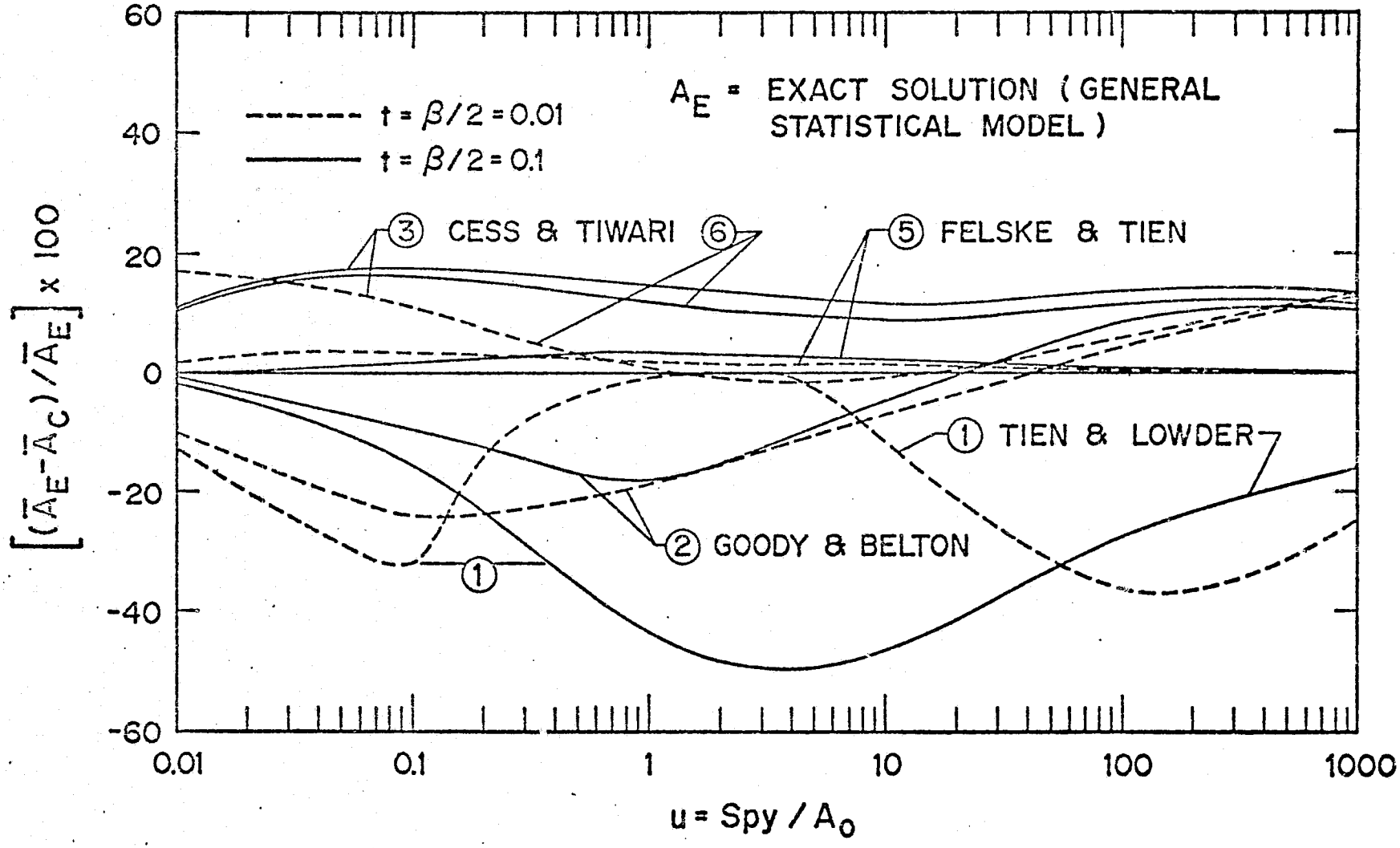

Fig. 3.15 Errors in the band absorptance correlations when compared with the exact solution (General Statistical Model) for t = 0.01 and 0.1.

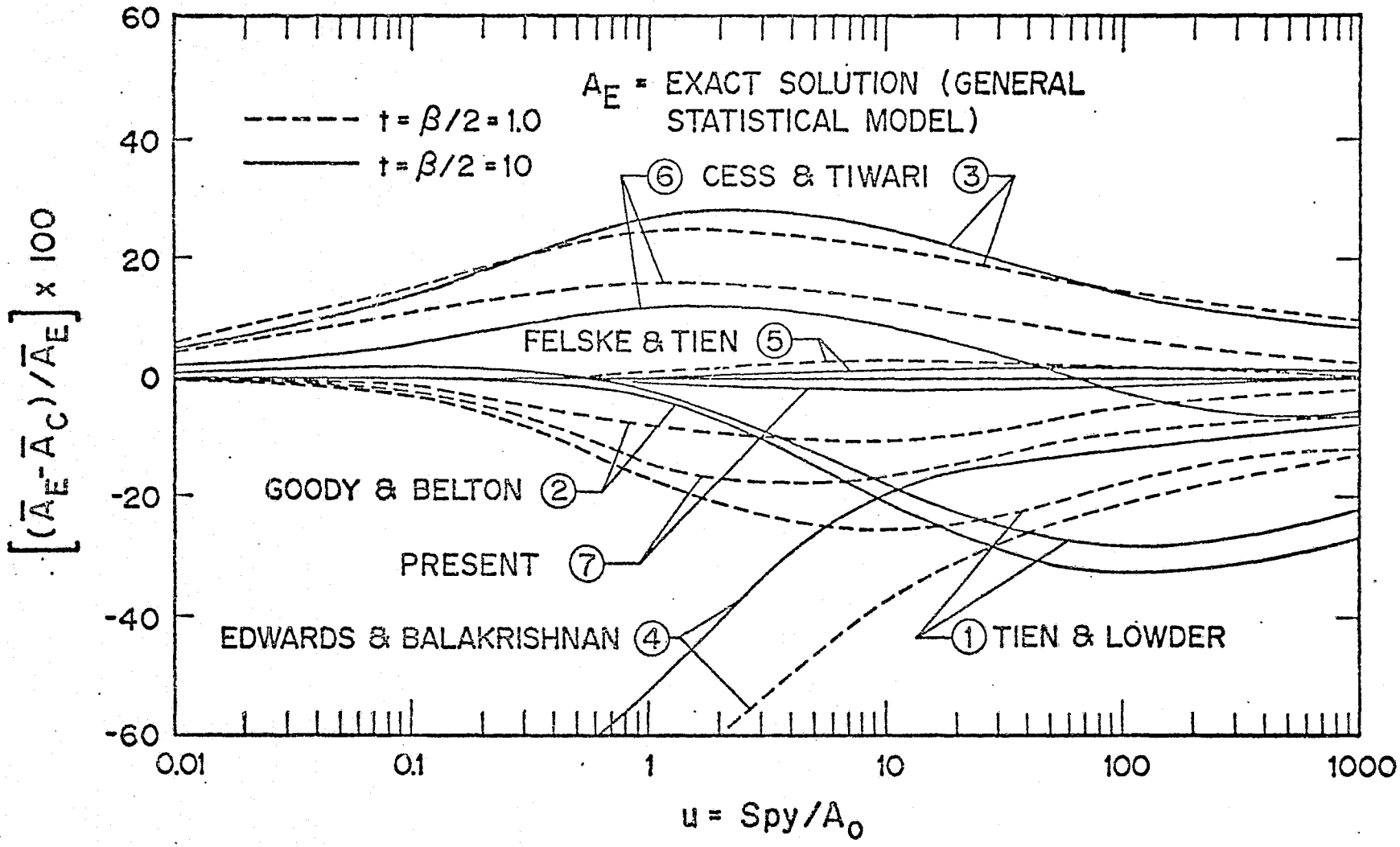

Fig. 3.16 Errors in the band absorptance correlations when compared with the exact solution (General Statistical Model) for t = 1 and 10.

and therefore could not be shown in Figure 3.14. For $t > 1$, the results of Eqs. (3.55) and (3.56) are identical for all path lengths. When compared with the exact solution based on the uniform statistical model [16, 17], the results of Eq. (3.56) indicate a maximum error of about 11% for $t = 1$ and 0.7% for $t = 10$. When compared with the exact solution based on the general statistical model (Figure 3.16), the results of Eq. (3.56) indicate a maximum error of about 18% for $t = 1$ and 2% for $t = 10$. The use of Eq. (3.56) should, therefore, be made in all cases at sufficiently high pressure ($P = 1$ atm and higher). Eq. (3.56) is especially useful for gases whose spectral behavior could be described by the Elsasser and uniform statistical models.

The comparison of results of Felske and Tien's correlation with the numerical solution of Eq. (3.69) indicates excellent agreement (Figures 3.15 and 3.16) for all β and u values. This, however, would be expected because the correlation was obtained from Eq. (3.69) which was derived from the general statistical model. The correlation, therefore, is very useful in radiative transfer analyses involving those molecules whose absorption-emission characteristics can be represented by the general statistical model.

3.6. Band Emissivity (Total Emissivity)

The concept of band emissivity (total emissivity or simply emissivity) has proven to be very important in many radiative transfer analyses. It is particularly useful in calculating atmospheric radiation fluxes and cooling rates. As with the band model correlations, the expressions for emissivity are useful in eliminating the integration over the complicated line structure of the atmospheric spectrum. A large amount of information concerning various relations for emissivity of different gases is available in the literature. Important formulations for emissivity of atmospheric constituents are given in [13, 111-114]. No attempt is made here to summarize all the information available in the literature. Instead, a few fundamental expressions for the emissivity are presented which, along with the band models discussed earlier, can be used in many atmospheric radiative transfer analyses.

For a homogeneous path of absorbing-emitting gases, the spectral emissivity is defined by

$$\varepsilon_\omega = A_\omega = 1 - \exp\left(-\kappa_\omega X\right) , \tag{3.82}$$

where $A_\omega = \alpha_\omega$ is the spectral absorption defined in Eq. (3.2). The total emissivity (or simply emissivity) refers to the emissivity over the entire energy spectrum and for a homogeneous path of absorber it is defined by

$$\varepsilon(X, p, T) = (\pi/\sigma T^4) \int_0^\infty A_\omega(X, p, T)\, B_\omega(T)\, d\omega , \tag{3.83}$$

where σ is the Stefan-Boltzmann constant.

For a single gas, whose absorption spectrum consists of bands of rotational lines, the column emissivity may be expressed by [13, 18]

$$\varepsilon(X, p, T) = \left[\sum_i B_i(T)\, A_i(X, p, T)\right] \Big/ \sum_i B_i(T) , \tag{3.84}$$

where $B_i(T)$ is the Planck function evaluated at the band center, $\sum_i B_i(T) = \sigma T^4$, and A_i represents the integrated absorptance of the ith band and is given by Eq. (3.2). For a single band gas, Eq. (3.84) reduces to

$$\left.\begin{aligned} &\varepsilon(X, p, T) = a(T)\, A_i(X, p, T) , \\ &\text{where} \\ &a(T) = \pi B_i(T)/(\sigma T^4) . \end{aligned}\right\} \tag{3.85}$$

By employing appropriate band absorptance relations for individual bands, theoretical expressions for emissivity of a gas can be obtained from Eq. (3.84). Band absorptance correlations, discussed in section 3.4, are especially useful for this purpose.

For many atmospheric applications, the process of radiative transfer corresponds to the limit of strong rotational lines [111,

114], and emissivity can be expressed in terms of a single parameter (see the discussions on the strong line approximation). For example, if one considers the statistical band model consisting of Lorentz lines, then the band absorptance for strong line approximation is given by Eq. (3.32b). A combination of Eqs. (3.32b) and (3.85) results in

$$\left.\begin{aligned} &\varepsilon(\zeta) = a(T)\, A_i(\zeta) = a(T)\, [1 - \exp(-\sqrt{\zeta})] \ , \\ &\text{where} \\ &\zeta = 2\beta^2 x/\pi = 4\gamma_L\, S_j X/d^2 \ . \end{aligned}\right\} \quad (3.86)$$

In the strong nonoverlapping line limit (square root limit), $A_j(\zeta) = \sqrt{\zeta}$ and Eq. (3.86) reduces to

$$\varepsilon(\zeta) = a(T)\sqrt{\zeta} \ . \quad (3.87)$$

By making use of Eq. (3.84), Eqs. (3.86) and (3.87) can be extended to the case of multiband gases. The constants appearing in $a(T)$ and ζ can be evaluated for a particular gas (with a single or multiple bands) under varying conditions.

The above relations for emissivity are written for a homogeneous path. In a real atmosphere, the temperature varies along a nonhomogeneous path and these relations should be appropriately modified. The emissivity for a nonhomogeneous atmosphere (for the path between levels z and z') can be expressed by

$$\left.\begin{aligned} &\varepsilon(z, z') = \int_0^\infty A_\omega(z, z') \left[B_\omega(z')/B(z')\right] d\omega \ , \\ &\text{where} \\ &B(z') = \int B_\omega(z)\, d\omega = \sigma T^4/\pi \ . \end{aligned}\right\} \quad (3.88)$$

Various relations for spectral absorptance can be used in Eq. (3.88) and the resulting equations can be properly scaled for nonhomogeneous atmospheric applications.

Several relations for emissivity of various gases are available in the literature [13, 18, 111-117]. Early experimental investigations on the emissivity of the gases such as CO, CO_2, H_2O, $CO_2 + H_2O$, SO_2, NH_3, NO_2, and CH_4 are summarized by Hottel in [116, 117]. Recent investigations are discussed in [18, 111-115].

It should be pointed out here that any single relation for the emissivity cannot be expected to apply over a wide range of atmospheric conditions. Furthermore, in radiative flux calculations not only the expressions for emissivity but its derivatives also are required. Different relations are needed for upward and downward flux calculations. These points are discussed in some detail by Goody [13] and Rodgers [111].

4. EVALUATION OF TRANSMITTANCE AND INTEGRATED ABSORPTANCE OF SELECTED INFRARED BANDS

In this section transmittance and integrated absorptance computations are made for several bands of different gases by employing the line-by-line and quasi-random band model formulations under conditions of pressure and temperature for which experimental measurements are available. The sole motivation for this was to examine the possibility of using the quasi-random band model formulation for transmittance computations as required in surface temperature retrieval and other data reduction procedures [4, 14, 15, 118, 119].

For a homogeneous path of an absorber, the monochromatic transmittance at any wave number location ω is given by

$$\tau(\omega) = \exp[-\kappa(\omega)\ \bar{u}] \ , \tag{4.1}$$

where $\kappa(\omega)$ is the absorption coefficient at ω in cm^{-1}-atm^{-1} and $\bar{u}$ represents the pressure path-length of the absorber in cm-atm. To calculate the transmittance from Eq. (4.1) it is essential to employ an appropriate spectral model for the absorption coefficient.

4.1. Transmittance Models and Computational Procedures

The line-by-line (direct integration) and quasi-random band models are used in calculating the spectral transmittance. The computational procedures are described in detail in [12, 14, 15, 120].

In the direct integration procedure the entire frequency range of interest is first divided into a large number of narrow intervals $\Delta\omega$. Each interval is then divided into a variable number of subintervals depending upon the number of lines within the interval. Two very narrow subintervals are created on each side of a line center. The transmittance is computed at four frequency locations in each subinterval and is averaged finally over each interval. Total absorption coefficient at any wave number ω consists of contributions from all the lines in the vicinity and is computed in two parts as

$$\kappa(\omega) = \kappa^{D}(\omega) + \kappa^{W}(\omega) \ , \tag{4.2}$$

where $\kappa^{D}(\omega)$ and $\kappa^{W}(\omega)$ are called the direct and wing contributions respectively. Direct contribution originates from lines in very close vicinity (on both sides) and for Lorentz lines this is obtained from

$$\kappa^{D}(\omega) = \sum_{n} S_n\gamma_n \Big/ \left\{\pi\left[(\omega - \omega_n)^2 + \gamma_n^2\right]\right\} \ , \tag{4.3}$$

where ω_n refers to the center of the nth contributing line. The wing contribution arises from lines which are farther from ω than the range of direct contribution and for Lorentz lines this is given by the expression

$$\kappa^{W}(\omega) = \sum_{n} S_n\gamma_n \Big/ \left[\Pi(\omega - \omega_n)^2\right] \ . \tag{4.4}$$

For complete information on the direct integration procedure references should be made to [15, 120].

In the quasi-random band model, the entire band span Δ is divided into a number of small subintervals of equal spectral width δ . The appropriate number of such intervals is obtained through numerical experimentations. The lines within each subinterval are distributed into five intensity decades and average intensity for each decade is obtained first. The average transmittance over δ due to a single line of intensity S_n is given by [15]

$$\bar{\tau}_n(\delta) = \frac{1}{\delta} \int_\delta \exp\left[-S_n \bar{u} f(\omega, \omega_n)\right] d\omega_n , \tag{4.5}$$

where it should be noted that the variable of integration is the line center location ω_n . If N is the number of lines in an intensity decade then the average transmittance due to all lines in that decade is given by

$$\bar{\tau}_d(\delta) = \left\{\frac{1}{\delta} \int_\delta \exp\left[-\bar{S}_n \bar{u} f(\omega, \omega_n)\right] d\omega_n\right\}^N , \tag{4.6}$$

where $\bar{S}_n$ is the average intensity of all the lines within the decade under consideration. The average transmittance due to all lines in the five intensity decades of the subinterval δ is given by

$$\bar{\tau}_k(\delta) = \prod_{d=1}^{5} \bar{\tau}_d(\delta) = \prod_{d=1}^{5} \left\{\frac{1}{\delta_k} \int_{\delta_k} \exp\left[-\bar{S}_n \bar{u} f(\omega, \omega_n)\right] d\omega_n\right\} , \tag{4.7}$$

where subscript k represents the kth spectral subinterval (i.e., δ_k) of the total spectral interval Δ . Eq. (4.7) represents the transmittance due to the lines within δ_k . The wings of the lines in the adjacent subintervals also make a significant contribution to the absorption in δ_k . The resultant transmittance over the subinterval δ_k , therefore, is given by

$$\bar{\tau}_k(\delta) = \bar{\tau}_{k-k}(\delta) \prod_{\substack{j=1 \\ j \neq k}}^{K} \bar{\tau}_{k-j}(\delta) , \tag{4.8}$$

where $\bar{\tau}_{k-j}(\delta)$ represents the transmittance in δ_k due to lines

in δ_j and K is the number of adjacent subintervals (on both sides) from which the wing contribution is considered significant. The average transmittance for the entire range Δ is expressed by

$$\bar{\tau}(\Delta) = \frac{1}{K} \sum_{k=1}^{K} \bar{\tau}_k(\delta) \quad . \tag{4.9}$$

For other computational details, references should be made to [14, 15].

4.2. Transmittance of Selected IR Bands

In this section, transmittances of selected infrared bands are calculated by employing the line-by-line and quasi-random band models and the results are compared with the experimental measurements of Burch et al. [121]. The bands selected for comparison are CO fundamental (4.6 μ), 4.5 μ N_2O, 4.3 μ CO_2, and 15 μ CO_2 bands. Transmittance results are presented in Figures 4.1-4.4 separately for each band. Line-by-line results are shown by the solid lines, quasi-random band model results by the histograms, and the experimental results by the broken lines. Integrated absorptance for these bands are presented in Table 4.1 for comparison. The results for 6.3 μ H_2O band are available in [118].

The values of the computational parameters (such as the number of narrow subintervals for the line-by-line and band models, the ranges of direct and wing contributions, etc.) used for each band and the reasons for using them are discussed in [118]. In Ref. [121], the experimental results were obtained by using different effective slit-widths for different bands. The theoretical results, therefore, were also degraded with the corresponding slit functions for comparison.

For CO fundamental band, transmittances were calculated for the spectral range of ω = 2070 - 2220 cm^{-1} and these are compared with the experimental results in Figure 4.1. The line-by-line results are seen to be in good agreement with the experimental results while the band model results are seen to exhibit appreciable differences (particularly in the P and R branches of the band).

Table 4.1. Comparison of Integrated Absorptances for Various Bands.

Band Identification and Frequency Range	Experimental Absorptance (Burch et al. 1962)	Line-by-Line Results		Band Model Results	
		Integrated Absorptance (cm^{-1})	Percentage Difference with Measurement	Integrated Absorptance (cm^{-1})	Percentage Difference with Measurement
CO 4.6 μ (1970-2270 cm^{-1})	73.90	70.32	-4.84	67.30	-8.93
N_2O 4.5 μ (2140-2290 cm^{-1})	57.00	56.01	-1.74	51.43	-9.77
CO_2 4.3 μ (2220-2420 cm^{-1})	73.80	74.09	0.39	69.72	-5.53
H_2O 6.3 μ (1200-2100 cm^{-1})	334.0	326.4	-2.28	323.1	-3.26
CO_2 15 μ (550-800 cm^{-1})	66.10	66.57	0.71	65.35	-1.13

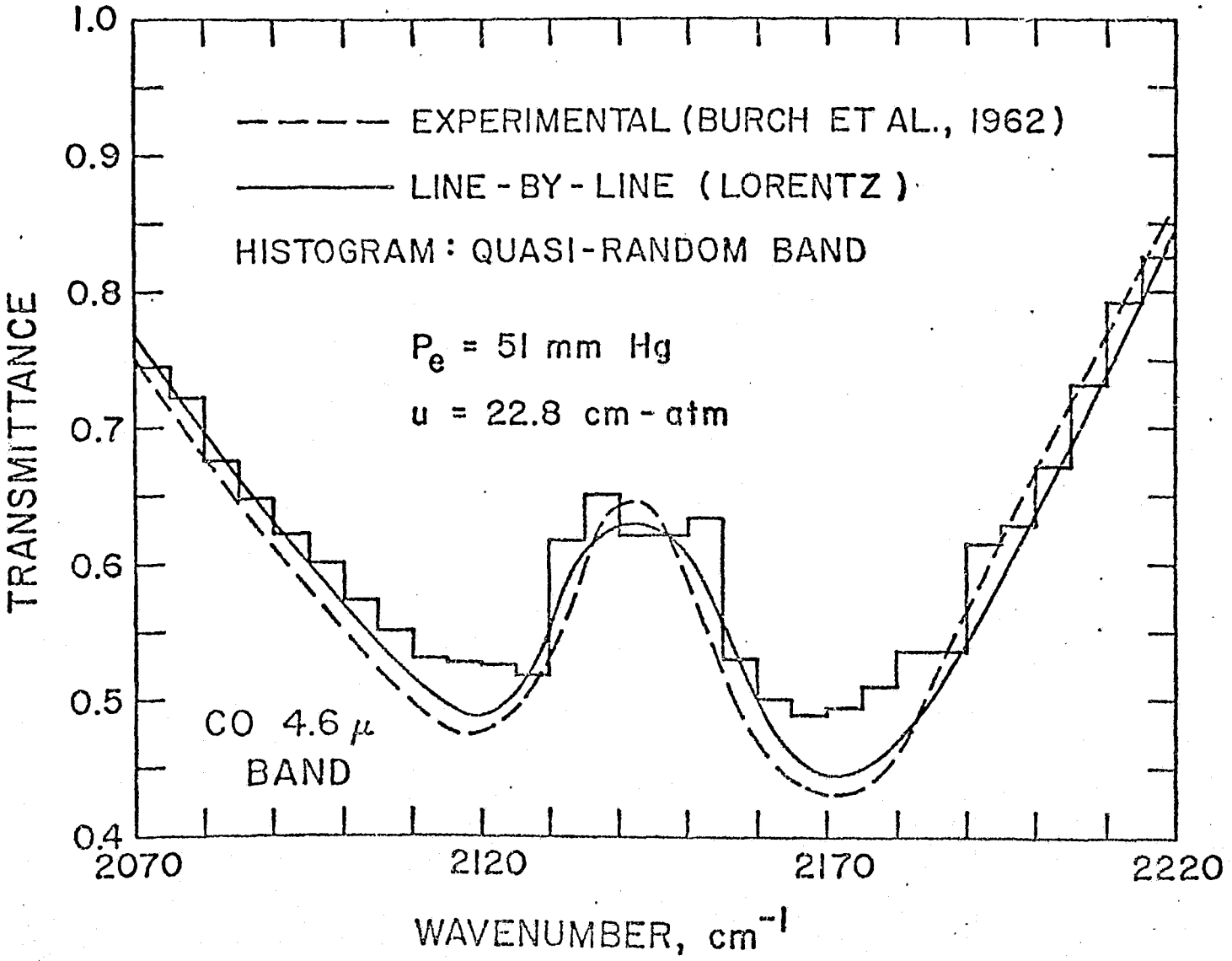

Fig. 4.1 Comparison of transmittances of CO fundamental band.

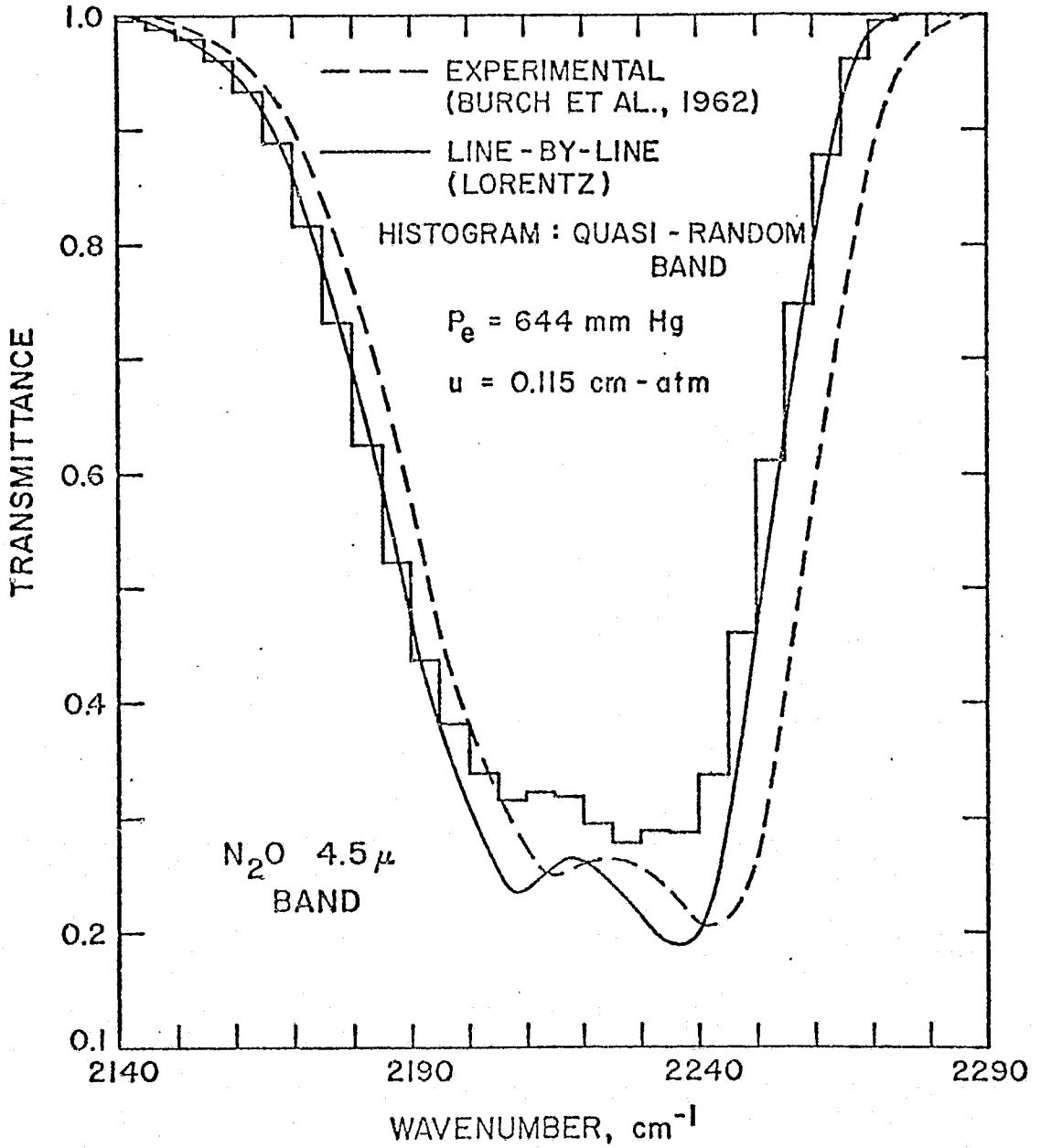

Fig. 4.2 Comparison of transmittances of 4.5μ N_2O band.

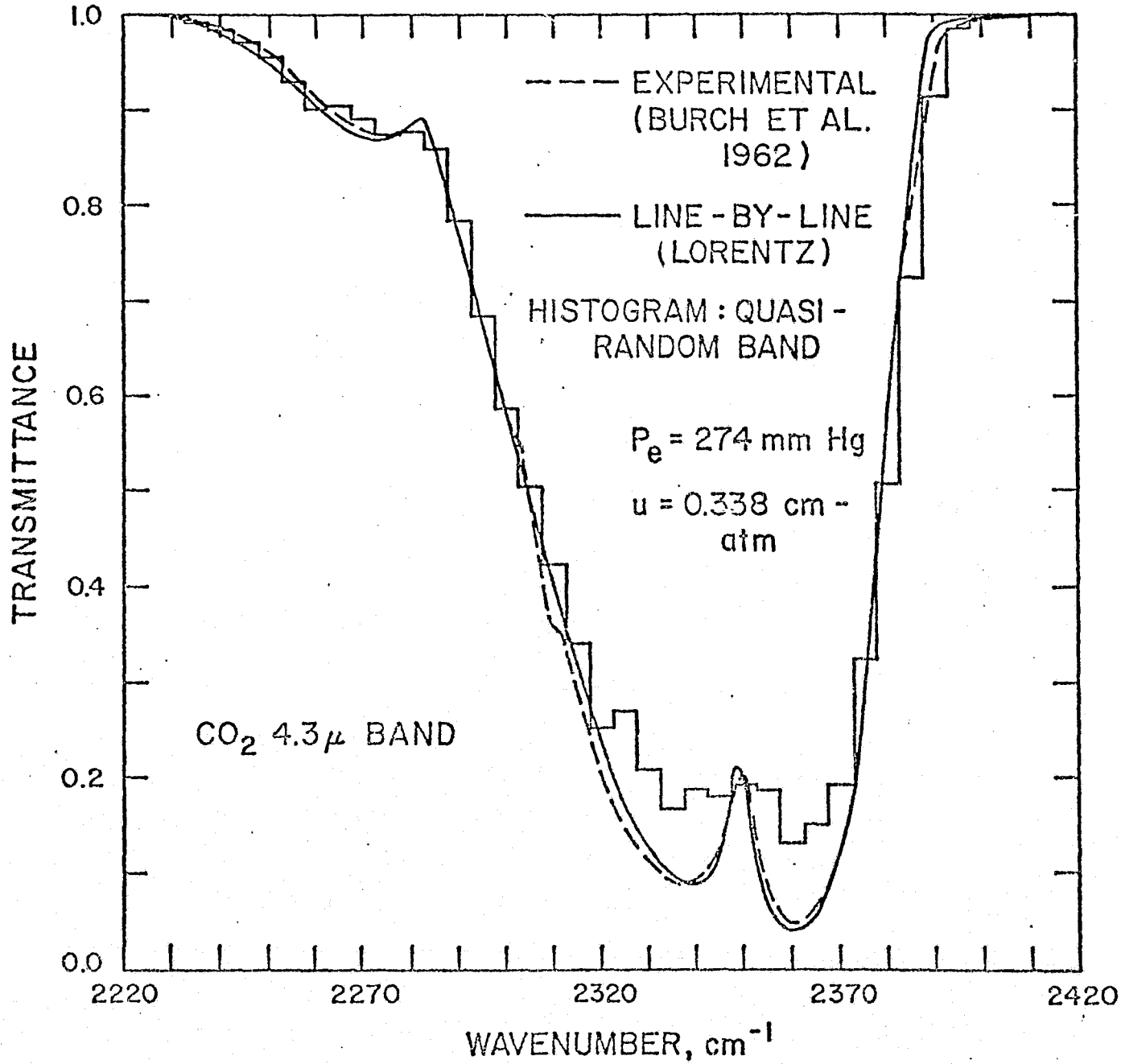

Fig. 4.3 Comparison of transmittances of 4.3μ CO_2 band.

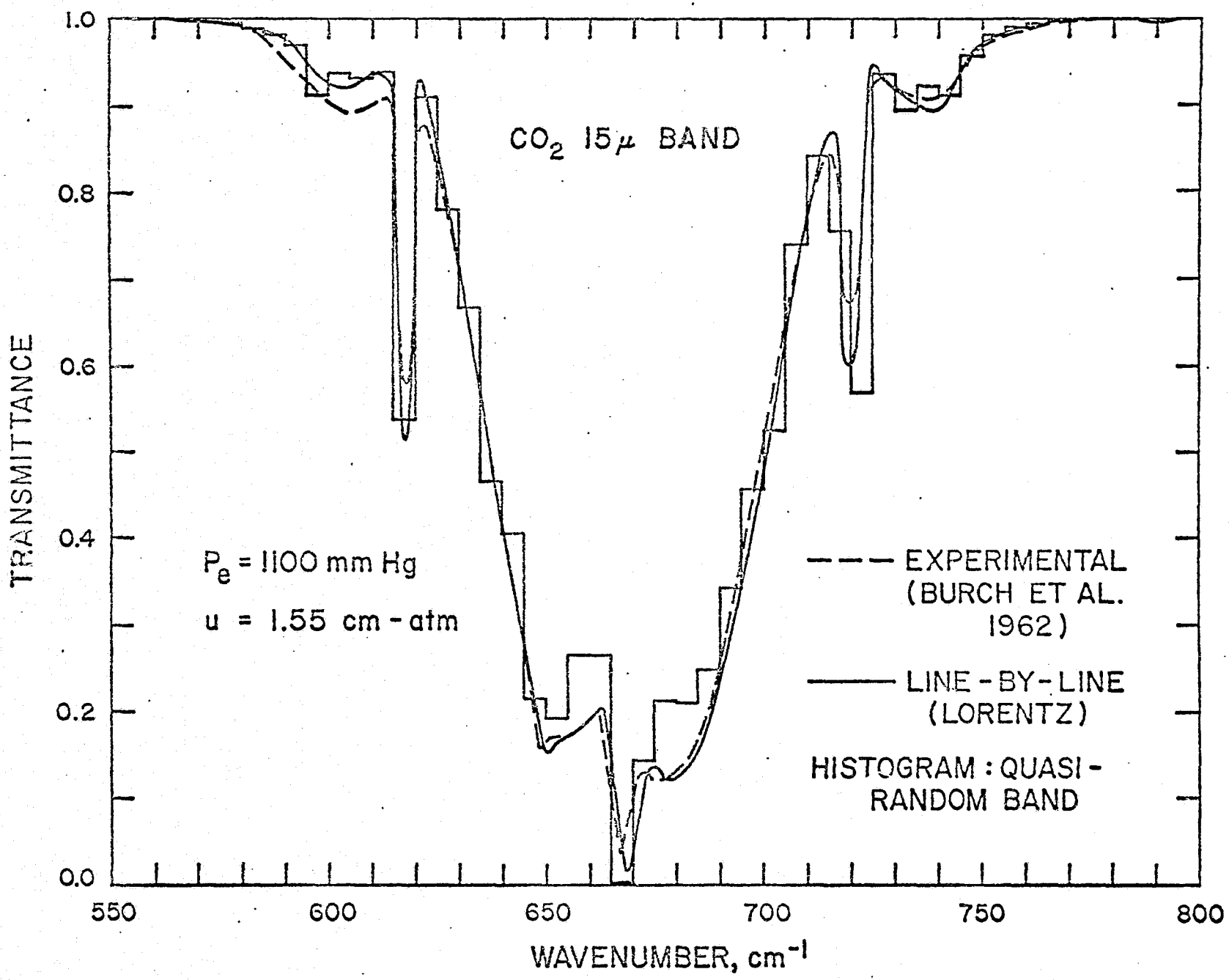

Fig. 4.4 Comparison of transmittances of 15μ CO_2 band.

Integrated absorptances for this band (presented in Table 4.1) are for slightly greater frequency range than that considered for transmittance calculations. This was necessary because the experimental value was for a greater frequency range. The results of Table 4.1 show that the line-by-line model absorptance is about five percent lower and the band model absorptance is about nine percent lower than the experimental value.

For 4.5 μ N_2O band, the spectral range selected for transmittance calculations is 2140 - 2290 cm^{-1} and the results are presented in Figure 4.2. With the exception of the fact that the experimental curve is shifted approximately 6 cm^{-1} toward the higher frequency side (with respect to the theoretical curves), the agreement between the line-by-line and experimental results is very good. The band model results again show appreciably lower absorption. Table 4.1 indicates that the line-by-line absorptance is less than two percent lower than the experimental value while the difference for the band model absorptance is approximately ten percent.

For 4.3 μ CO_2 band, the comparison of theoretical and experimental transmittances is shown in Figure 4.3 for the spectral range of 2220 - 2420 cm^{-1} . The agreement between the experimental and the line-by-line results is seen to be excellent. The band model results again exhibit a slightly lower absorption. It can be seen from Table 4.1 that the integrated line-by-line absorptance is within 0.5 percent of the experimental value while the band model absorptance is approximately 5.5 percent lower.

For 15 μ CO_2 band, the transmittance results are presented in Figure 4.4 and the agreement between the three results is seen to be excellent. Table 4.1 shows that the theoretical results agree with the experimental ones within one percent.

From the results presented in this section it is concluded that the line-by-line results are in better agreement with the experimental values than the quasi-random band model results.

In view of high accuracy required for the temperature retrieval and other data reduction work [4, 14, 15, 119], it would be

desirable to use the line-by-line model. In other atmospheric works, however, use of the quasi-random band model may be justified.

5. UPWELLING ATMOSPHERIC RADIATION

It is possible to infer concentrations of various pollutants from an appropriate analysis of upwelling radiation measurements obtained in passive mode experiments [4, 5, 15]. Since variables like surface temperature, surface emittance, concentration of water vapor and other more abundant species (e.g., CO_2) affect the upwelling radiance to a greater extent than the less abundant pollutants like CO, a theoretical study of the effects of these variables on the upwelling radiance is essential in order to be able to obtain meaningful information regarding pollutants. In this section, basic equations for calculating the upwelling atmospheric radiance are presented. These account for the various sources of radiation coming out at the top of the atmosphere. The line-by-line and quasi-random band models are used for the evaluation of transmittance and upwelling radiance in the spectral region of CO fundamental band (2070 - 2220 cm^{-1}). The theoretical procedure, however, can be extended easily to any other spectral range. Model calculations have been performed to study the effect of different interferring gases, water vapor profiles, surface temperature and surface emittance on the upwelling radiance and signal change.

As shown in Figure 5.1, the radiation emergent from the atmosphere, $E(\omega)$, may be given by the expression [4, 7]

$$E(\omega) = E_G(\omega) + E_R(\omega) + E_\phi(\omega) + E_{R\phi}(\omega) \ , \qquad (5.1)$$

where

$E_G(\omega)$ = thermal radiation emitted by underlying surface and atmosphere

$E_R(\omega)$ = incident solar radiation reflected by the surface

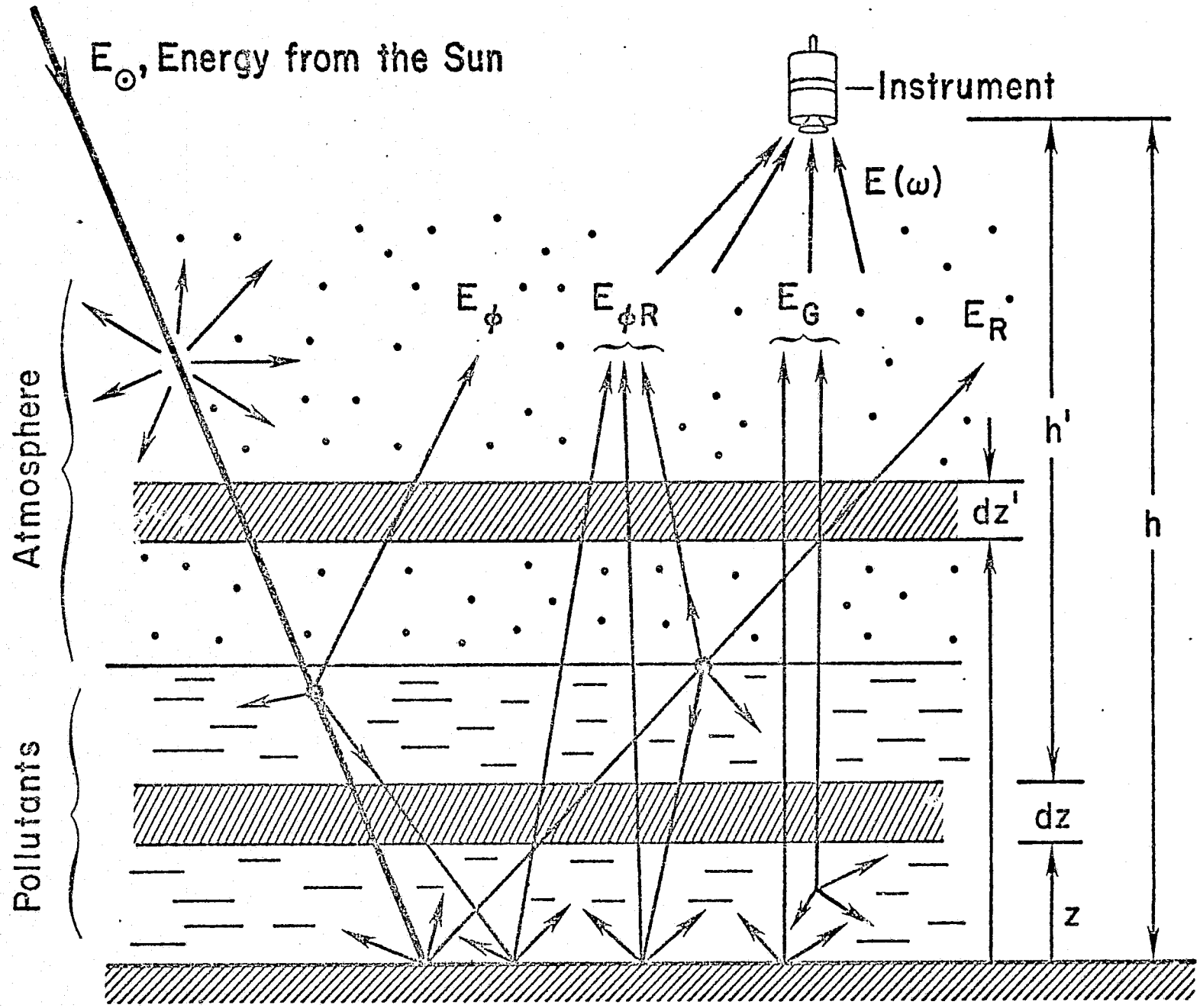

Fig. 5.1 Radiative energy received by an aircraft or satellite mounted instrument.

$E_{\phi}(\omega)$ = radiation scattered by single or multiple scattering processes in the atmosphere without having been reflected from the surface

$E_{R\phi}(\omega)$ = scattered energy which has undergone a reflection from the surface.

In general, these quantities are functions of surface temperature, atmospheric temperature, surface emittance, surface reflectance, sun zenith angle, scattering characteristics of particles, and transmittance of the atmosphere.

In the spectral region of infrared measurements, the effect of scattering is negligible. The incident solar radiation reflected by the surface, however, is important especially if the surface reflectance is assumed to be high (0.2 and higher).

Upon neglecting the scattering and solar radiation, the expression for thermal radiation emerging from a plane-parallel atmosphere can be written as

$$E(\omega) = E_G(\omega) = \varepsilon(\omega)\ B(\omega, T_s)\ \tau(\omega, o) + \int_o^h B(\omega, T(z))\ [d\tau(\omega, z)/dz]\ dz\ , \tag{5.2}$$

where $\varepsilon(\omega)$ is the surface emittance, $B(\omega, T)$ is the Plank's blackbody function, T_s is the surface temperature, $T(z)$ is the temperature at altitude z, and $\tau(\omega, z)$ is the monochromatic transmittance of the atmosphere. The first term on the right hand side of this equation represents the radiation from the surface while the second term is the radiation from the atmosphere.

The contribution from sunlight reflected from the surface becomes significant at shorter wavelengths. This contribution is given by the component $E_R(\omega)$ as

$$E_R(\omega) = (1/\pi)\ [1 - \varepsilon(\omega)]\ \cos\theta\ H_s(\omega)\ [\tau(\omega)]^{\zeta}\ , \tag{5.3}$$

where θ is the sun zenith angle and $\zeta = 1 + f(\theta)$. Function $f(\theta) = \sec\theta$ for $o \leq \theta \leq 60°$ and equals to Ch θ for $\theta > 60°$ with Ch θ denoting the Chapman function. $H_s(\omega)$ is the sun

irradiance on top of the atmosphere, and $\tau(\omega)$ is the transmission vertically through the atmosphere.

The total energy emergent from the atmosphere is obtained by integrating either Eq. (5.1) or (5.2) over the specified spectral interval $\Delta\omega$ as

$$E_D = E_{\Delta\omega} = \int_{\Delta\omega} E(\omega)\, d\omega \ . \tag{5.4}$$

The procedure for calculating the upwelling radiance, by employing the line-by-line and quasi-random band model for transmittance, is discussed in detail in [15] and computer programs are provided. A summary of the procedure is given here.

5.1. Procedure for Calculating the Upwelling Radiance

In radiation modeling for pollution measurement in a nonhomogeneous atmosphere, the upwelling radiation is calculated by dividing the atmosphere into an appropriate number of sublayers. Each sublayer is assumed to be homogeneous in species concentration, temperature and pressure.

In a specified spectral interval in which a particular pollutant absorbs, the total energy emergent from the atmosphere is obtained from Eq. (5.4). If in this interval, n independent measurements (corresponding to the number of homogeneous layers) could be made to find E_{D1}, E_{D2}, --- E_{Dn}, then the uniform concentration of the pollutant in each layer (and therefore the concentration profile in the actual atmosphere) could be determined from Eq. (5.4). Because of low concentrations of pollutants in the atmosphere, however, n such measurements are not feasible. Thus, only one independent measurement is usually made and an average value of the particular pollutant concentration in the atmosphere is obtained. Even if only one value of the pollutant concentration can be obtained from an independent measurement, it is essential to divide the nonhomogeneous atmosphere into several homogeneous layers for the purpose of data reduction. This is because the pressure, temperature, and amount of interfering molecules vary in the

atmosphere, and spectroscopic parameters and pressure path lengths are strong functions of these variables.

By employing the Lorentz line-by-line model for atmospheric transmittance, the upwelling radiance at the top of the atmosphere is obtained from Eq. (5.4) for each narrow spectral interval $\Delta\omega$. The exact procedure for doing this is to evaluate the average value of the Planck function for this interval first, then by using the mean value of the transmittance for the interval, evaluate the upwelling radiance at the top of the atmosphere. The total upwelling radiance ($E = \Sigma E_{\Delta\omega}$) at the top of the atmosphere for the entire spectral range Δ is obtained by summing the radiances of individual intervals.

By employing the quasi-random band model, the total upwelling radiance at the top of the atmosphere can be evaluated from Eq. (5.4). First, the net (integrated) radiance is obtained at the top of the atmosphere for each subinterval by calculating the Planck function and the average transmittance for that subinterval. The total radiance for the entire range Δ is then obtained by summing the integrated radiances of each subinterval.

The signal change $SC = \Delta E$ (in watts/cm^2 - sr) can be calculated by employing Eq. (5.4) as

$$SC = \Delta E = \int_{\Delta\omega} \left[E(\omega, \tau_o) - E(\omega, \tau_p) \right] d\omega \,, \qquad (5.5)$$

where τ_o represents the transmittance of a "clean" atmosphere in which the pollutant concentration is zero, and τ_p refers to the transmittance of the atmosphere in the presence of the pollutant. The numerical procedure for evaluating Eq. (5.5) is identical to that described for calculating the upwelling atmospheric radiance.

Since Applications Incorporated (NASA-Contractor, responsible for the development of non-dispersive correlation instrument for pollution measurement [4, 5]) has compiled spectral line parameters (position, strength, width, and lower energy level) for lines of CO fundamental band and for lines of other molecules which interfere with the CO band. In the calculation of transmittances,

these line parameters are directly read from a tape provided by SAI [5] to NASA-Langley.

Solar irradiances at the top of the atmosphere, at a few selected wave numbers, are also available from the SAI tape [5]. Values obtained from the tape, for the spectral range of present interest, are tabulated in [15]. In the evaluation of contribution of the reflected solar radiation to the upwelling radiance, the solar irradiance for each spectral subinterval is obtained from a linear interpolation of the tabulated values [15].

By employing the Lorentz line-by-line and quasi-random band model for atmospheric transmittance, upwelling radiance and signal change were calculated for several illustrative cases.

5.2. Results of Model Calculations

The results of integrated upwelling radiance at the top of the troposphere (i.e., at 10 km) for different CO concentrations (uniformly distributed through the troposphere), in the presence of various interfering molecules, are illustrated in Figure 5.2. The solid curves represent the results of the line-by-line model and broken curves for the quasi-random band model. As would be expected, the upwelling radiance E decreases with increasing CO concentration and with the inclusion of different interfering molecules. Inclusion of O_3 causes a slight decrease in radiance (not exceeding 0.5%) and it was difficult to illustrate this decrease in Figure 5.2. The agreement between the line-by-line and the quasi-random band model results is seen to be excellent for the case of $CO + H_2O$. The slightly lower radiances for the next two cases is attributed to the over-estimation of absorption by the band model. The reason for this lies in the assumption of random distribution of many lines (in the presence of interfering molecules) in the subintervals of the band model. In the actual spectra, however, the lines are more closely spaced in some regions than in others. The variation in the signal change, ΔE , with the CO concentration is illustrated in Figure 5.3. These results follow the general trend of the results presented in Figure 5.2.

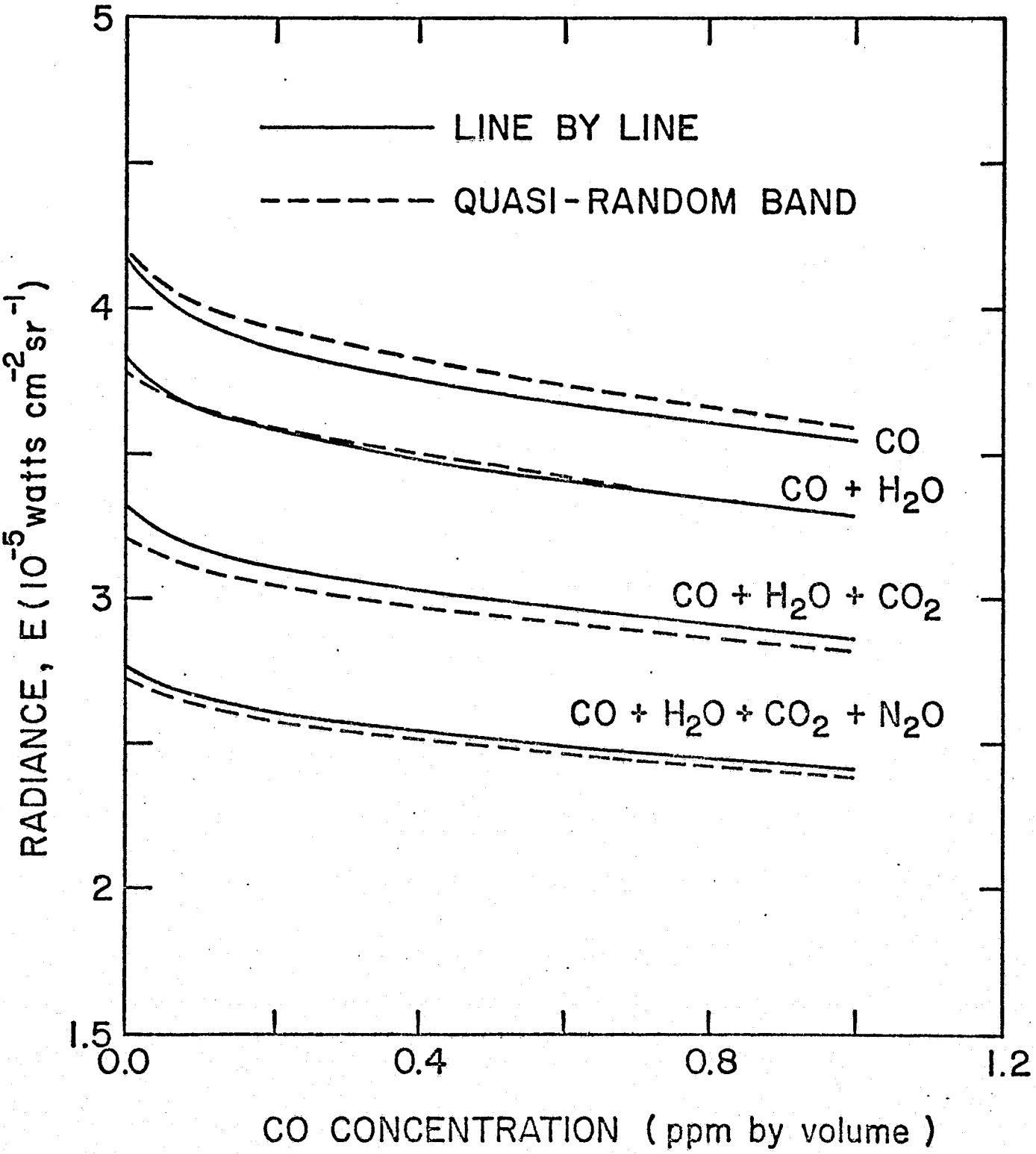

Fig. 5.2 Upwelling radiance as a function of CO concentration in the presence of interfering molecules, T_s = 288°K, ε = 0.8.

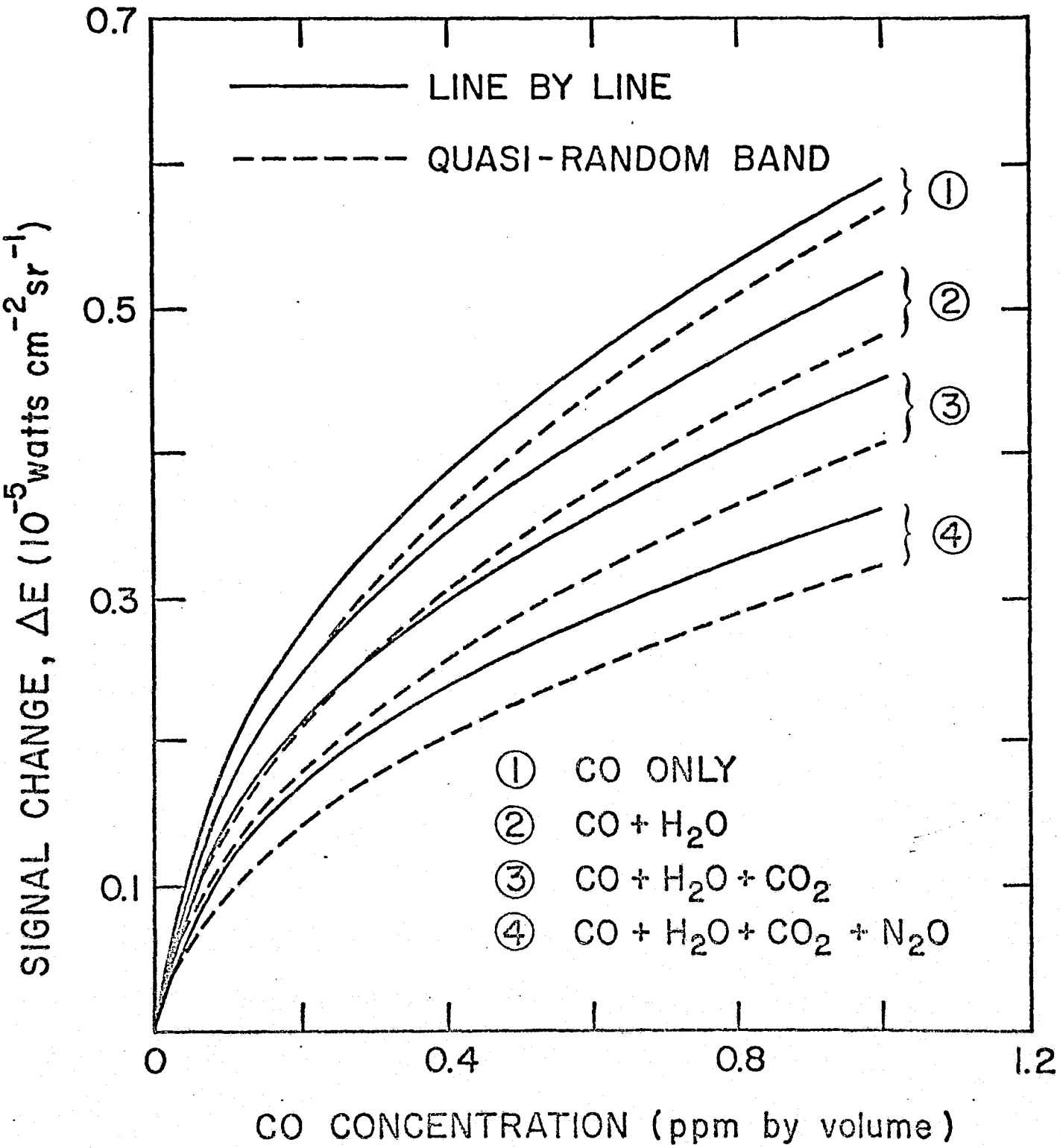

Fig. 5.3. Signal change as a function of CO concentration in the presence of different interfering molecules, T_s = 288°K, ε = 0.8.

The influence of different amounts of water vapor on the upwelling radiance and the signal change is shown in Figures 5.4 and 5.5 respectively. Increased water vapor concentration results in increased absorption in the atmosphere. This, in turn, results in lower values for upwelling radiance and signal change. It should be noted that the effect of CO concentration on the signal change would be relatively small in the presence of larger quantity of water vapor.

Figure 5.6 shows the upwelling radiances for surface temperatures of 280, 290, and 300°K and a surface emittance of 0.8. The strong dependence of the upwelling radiance on the surface temperature is obvious from these results. The relatively lower radiance values obtained with the band model are indicative of slight over-estimation of absorption by this model.

Figure 5.7 shows the signal change for three different values of surface emittance and for a surface temperature of 288°K. As explained earlier, the radiances obtained from the band model are lower than the line-by-line model because of over-estimation of absorption by the band model. The relative increase of the difference for the lower ε-values is due to lower total emission from the earth for the small values of surface emittance. In these cases, therefore, the increased absorption by the band model has a greater relative effect on the radiance and signal change.

Figure 5.8 shows the variation of the upwelling radiance with the surface temperature for a fixed concentration of CO (1 ppm by volume) in the atmosphere and for $\varepsilon = 0.8$. The strong dependence of radiance on the surface temperature may be easily explained on the basis of the Stefan's law. However, because of the interference from the infrared active atmospheric molecules, the results obtained here do not exhibit an exact fourth power relationship.

Figure 5.9 shows the variation of radiance with the surface emittance for a fixed CO concentration (1 ppm by volume) and $T_s = 288°K$. As would be expected, the results indicate the linear dependence of radiance on the surface emittance. In general, the ground emittance varies with the wave number. However, for the

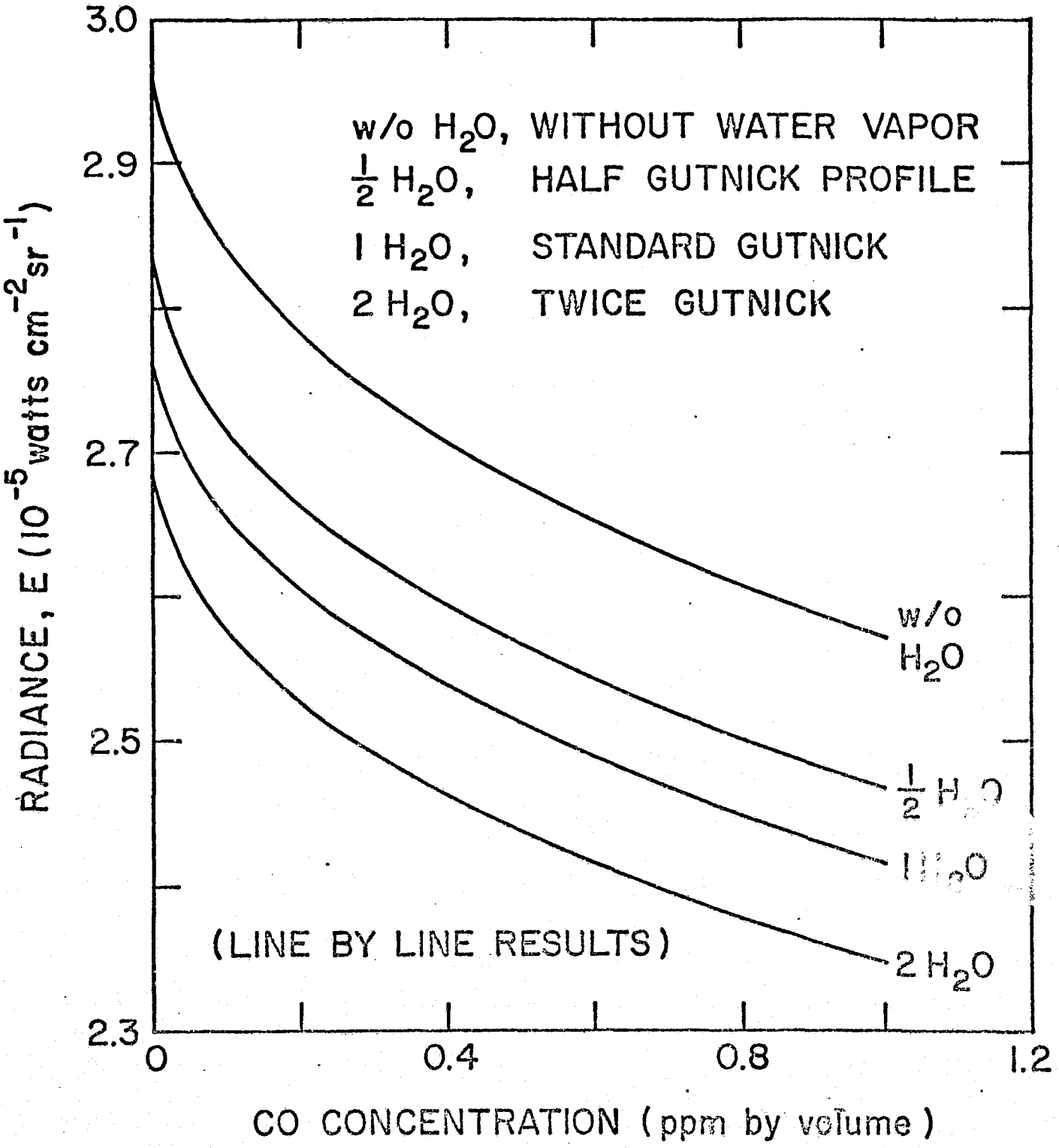

Fig. 5.4 Upwelling radiance as a function of CO concentration for different water vapor profiles, T_s = 288°K, ε = 0.8.

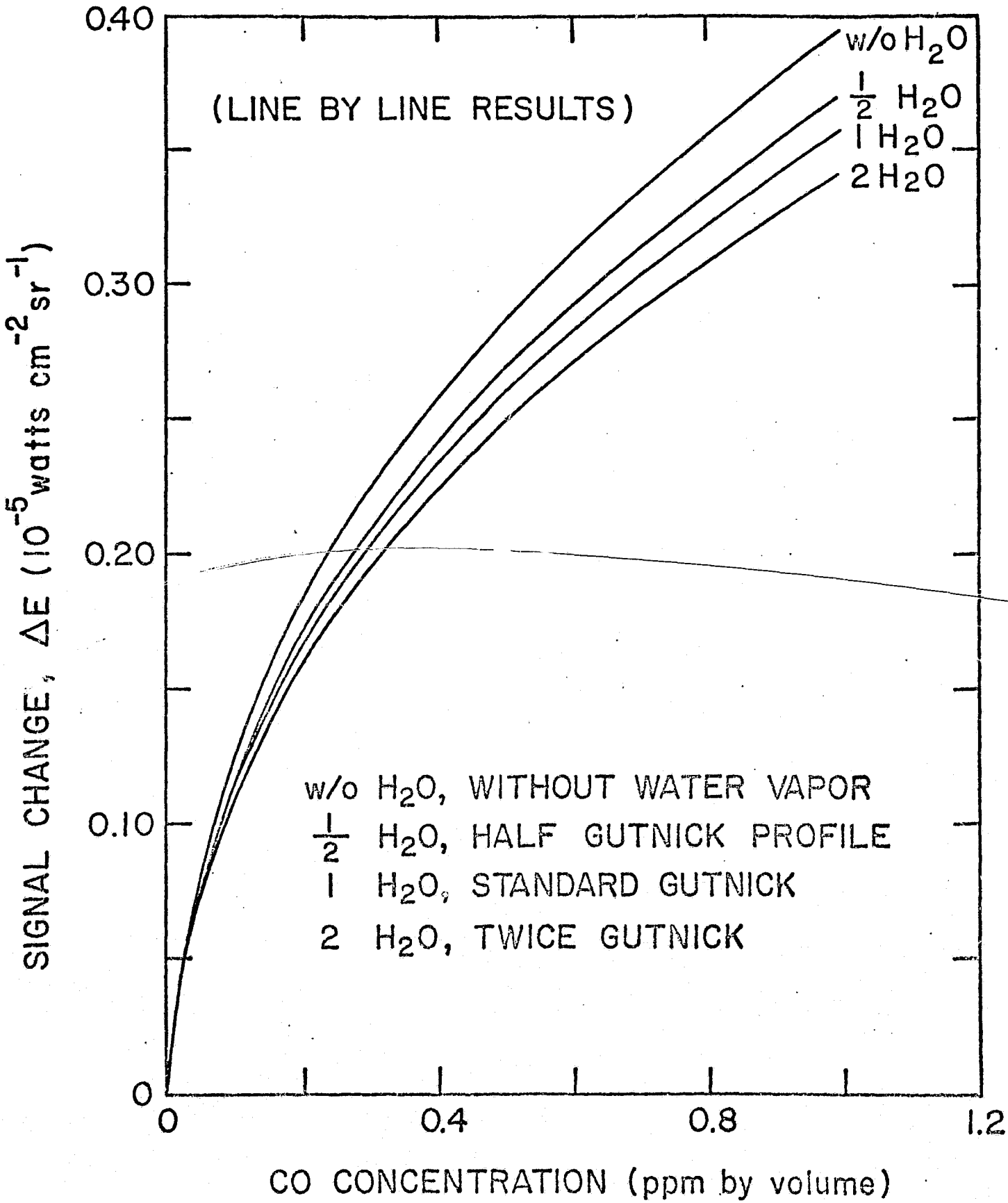

Fig. 5.5 Effects of water vapor concentration on the signal change $T_s = 288°K$, $\varepsilon = 0.8$.

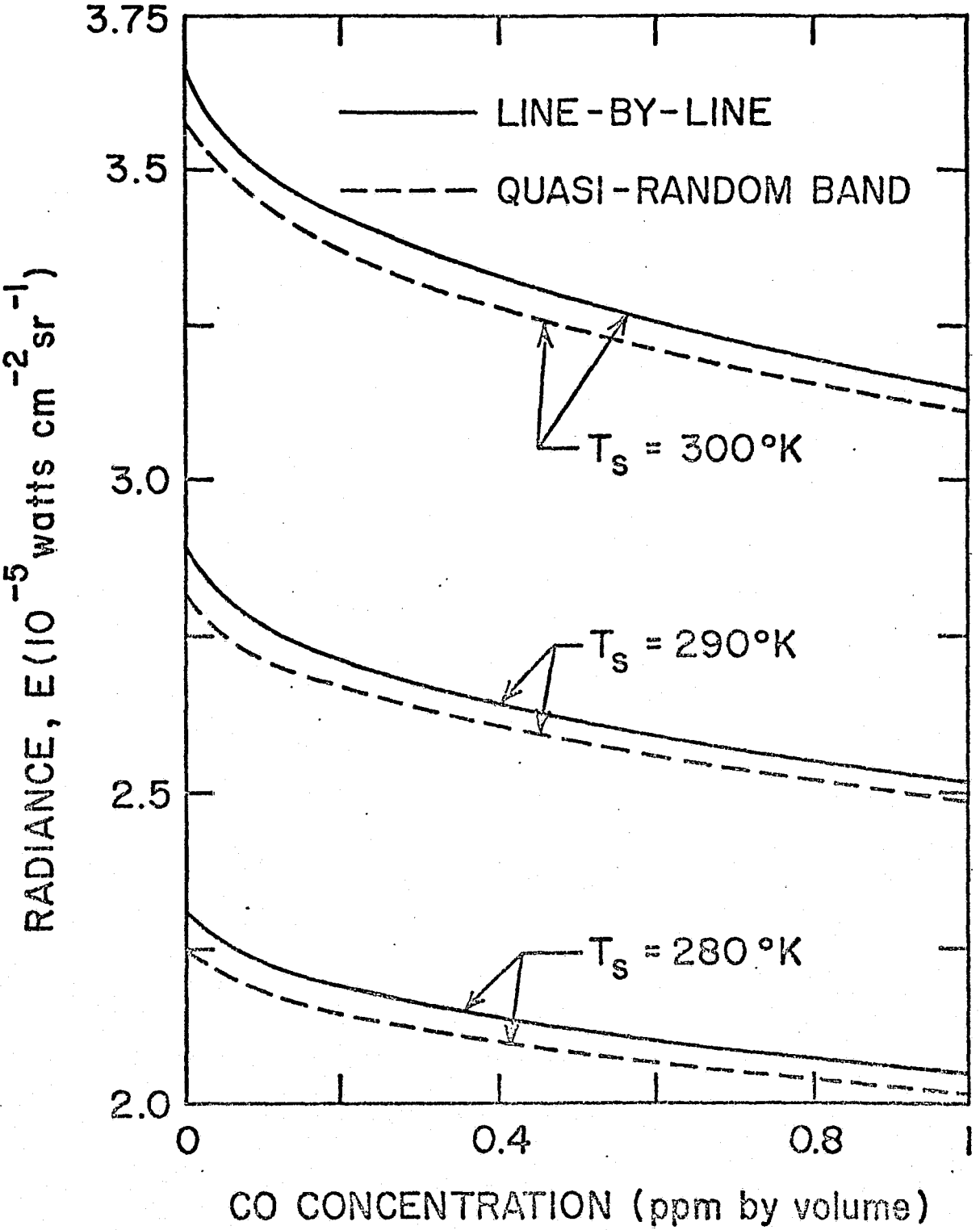

Fig. 5.6 Upwelling radiance as a function of CO concentration for three different surface temperatures (surface emittance $\varepsilon = 0.8$).

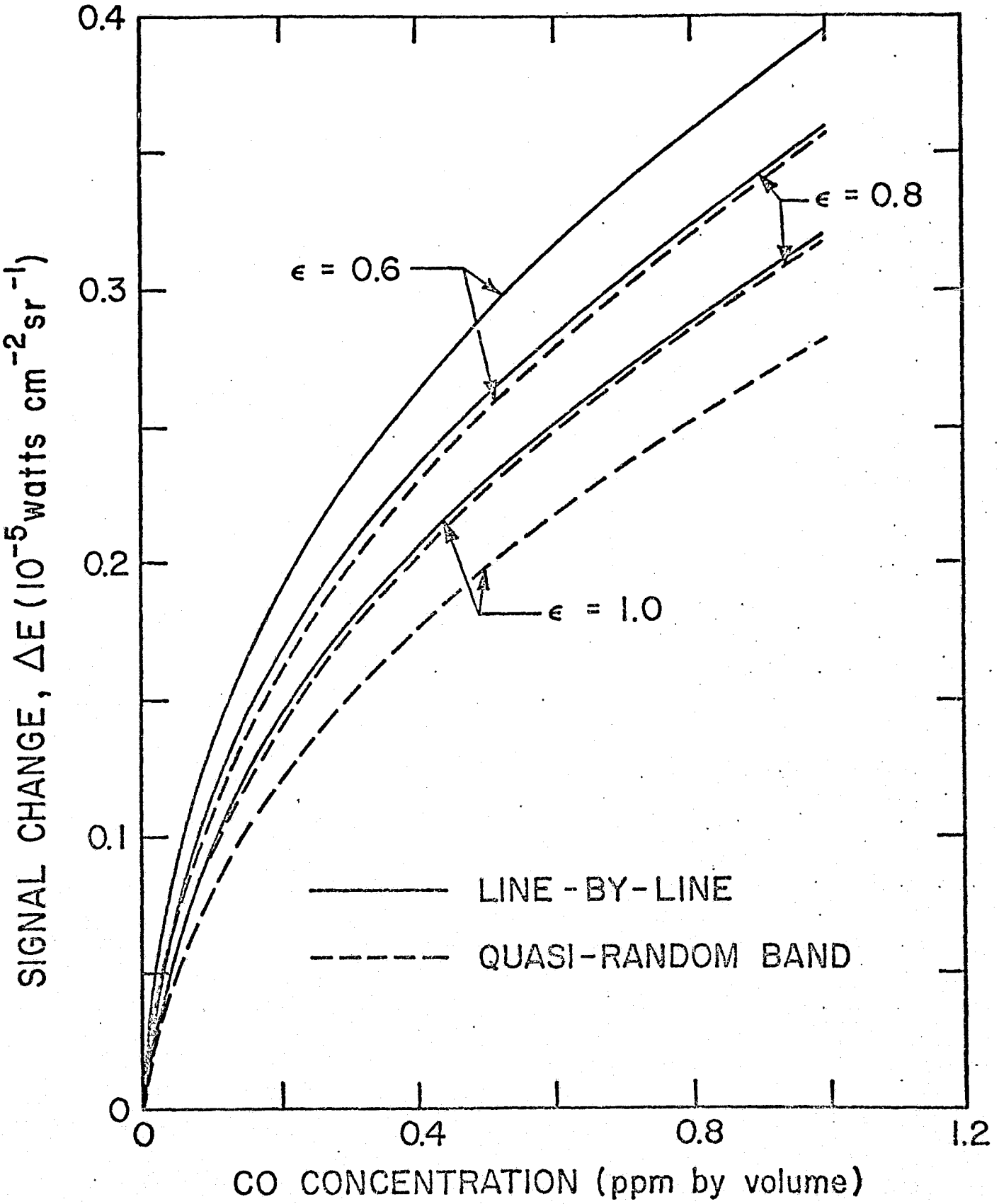

Fig. 5.7 Signal change as a function of CO concentration for three different surface emittances, T_s = 288°K.

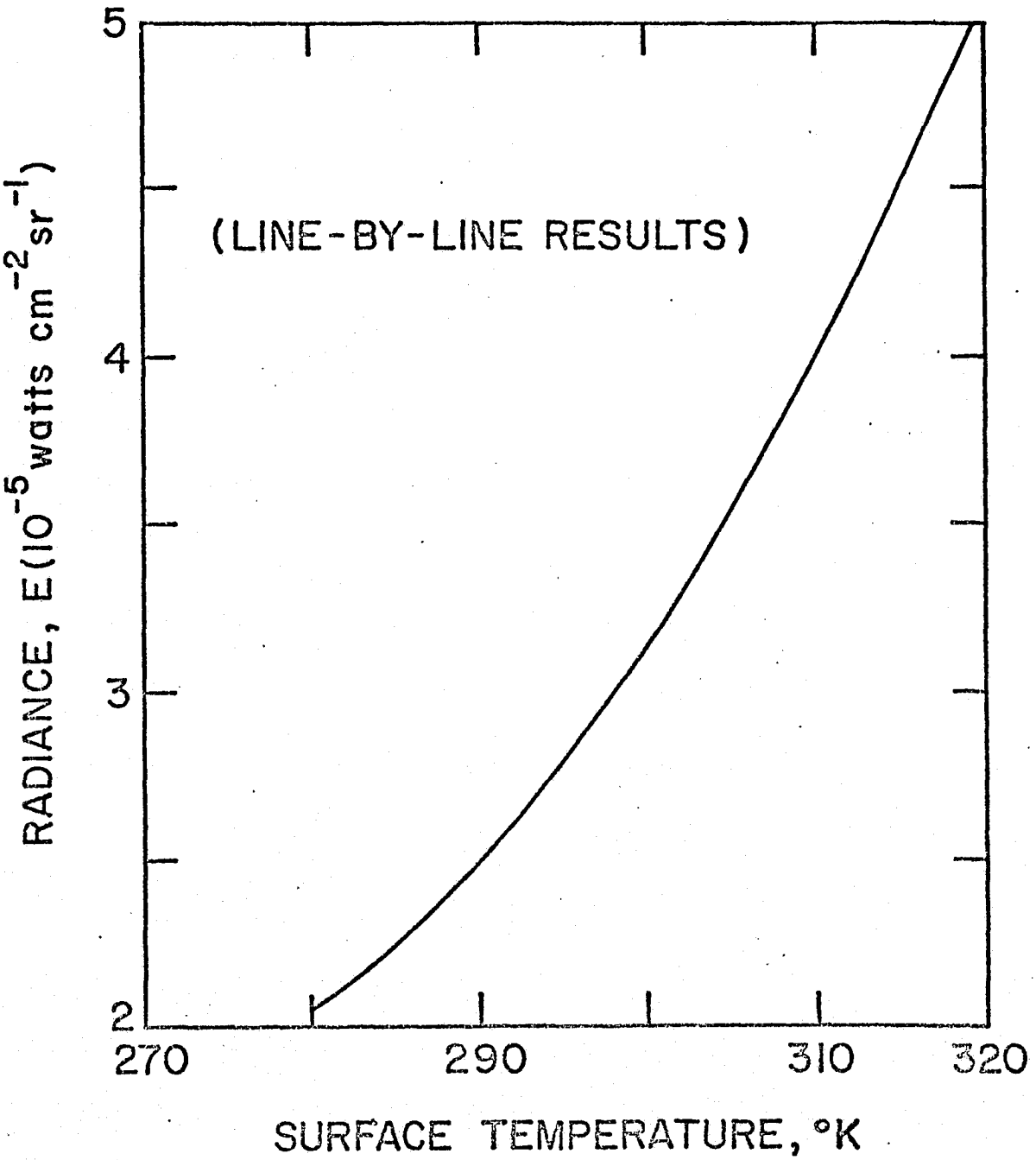

Fig. 5.8 Upwelling radiance as a function of surface temperature for a fixed CO concentration (1 ppm by volume), $\varepsilon = 0.8$.

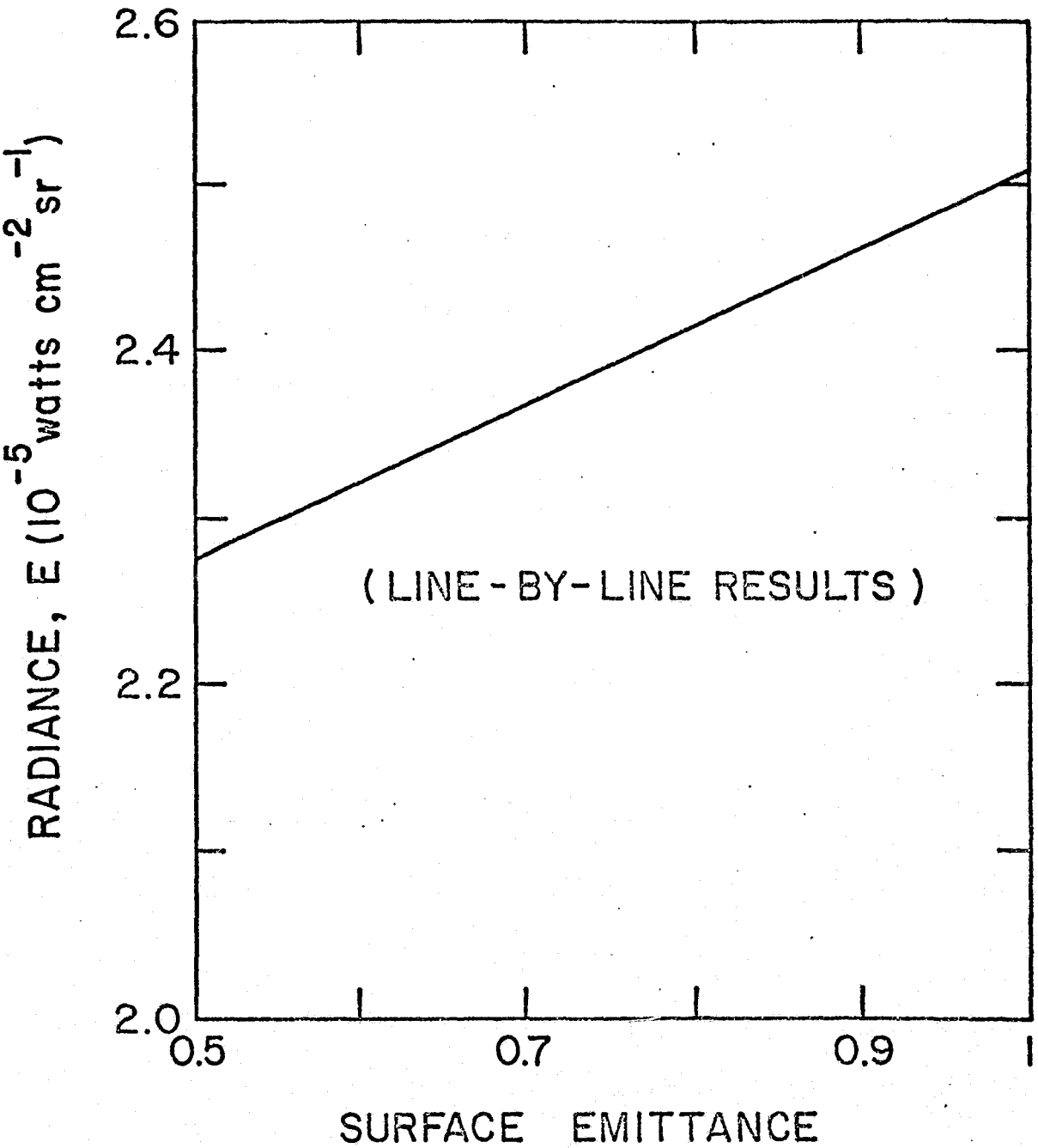

Fig. 5.9 Upwelling radiance as a function of surface emittance for a fixed CO concentration (1 ppm by volume), T_s = 288°K.

spectral range of CO fundamental band, it was shown in reference [4] that the radiance is not influenced by a significant amount when the wave number dependent ground emittance is replaced by an averaged value.

Figure 5.10 shows a comparison of the results obtained from the line-by-line program developed in [15] and another line-by-line program (called POLAYER) developed by the Science Applications Inc. [5]. In computing the total absorption coefficient at any wave number, the program of Reference [15] considers contributions from all the lines up to a fixed wave number location (on both sides) of 45.5 cm^{-1} from the wave number under consideration. This value of 45.5 cm^{-1} for the so-called wing effect was chosen after several numerical experimentations. The POLAYER, on the other hand, considers the effect of a fixed number of 20 lines on each side of the wave number under consideration. This causes the range of wing effect to change depending upon the density of lines in the spectrum. Thus, in some cases, POLAYER will not consider the influence of lines which are only 1 cm^{-1} away from the wave number under consideration. This, of course, will result in underestimation of absorption. This, at least in part, is responsible for the higher integrated radiance (and, therefore, larger signal change) for the POLAYER program.

6. CONCLUDING REMARKS

The purpose of this study was to review different line and band models for infrared spectral absorption, compare their absorptances and transmittances, indicate their limitations, and establish their usefulness for atmospheric applications.

From the comparison of results of the three line profiles (Lorentz, Doppler, and Voigt), it is concluded that the Voigt line profile should be employed in calculating the transmittance for the middle to upper troposphere and lower stratosphere. The use of the Lorentz line profile is justified for lower tropospheric applications.

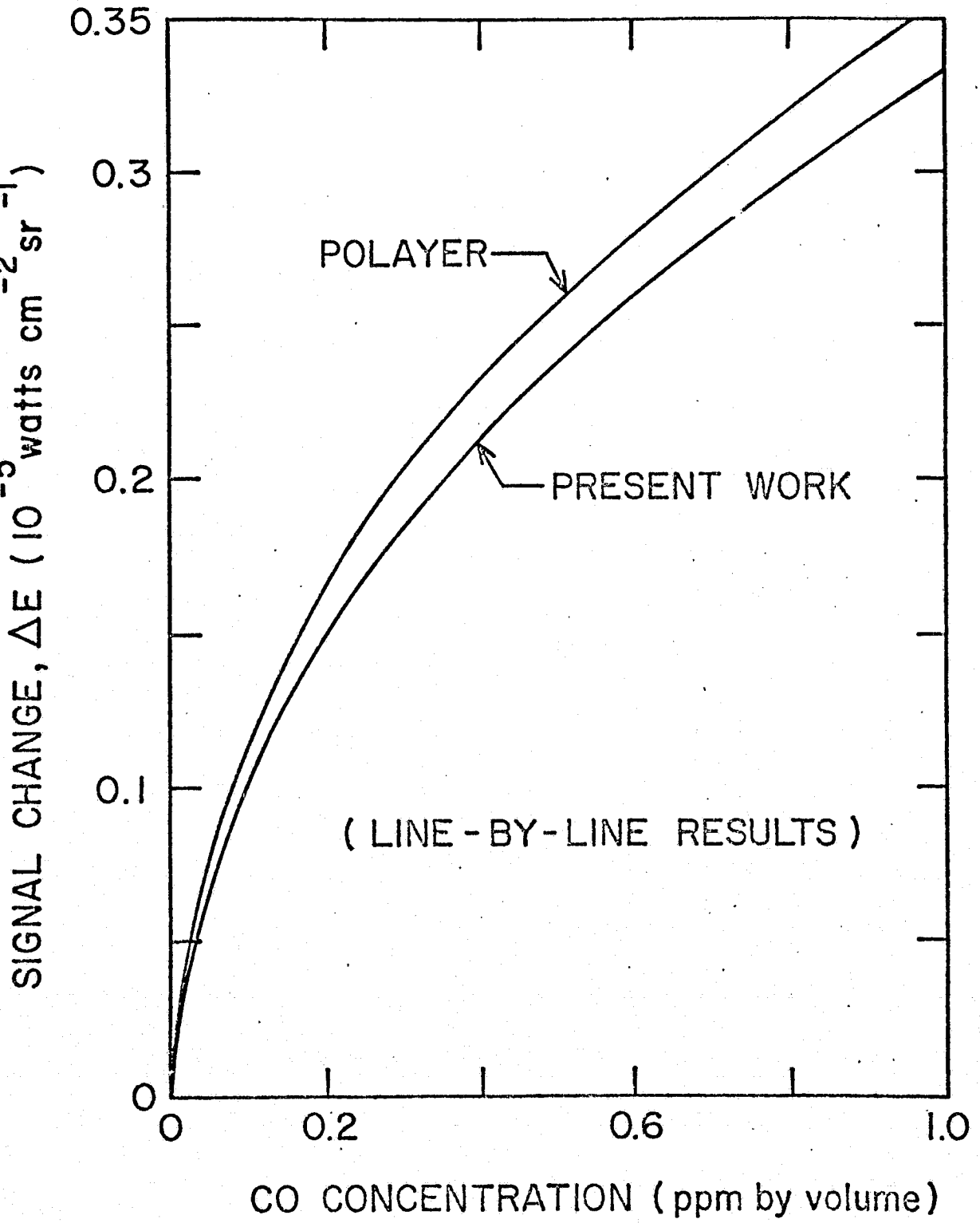

Fig. 5.10 Comparison of signal change results obtained from the program POLAYER and the present LINBLIN program, T_s = 288°K, ε = 0.8. On the average, LINBLIN values are 2% lower than POLAYER values.

From the comparison of wide band absorptance of various band models, it is concluded that the correlation presented by Felske and Tien provides fairly accurate results for all pressures and path lengths. At relatively high pressure, however, the simple correlation given by Tiwari and Batki provides a uniformly better approximation for the total band absorptance.

The homogeneous path transmittances were calculated for CO fundamental, 4.5 μ N_2O , 4.3 μ CO_2 , and 15 μ CO_2 bands by employing the line-by-line and quasi-random band models. Comparisons of these results with available experimental measurements indicate that in sensitive atmospheric applications (such as surface temperature retrieval and detection of CO concentration), the use of the line-by-line model is desirable.

By employing the line-by-line and quasi-random models, results were obtained to study the effects of different interferring molecules, water vapor profiles, ground temperatures, and ground emittances on the upwelling radiance and signal change in the spectral range of CO fundamental band. Physically realistic values of various parameters were used in the model calculations. This information is very useful in interpreting the data obtained from an aircraft or satellite mounted instrument to determine the pollutant concentration in the atmosphere.

REFERENCES

1. McClatchey, R. A., Fenn, R. W., Selby, J.E.A., Volz, F. E., and Garing, J. S., "Optical Properties of the Atmosphere," 3rd ed., AFCRL-72-0497, Aug. 1972, Air Force Cambridge Research Laboratories, Bedford, Mass.

2. Selby, J.E.A. and McClatchey, R. A., "Atmospheric Transmittance from 0.25 μm: Computer Code LOWTRAN 3," AFCRL-TR-75-0255, Oct. 1975, Environmental Research Cambridge Research Laboratories, Bedford, Mass.

3. McClatchey, R. A., Benedict, W. S., Clough, S. A., Burch, D. E., Calfee, R. F., Fox, K., Rothman, L. S., and Garing, J. S., "AFCRL Atmospheric Line Parameters Compilation," AFCRL-TR-73-0096, Jan. 1973, Air Force Cambridge Research Laboratories, Bedford, Mass.

4. Ludwig, C. B., Griggs, M., Malkmus, W., and Bartle, E. R., "Air Pollution Measurements from Satellites," NASA CR-2324, Nov. 1973. Also refer to other references of this report (Refs. 3 and 139 in particular).

5. Science Application Incorporated (SAI), "Line-by-Line Program (POLAYER) for Evaluation of Radiance and Signal Change, and Compilation of Spectroscopic Parameters for the Spectral Range of CO Fundamental Band (1973 Version)." Available at NASA Langley Research Center, Hampton, Va.

6. Tiwari, S. N., "Appropriate Line Profiles for Radiation Modeling in the Detection of Atmospheric Pollutants," TR-73-T3, March 1973, School of Engineering, Old Dominion University, Norfolk, Va.

7. Tiwari, S. N. and Reichle, H. G., "Application of Infrared Line Models in the Detection of Atmospheric Pollutants," AIAA Paper 74-651, Presented at AIAA/ASME Thermophysics and Heat Conference, July 15-17, 1974, Boston, Mass.

8. Tiwari, S. N. and Batki, R. R., "Infrared Line Models for Atmospheric Radiation," TR-74-T4, July 1974, School of Engineering, Old Dominion University, Norfolk, Va.

9. Elsasser, W. M., "Heat Transfer by Infrared Radiation in the Atmosphere," Harvard Meteorological Studies, No. 6, Harvard Univ. Press, Cambridge, Mass., 1942.

10. Plass, G. N., "Models for Spectral Band Absorption," Journal of the Optical Society of America, Vol. 48, No. 10, Oct. 1958, pp. 690-703.

11. Plass, G. N., "Useful Representations for Measurements of Spectral Band Absorption," Journal of the Optical Society of America, Vol. 50, No. 9, Sept. 1960, pp. 868-875.

12. Wyatt, P. J., Stull, V. R., and Plass, G. N., "Quasi-Random Model of Band Absorption," Journal of the Optical Society of America, Vol. 52, No. 11, Nov. 1962, pp. 1209-1217.

13. Goody, R. M., Atmospheric Radiation I: Theoretical Basis, Oxford Univ. Press, London and New York, 1964.

14. Kunde, V. G., "Theoretical Computations of the Outgoing Infrared Radiance from a Planetary Atmosphere," TN D-4045, Aug. 1967, NASA.

15. Gupta, S. K. and Tiwari, S. N., "Evaluation of Upwelling Infrared Radiance from Earth's Atmosphere," TR-75-T14, Nov. 1975, School of Engineering, Old Dominion University, Norfolk, Va.

16. Tiwari, S. N. and Batki, R. R., "Infrared Band Models for Atmospheric Radiation," TR-75-T17, Nov. 1975, School of Engineering, Old Dominion University, Norfolk, Va.

17. Tiwari, S. N., "Band Models and Correlations for Infrared Radiation," AIAA Paper 75-699, Presented at the AIAA 10th Thermophysics Conference, May 27-29, 1975, Denver, Colo. Also Published in 1975-AIAA Progress in Astronautics and Aeronautics: Radiative Transfer and Thermal Control.

18. Tien, C. L., "Thermal Radiation Properties of Gases," Advances in Heat Transfer, Vol. V, Academic Press, New York, 1968.

19. Cess, R. D. and Tiwari, S. N., "Infrared Radiative Energy Transfer in Gases," Advances in Heat Transfer, Vol. VIII, Academic Press, New York, 1972.

20. Edwards, D. K. "Molecular Gas Band Radiation," Advances in Heat Transfer, Vol. XII, Academic Press, New York, 1976.

21. Mitchell, A.C.G. and Zemansky, W. M., Resonance Radiation and Excited Atoms, Cambridge Univ. Press., Cambridge, Mass., 1934 (reprinted 1961).

22. Penner, S. S., Quantitative Molecular Spectrsocopy and Gas Emissivities, Addison-Wesley, Reading, Mass., 1959.

23. Baranger, M., "Spectral Line Broadening in Plasmas," in Atomic and Molecular Processes, edited by D. R. Bates, Academic Press, New York, 1962.

24. Allen, L. H., Astrophysics - The Atmosphere of the Sun and Stars, 2nd ed., Ronald Press Co., New York, 1963.

25. Griem, H. R., Plasma Spectroscopy, McGraw-Hill Book Co., New York, 1964.

26. Cooper, J., "Plasma Spectroscopy," in Report on Progress in Physics, Vol. 29, 1966, pp. 35-130.

27. Jefferies, J. T., Spectral Line Formation, Ginn-Blaisdell, New York, 1968.

28. Kondratyev, K. Ya., Radiation in Atmosphere, Academic Press, New York, 1969.

29. Armstrong, B. H. and Nicholls, R. W., Emission, Absorption and Transfer of Radiation in Heated Atmosphere, Pergamon Press, New York, 1972.

30. Yamamoto, G., Tanaka, M., and Aoki, T., "Estimation of Rotational Line Widths of Carbon Dioxide Bands," Journal of Quantitative Spectroscopy and Radiative Transfer, Vol. 9, No. 3, March 1969, pp. 371-382.

31. Ely, R. and McCubbin, T. K., Jr., "The Temperature Dependence of the Self Broadened Half-Width of the P-20 Line in the 001-100 Band of CO_2," Applied Optics, Vol. 9, No. 5, May 1970, pp. 1230-1231.

32. Tubbs, L. D. and Williams, D., "Broadening of Infrared Absorption Lines at Reduced Temperatures: Carbon Dioxide," Journal of the Optical Society of America, Vol. 62, No. 2, Feb. 1972, pp. 284-289.

33. Reiche, F., Verhandl. deut. Physik. Ges., Vol. 15, p. 3, 1913.

34. Born, M., Optik, pp. 482-486, Julius Springer, Berlin, 1933.

35. Van de Hulst, H. C. and Reesinck, J. M., "Line Breadths and Voigt Profiles," Astrophysical Journal, Vol. 106, No. 1, July 1947, pp. 121-127.

36. Harris, D. L. III, "On the Line-Absorption Coefficient due to Doppler Effect and Damping," Astrophysical Journal, Vol. 108, No. 1, July 1948, pp. 112-115.

37. Penner, S. S. and Kavanagh, R. W., "Radiation from Isolated Spectral Lines with Combined Doppler and Lorentz Broadening," Journal of the Optical Society of America, Vol. 43, No. 5, May 1953, pp. 385-388.

38. Plass, G. N. and Fivel, D. I., "Influence of Doppler Effect and Damping on Line Absorption Coefficient and Atmospheric Radiation Transfer," The Astrophysical Journal, Vol. 117, No. 1, Jan. 1953, pp. 225-233.

39. Posener, D. W., "The Shape of Spectral Lines: Table of the Voigt Profile," Australian Journal of Physics, Vol. 12, No. 2, June 1959, pp. 184-196.

40. Fried, B. D. and Conte, S. D., The Plasma Dispersion Function, Academic Press, New York, 1961.

41. Hummer, D. G., "The Voigt Function: An Eight-Significant-Figure Table and Generating Procedure," NBS JILA Report 24, Univ. of Colorado, Colo., 1964.

42. Hummer, D. G., "Expansion of Dawson's Function in a Series of Chebyshev Polynomials," Mathematics of Computation, Vol. 18, No. 86, April 1964, pp. 317-319.

43. Hummer, D. G., "The Voigt Function: An Eight Significant-Figure Table and Generating Procedure," Memoirs Royal Astronomical Society (G. B.), Vol. 70, Part 1, 1965, pp. 1-32.

44. Finn, G. D. and Mugglestone, D., "Tables of the Line Broadening Function H (a,v)," Royal Astronomical Society (LONDON) Monthly Notice, Vol. 129, No. 2, Feb. 1965, pp. 221-236.

45. Young, C., "Table for Calculating the Voigt Profile," TR-05863-7-T, July 1965, College of Engineering, Univ. of Michigan, Ann Arbor, Mich.

46. Young, C., "Calculation of the Absorption Coefficient for Lines with Combined Doppler and Lorentz Broadening," Journal of Quantitative Spectroscopy and Radiative Transfer, Vol. 5, No. 3, May-June 1965, pp. 549-552.

47. Armstrong, B. H., "Spectrum Line Profiles: The Voigt Function," Journal of Quantitative Spectroscopy and Radiative Transfer, Vol. 7, No. 1, Jan.-Feb. 1967, pp. 61-88.

48. Chiarella, C. and Reichel, A., "On the Evaluation of Integrals Related to the Error Function," Mathematics of Computation, Vol. 22, No. 101, Jan. 1968, 1968, pp. 137-143.

49. Gautschi, W., "Complex Error Function," Association for Computing Machinery and Communications, Vol. 12, No. 11, Nov. 1969, p. 635.

50. Gautschi, W., "Efficient Computation of the Complex Error Function," SIAM, Journal of Numerical Analysis, Vol. 7, No. 1, March 1970, pp. 187-198.

51. Whiting, E. E., "An Empirical Approximation to the Voigt Profile," Journal of Quantitative Spectroscopy and Radiative Transfer, Vol. 8, No. 6, June 1968, pp. 1379-1384.

52. Kielkopf, J. F., "New Approximation to the Voigt Function with Applications to Spectral Line Profile Analysis," Journal of the Optical Society of America, Vol. 63, No. 8, Aug. 1973, pp. 987-995.

53. Simmons, F. S., "Radiance and Equivalent Widths of Lorentz Lines for Non-isothermal Paths," Journal of Quantitative Spectroscopy and Radiative Transfer, Vol. 7, No. 1, Jan.-Feb. 1967, pp. 111-121.

54. Yamamoto, G. and Aida, M., "Transmission in a Non-Homogeneous Atmosphere with an Absorbing Gas of Constant Mixing Ratio," Journal of Quantitative Spectroscopy and Radiative Transfer, Vol. 10, No. 6, June 1970, pp. 593-608.

55. Cogley, A. C., "Radiative Transport of Lorentz Lines in Non-Isothermal Gases," Journal of Quantitative Spectroscopy and Radiative Transfer, Vol. 10, No. 9, Sept. 1970, pp. 1065-1075.

56. Tien, C. L., "A Simple Approximate Formula for Radiation from a Line with Resonance Contour," Journal of Quantitative Spectroscopy and Radiative Transfer, Vol. 6, No. 6, Nov.-Dec. 1966, pp. 893-894.

57. Varanasi P., Referred by C. L. Tien in Journal of Quantitative Spectroscopy and Radiative Transfer, Vol. 6, No. 6, Nov.-Dec. 1966, pp. 893-894.

58. Goldman, A., "On Simple Approximations to the Equivalent Width of a Lorentz Line," Journal of Quantitative Spectroscopy and Radiative Transfer, Vol. 8, No. 2, Feb. 1968, pp. 829-831.

59. Yamada, H. Y., "Total Radiances and Equivalent Widths of Doppler Lines for Nonisothermal Paths," Journal of Quantitative Spectroscopy and Radiative Transfer, Vol. 7, No. 6, Nov.-Dec. 1967, pp. 997-1003.

60. Jansson, P. A. and Korb, C. L., "A Table of the Equivalent Widths of Isolated Lines with Combined Doppler and Common Broadened Profiles," Journal of Quantitative Spectroscopy and Radiative Transfer, Vol. 8, No. 7, July 1968, pp. 1399-1409.

61. Kyle, T. G., "Absorption by Doppler-Lorentz Atmospheric Lines," Journal of Quantitative Spectroscopy and Radiation Transfer, Vol. 8, No. 8, Aug. 1968, pp. 1455-1462.

62. Yamada, H. Y., "Total Radiances and Equivalent Widths of Isolated Lines with Combined Doppler and Collision Broadened Profiles," Journal of Quantitative Spectroscopy and Radiative Transfer, Vol. 8, No. 8, Aug. 1968, pp. 1463-1473.

63. Curtis, A. R., Unpublished work discussed in References 64 and 65.

64. Gille, J. C. and Ellingson, R. G., "Correction of Random Exponentia' Band Transmission for Doppler Effects," Applied Optics, Vol. 7, No. 3, March 1968, pp. 471-474.

65. Rodgers, C. B. and Williams, A. P., "Integrated Absorption of a Spectral Line with the Voigt Profile," Journal of Quantitative Spectroscopy and Radiative Transfer, Vol. 14, No. 4, April 1974, pp. 319-323.

66. Yamamota, G. and Aida, M., "Transmission Due to Overlapping Lines," Journal of Quantitative Spectroscopy and Radiative Transfer, Vol. 7, No. 1, Jan.-Feb. 1967, pp. 123-141.

67. Kaplan, L. D., "Regions of Validity of Various Absorption - Coefficient Approximations," Journal of Meteorology, Vol. 10, No. 2, April 1953, pp. 100-104.

68. Craig, R. A., "A Note on the Transmissivity of an Elsasser Band," Journal of the Atmospheric Sciences, Vol. 20, No. 1, Jan. 1963, pp. 66-68.

69. Seitz, W. S. and Lundholm, D. V., "Elsasser Model for Band Absorption; Series Representation of a Useful Integral," Journal of the Optical Society of America, Vol. 54, No. 3, March 1964, pp. 315-318.

70. Zachor, A. S., "Absorptance and Radiative Transfer by a Regular Band," Journal of Quantitative Spectroscopy and Radiative Transfer, Vol. 7, No. 6, Nov.-Dec. 1967, pp. 857-870.

71. Kaplan, L. D., 1953 Proceedings of the Toronto Meteorological Conference, 1954, Royal Meteorological Society, p. 43.

72. Kyle, T. G., "Absorption of Radiation by Uniformly Spaced Doppler Lines," Astrophysical Journal, Vol. 148, No. 3, Part I, June 1967, pp. 845-848.

73. Golden, S. A., "The Doppler Analog of the Elsasser Band Model," Journal of Quantitative Spectroscopy and Radiative Transfer, Vol. 7, No. 3, May-June 1967, pp. 483-494.

74. Golden, S. A., "The Doppler Analog of the Elsasser Band Model-II, The Integrated Emissivity," Journal of Quantitative Spectroscopy and Radiative Transfer, Vol. 8, No. 3, March 1968, pp. 877-897.

75. Young, S. J., "Band Model Formulation for Inhomogeneous Optical Paths," Journal of Quantitative Spectroscopy and Radiative Transfer, Vol. 15, No. 6, June 1975, pp. 483-501.

76. Young, S. J., "Addendum to: Band Model Formulation for Inhomogeneous Optical Paths," Journal of Quantitative Spectroscopy and Radiative Transfer, Vol. 15, No. 12, Dec. 1975, pp. 1137-1140.

77. Golden, S. A., "The Voigt Analog of an Elsasser Band," Journal of Quantitative Spectroscopy and Radiative Transfer, Vol. 9, No. 8, Aug. 1969, pp. 1067-1081.

78. Malkmus, W., "Random Lorentz Band Model with Exponential-Tailed S^{-1} Line Intensity Distribution Function," Journal of the Optical Society of America, Vol. 57, No. 3, March 1967, pp. 323-329.

79. Malkmus, W., "Random Band Models with Lines of Pure Doppler Shape," Journal of the Optical Society of America, Vol. 58, No. 9, Sept. 1968, pp. 1214-1217.

80. Rodgers, C. D., "Some Extensions and Applications of the New Random Model for Molecular Band Transmission," Journal of Royal Meteorological Society, Vol. 94, No. 399, Jan. 1968, pp. 99-102.

81. Curtis, A. R., "Discussion of a Statistical Model for Water Vapour Absorption," Quarterly Journal of Royal Meteorological Society, Vol. 78, No. 338, Oct. 1952, pp. 638-641.

82. Godson, W. L., "The Evaluation of Infrared Radiative Fluxes due to Atmospheric Water Vapour," Quarterly Journal Royal Meteorological Society, Vol. 79, No. 341, July 1953, pp. 367-379.

83. Walshaw, C. D. and Rodgers, C. D., "The Effect of Curtis-Godson Approximation on the Accuracy of Radiative Heating-Rate Calculations," Quarterly Journal of Royal Meteorological Society, Vol. 89, No. 379, Jan. 1963, pp. 122-130.

84. Goody, R. M., "The Transmission of Radiation Through an Inhomogeneous Atmosphere," Journal of the Atmospheric Sciences, Vol. 21, No. 6, Nov. 1964, pp. 576-581.

85. Armstrong, B. H., "Analysis of Curtis-Godson Approximation and Radiation Transmission Through Inhomogeneous Atmospheres," Journal of the Atmospheric Sciences, Vol. 25, No. 2, March 1968, pp. 312-322.

86. Yamamoto, G. Aida, M., and Yamamoto, S., "Improved Curtis-Godson Approximation in a Non-Homogeneous Atmosphere," Journal of the Atmospheric Sciences, Vol. 29, No. 6, Sept. 1972, pp. 1150-1155.

87. Lindquist, G. H. and Simmons, F. S., "A Band Model Formulation for Very Non-Uniform Paths," Journal of Quantitative Spectroscopy and Radiative Transfer, Vol. 12, No. 5, May 1972, pp. 807-820.

88. Weinreb, M. P. and Neuendorffer, A. C., "Method to Apply Homogeneous-Path Transmittance Models to Inhomogeneous Atmosphere," Journal of the Atmospheric Sciences, Vol. 30, No. 4, May 1973, pp. 662-666.

89. Aida, M., "A Statistical Method to Estimate the Vertical Transmission Through Horizontally Non-Homogeneous Media," Journal of Quantitative Spectroscopy and Radiative Transfer, Vol. 15, No. 6, June 1975, pp. 503-511.

90. McMillin, L. M., and Fleming, H. E., "Atmospheric Transmittance of an Absorbing Gas: A Computationally Fast and Accurate Transmittance Model for Absorbing Gases with Constant Mixing Ratios in Inhomogeneous Atmospheres," Applied Optics, Vol. 15, No. 2, Feb. 1976, pp. 358-363.

91. Edwards, D. K. and Menard, W. A., "Comparison of Methods for Correlation of Total Band Absorption," Applied Optics, Vol. 3, No. 5, May 1964, pp. 621-625.

92. Edwards, D. K., Glassen, L. K., Hauser, W. C., and Tuchscher, J. S., "Radiation Heat Transfer in Nonisothermal Nongray Gases," Journal of Heat Transfer, Vol. 89, Series C, No. 3, Aug. 1967, pp. 219-229.

93. Edwards, D. K. and Balakrishnon, A., "Slab Band Absorptance for Molecular Gas Radiation," Journal of Quantitative Spectroscopy and Radiative Transfer, Vol. 12, No. 10, Oct. 1972, pp. 1379-1387.

94. Felske, J. D. and Tien, C. L., "A Theoretical Closed Form Expression for the Total Band Absorptance of Infrared-Radiating Gases," International Journal of Heat and Mass Transfer, Vol. 17, No. 1, Jan. 1974, pp. 155-158.

95. Echigo, R., Hasegawa, S., and Miyazaki, Y., "Composite Heat Transfer with Thermal Radiation in Non-Gray Medium-Part I Interaction of Radiation with Conduction," International Journal of Heat and Mass Transfer, Vol. 14, No. 12, Dec. 1971, pp. 2001-2015.

96. Tiwari, S. N. and Cess, R. D., "Heat Transfer to Laminar Flow of Non-Gray Gases Through a Circular Tube," Applied Scientific Research, Vol. 25, No. 3/4, Dec. 1971, pp. 155-170.

97. Donovan, T. E. and Breif, R., "Laminar Convection with an Absorbing and Emitting Gas," Applied Scientific Research, Vol. 31, No. 2, Aug. 1975, pp. 110-122.

98. Martin, J. K. and Hwang, C. C., "Combined Radiant and Convective Heat Transfer to Laminar Steam Flow Between Gray Parallel Plates with Uniform Heat Flux," Journal of Quantitative Spectroscopy and Radiative Transfer, Vol. 15, No. 12, Dec. 1975, pp. 1071-1081.

99. Edwards, D. K. and Balakrishnon, A., "Thermal Radiation by Combustion Gases," International Journal of Heat and Mass Transfer, Vol. 16, No. 1, Jan. 1973, pp. 25-40.

100. Wassel, A. T. and Edwards, D. K., "Molecular Gas Band Radiation in Cylinders," Journal of Heat Transfer, Vol. 96, Series C, No. 1, Feb. 1974, pp. 21-26.

101. Wassel, A. T., Edwards, D. K., and Cotton, I., "Molecular Gas Radiation and Laminar or Turbulent Heat Diffusion in a Cylinder with Internal Heat Generation," International Journal of Heat and Mass Transfer, Vol. 18, No. 11, Nov. 1975, pp. 1267-1276.

102. Wassel, A. T. and Edwards, D. K., "Molecular Gas Radiation in a Laminar or Turbulent Pipe Flow," Journal of Heat Transfer, Vol. 98, Series C, No. 1, Feb. 1976, pp. 101-107.

103. Gilles, S. E. and Vincenti, W. G., "Coupled Radiative and Vibrational Nonequilibrium in a Diatomic Gas, with Application to Gas Dynamics," Journal of Quantitative Spectroscopy and Radiative Transfer, Vol. 10, No. 2, Feb. 1970, pp. 71-97.

104. Cess, R. D., Mighdoll, P., and Tiwari, S. N., "Infrared Radiative Heat Transfer in Nongray Gases," International Journal of Heat and Mass Transfer, Vol. 10, No. 11, Nov. 1967, pp. 1521-1532.

105. Hsieh, T. C. and Greif, R., "Theoretical Determination of the Absorption Coefficient and the Total Band Absorptance Including a Specific Application to Carbon Monoxide," International Journal of Heat and Mass Transfer, Vol. 15, No. 8, Aug. 1972, pp. 1477-1487.

106. Lin, C. C. and Chan, S. H., "A General Slab Band Absorptance for Infrared Radiating Gases," Journal of Heat Transfer, Vol. 97, Series C, No. 3, Aug. 1975, pp. 478-480.

107. Tien, C. L. and Lowder, J. E., "A Correlation for Total Band Absorptance of Radiating Gases," International Journal of Heat and Mass Transfer, Vol. 9, No. 7, July 1966, pp. 698-701.

108. Goody, R. M. and Belton, M.J.S., "Radiative Relaxation Times for Mars (A Discussion of Martian Atmospheric Dynamics)," Planetary and Space Science, Vol. 15, No. 2, Feb. 1967, pp. 247-256.

109. Tien, C. L. and Ling, G. R., "On a Simple Correlation for Total Band Absorptance of Radiating Gases," International Journal of Heat and Mass Transfer, Vol. 12, No. 9, Sept. 1969, pp. 1179-1181.

110. Cess, R. D. and Ramanathan, V., "Radiative Transfer in the Atmosphere of Mars and that of Venus Above the Cloud Deck," Journal of Quantitative Spectroscopy and Radiative Transfer, Vol. 12, No. 5, May 1972, pp. 933-945.

111. Rodgers, C. D., "The Use of Emissivity in Atmospheric Radiative Calculations," Quarterly Journal of Royal Meteorological Society, Vol. 93, No. 395, Jan. 1967, pp. 45-54.

112. Manabe, S. and Wetherald, R. T., "Thermal Equilibrium of the Atmosphere with a Given Distribution of Relative Humidity," Journal of the Atmospheric Sciences, Vol. 24, No. 3, May 1967, pp. 241-259.

113. Taylor, P. B. and Foster, P. J.,"The Total Emissivities of Luminous and Non-Luminous Flames," International Journal of Heat and Mass Transfer, Vol. 17, No. 12, Dec. 1974, pp. 1591-1605.

114. Cess, R. D., "Radiative Transfer due to Atmospheric Water Vapor: Global Considerations of the Earth's Energy Balance," Journal of Quantitative Spectroscopy and Radiative Transfer, Vol. 14, No. 9, Sept. 1974, pp. 861-871.

115. Penner, S. S., "Equilibrium Radiation Properties of Gases," Handbook of Heat Transfer, edited by W. M. Rohsenow and J. P. Hartnett, Section 15, Part D, pp. 15-72, McGraw-Hill, New York, 1973.

116. Hottel, H. C., Heat Transmission, edited by W. H. McAdams, Chapter IV, McGraw-Hill, New York, 1954.

117. Hottel, H. C. and Sarofim, A. F., Radiative Transfer, McGraw-Hill, New York, 1967.

118. Gupta, S. K. and Tiwari, S. N., "Evaluation of Transmittance of Selected Infrared Bands," TR-76-T7, April 1976, School of Engineering, Old Dominion University, Norfolk, Va.

119. Gupta, S. K. and Tiwari, S. N., "Retrieval of Surface Temperature by Remote Sensing," TR-76-T8, April 1976, School of Engineering, Old Dominion University, Norfolk, Va.

120. Kunde, V. G. and Maguire, W. C., "Direct Integration Transmittance Model," Journal of Quantitative Spectroscopy and Radiative Transfer, Vol. 14, No. 8, Aug. 1974, pp. 803-817.

121. Burch, D. E., Gryvnak, D. A., Singleton, E. B., France, W. L., and Williams, D., "Infrared Absorption by Carbon Dioxide, Water Vapor, and Minor Atmospheric Constituents," AFCRL-62-698, July 1962, Air Force Cambridge Research Laboratories, Bedford, Mass.